PRODUCTION AND DEVELOPMENT OF ALUMINIDE COATINGS BY CHEMICAL VAPOR DEPOSITION ON NICKEL BASED SUPERALLOYS FOR TURBINE ENGINE APPLICATIONS

A THESIS SUBMITTED TO
THE GRADUATE SCHOOL OF NATURAL AND APPLIED SCIENCES
OF
MIDDLE EAST TECHNICAL UNIVERSITY

BY

UMUTCAN ERTÜRK

IN PARTIAL FULFILLMENT OF THE REQUIREMENTS
FOR
THE DEGREE OF MASTER OF SCIENCE
IN
METALLURGICAL AND MATERIALS ENGINEERING

AUGUST 2017

Approval of the thesis:

PRODUCTION AND DEVELOPMENT OF ALUMINIDE COATINGS BY CHEMICAL VAPOR DEPOSITION ON NICKEL BASED SUPERALLOYS FOR TURBINE ENGINE APPLICATIONS

submitted by **UMUTCAN ERTÜRK** in partial fulfillment of the requirements for the degree of **Master of Science in Metallurgical and Materials Engineering Department, Middle East Technical University** by,

Prof. Dr. Gülbin Dural Ünver
Dean, Graduate School of **Natural and Applied Sciences** _____

Prof. Dr. C. Hakan Gür
Head of Department, **Metallurgical and Materials Engineering** _____

Assist. Prof. Dr. M. Bilge İmer
Supervisor, **Metallurgical and Materials Eng. Dept., METU** _____

Examining Committee Members:

Prof. Dr. Macit Özenbaş
Metallurgical and Materials Eng. Dept., METU _____

Assist. Prof. Dr. M. Bilge İmer
Metallurgical and Materials Eng. Dept., METU _____

Prof. Dr. Kadri Aydınol
Metallurgical and Materials Eng. Dept., METU _____

Assist. Prof. Dr. Mert Efe
Metallurgical and Materials Eng. Dept., METU _____

Assist. Prof. Dr. Caner Şimşir
Manufacturing Eng. Dept., Atılım University _____

Date: August 18, 2017

I hereby declare that all information in this document has been obtained and presented in accordance with academic rules and ethical conduct. I also declare that, as required by these rules and conduct, I have fully cited and referenced all material and results that are not original to this work.

Name, Last name : Umutcan Ertürk

Signature :

ABSTRACT

PRODUCTION AND DEVELOPMENT OF ALUMINIDE COATINGS BY CHEMICAL VAPOR DEPOSITION ON NICKEL BASED SUPERALLOYS FOR TURBINE ENGINE APPLICATIONS

Ertürk, Umutcan
M.S., Department of Metallurgical and Materials Engineering
Supervisor: Assist. Prof. Dr. M. Bilge İmer

August 2017, 169 pages

Diffusion coatings including aluminide coatings are utilized to improve the high temperature oxidation and corrosion resistance of turbine blades. Through the advancement in the aluminizing methods, higher purity and more homogeneously distributed coatings have been realized. The chemical vapor deposition (CVD) is the most advanced technique utilized for aluminizing process. The versatility of CVD provides a large possibility to control process variables such as temperature, pressure, gas flows and ratios, and aluminum activity. However, the main challenge of CVD method is optimizing the process parameters to obtain high growth rate and outer layer/interdiffusion zone (IDZ) ratio while satisfying required coating microstructure and composition. In addition, improvement in the durability of aluminide coating is also an important design criterion to extend the lifetime of turbine blades which could be achieved by the addition of reactive or alloying elements to the coating.

In this dissertation, production of aluminide coatings by CVD was investigated to effectively increase growth rate and outer coating layer/IDZ ratio by optimizing the process variables. The influence of temperature, pressure, chlorinator temperature, gas flows and ratios, aluminum activity, and process time were studied on the formation of aluminide coating by univariate experimental analysis. Also, the effect of substrate properties, such as surface roughness, composition, and sample thickness was separately studied.

Moreover, co-deposition of reactive (Zr, Hf, Y) and alloying (Cr, Co) elements were investigated to incorporate ternary elements to aluminide coating in desired concentration and distribution. Additionally, the impact of these ternary elements on the hot corrosion behavior of aluminide coatings was evaluated by isothermal hot corrosion test to extend the life time of turbine blades.

Keywords: Chemical vapor deposition, aluminizing, diffusion coating, aluminide coating, hot corrosion.

ÖZ

TÜRBİN MOTORU UYGULAMALARI İÇİN ALÜMİNİT KAPLAMALARIN NİKEL BAZLI SÜPERALAŞIM ÜZERİNE KİMYASAL BUHAR BİRİKTİME YÖNTEMİ İLE UYGULANMASI VE GELİŞTİRİLMESİ

Ertürk, Umutcan
Yüksek Lisans, Metalurji ve Malzeme Mühendisliği
Tez Yöneticisi: Yard. Doç. Dr. M. Bilge İmer

Ağustos 2017, 169 sayfa

Difüzyon tipi bir kaplama olan alüminit kaplamalar türbin kanatlarının yüksek sıcaklık oksidasyon ve korozyon dirençlerini iyileştirmek için kullanılmaktır. Alüminit kaplama yöntemlerinde gerçekleşen ilerleme sayesinde, yüksek saflık ve homojenlikte kaplamalar elde edilebilmektedir. Kimyasal buhar birikimi (CVD), alüminit kaplama işlemi için kullanılan en gelişmiş tekniktir. CVD'nin çok yönlülüğü sıcaklık, basınç, alüminyum aktivitesi, gaz akışları ve oranları gibi proses değişkenlerini kontrol etmek için büyük bir olanak sağlar. CVD yönteminin zorluğu ise istenilen kaplama mikroyapısı ve kimyasal kompozisyonunu yüksek büyüme hızı ve yüksek dış katman /interdifüzyon bölgesi (IDZ) oranı ile birlikte elde edebilmek için proses parametrelerini optimize etmektir. Ayrıca, CVD yöntemi ile kaplamaya reaktif veya alaşım elementlerinin eş-zamanlı eklenmesi vasıtasıyla alüminit kaplama özellikleri geliştirilebilmektedir. Bu sayede türbin kanatlarının kullanım ömürleri önemli ölçüde uzatılabilmektedir.

Bu tez çalışmasında, proses değişkenlerini optimize ederek kaplama büyütme hızı ve dış katman/IDZ oranını etkili bir şekilde arttırmak için CVD ile alüminit kaplamaların üretimi araştırılmıştır. Tek değişkenli kaplama deneyleri ile sıcaklık, basınç, klorinatör sıcaklığı, gaz akışları ve oranları, alüminyum aktivitesi ve kaplama süresinin alüminit kaplama oluşumu üzerindeki etkileri incelenmiştir. Ayrıca, altlık malzeme yüzey pürüzlülüğü, bileşimi ve numune kalınlığının alüminit kaplama üzerndeki etkileri de incelenmiştir.

CVD optimizasyon çalışmalarının yanı sıra, reaktif (Zr, Hf, Y) ve alaşım (Cr, Co) elementlerinin CVD ile alüminit kaplamaya eş zamanlı olarak eklenmesi araştırılmıştır. Ayrıca, kaplamaya eklenen elementlerin alüminit kaplamaların yüksek sıcaklık korozyon direnci üzerindeki etkisi, izotermal sıcak korozyon testi gerçekleştirilerek karşılaştırmalı olarak incelenmiştir.

Anahtar Kelimeler: Kimyasal buhar biriktirme, aluminit kaplama, yüksek sıcaklık korozyonu.

To my beloved family

ACKNOWLEDGEMENTS

First of all, I would like to express my sincere gratitude to Dr. Bilge İmer, for her support, patience, encouragement, and confıdence on me from the very first day.

This work is supported by Tübitak KAMAG (Kamu Kurumları Araştırma ve Geliştirme Projelerini Destekleme Programı). I would like to express my gratitude to Tübitak KAMAG, EÜAŞ (Elektrik Üretim A.Ş.), Tübitak MAM, Gürmetal and SDM for their support in this study.

I am very grateful to academicians, management personnel, technicians, and fellow students in Metallurgical and Materials Engineering Department - METU for all the support. Additionally, I want to thank SEM technician Serkan Yılmaz and XRD technician Nilüfer Özel. I also want to appreciate Zafer Artvin who is employee of METU Central Laboratory for his kind attention during “EPMA - WDS” analysis.

I would like to thank Orcan Kolankaya, İlker Yerbay, Dr. Süha Türkeş, Dr. Koray Yurtışık from METU Welding Technology and Non-Destructive Testing Research Laboratory for their help on welding and NDT analysis of CVD piping.

It has been my pleasure and honor to work and share with my colleagues Mustafa Tarık Boyraz, Seren Özer, Doğuhan Sarıtürk, Ali Fırat Dinler and Fırat Güler. Also, I am very grateful for their support and friendship during this study.

Additionally, I want to thank Phil Minett, Mark Bowry, and John Yeatman from Archer Technicoat for their help to keep CVD system running.

Furthermore, I would like to thank Alp Turgaç from SDM for his help on hot corrosion tests.

In addition, I would like to appreciate my friends Burak Çakırlar, Baran Güler (Bargül), Berkay Bayramin (Berk), Elif Özlem Güner, Berhan Melek, İshak Can Aydın, Kaan Aydın, Mert Dereli, Şamil Dereli, Mete Emre Gökdoğan, and Umut Yetiştiren for their support during this work.

My deepest gratitude goes to my parents and İrem Özcan for their endless support during this study as in the entire of my lifetime.

TABLE OF CONTENTS

LIST OF TABLES

TABLES

LIST OF FIGURES

FIGURES

LIST OF ABBREVIATIONS

CVD	Chemical Vapor Deposition
EDS	Energy Dispersive Spectroscopy
EPMA	Electron Probe Micro Analysis
FCC	Face Centered Cubic
HIP	Hot Isostatic Pressing
HTHC	High Temperature Hot Corrosion
IDZ	Interdiffusion Zone
LTHC	Low Temperature Hot Corrosion
PLC	Programmable Logic Controller
RE	Reactive Element
SEM	Scanning Electron Microscopy
TGO	Thermally Grown Oxide
WDS	Wavelength Dispersive Spectroscopy
XRD	X-ray Diffraction

CHAPTER 1

INTRODUCTION

1.1 General

Almost all industrial processes operate in very aggressive conditions defined by high temperature, extreme loads and stresses, oxidative and corrosive environment. Gas turbine engines are typical examples of machines working in extreme conditions. Process temperatures could reach up to 1650 ˚C in the hot section of gas turbine engines and components exposed to oxidative and corrosive exhaust gases at high temperature [1]. To provide required reliability and durability of components, nickel and cobalt based superalloys are widely used in turbine components such as turbine blades, due to their capability to sustain strength and oxidation/corrosion resistance above 650 ˚C [2].

To improve turbine engine performance and fuel efficiency by increasing operating temperature of turbine engines, compositional modifications were made to superalloys but caused a degradation in oxidation and corrosion resistance [3]. Degradation of turbine blade surfaces resulting from high temperature oxidation and hot corrosion deteriorates mechanical properties of blades and shortens life cycles. Therefore, protective coatings were developed to compensate the reduction in oxidation and hot corrosion resistance. The idea of applying protective coatings on nickel based superalloys was first practiced in the 1960s [4]. Diffusion aluminide coatings are the most widely used coatings in turbine blades than overlay coatings including MCrAlY types. These aluminide coatings were applied by pack process since the 1970s [5]; however, chemical vapor deposition (CVD) is the most present and advanced method so far.

Aluminide coatings generally have a two-layer structure which consists of the outer coating layer and interdiffusion zone (IDZ). At the outer layer, β-NiAl is the most preferential phase of Ni-Al binary phase system rather than Ni_3Al or Ni_2Al_3 phases. Between outer β-NiAl layer and substrate, interdiffusion zone forms by gradually adjusting the concentration difference of the aluminide coating and substrate elements by diffusion. While these species are diffusing, phases such as α-Cr, Ni_3Al, Ni_2Al_3 precipitates along this zone due to their low solubility in various region of aluminide coating. The function of aluminide coating is to form protective Al_2O_3 scale, which is called as thermally grown oxide (TGO), on the coating surfaces. Dense, continuous and adherent oxide layer prevents further oxidation of components by acting as a diffusion barrier for oxygen.

Main degradation mechanisms of aluminide coatings are oxide spallation due to weak scale adherence, unstable scale growth, and aluminum depletion. Types of phases formed at the surface, outer layer/IDZ thickness ratio, and coating homogeneity directly affect the lifetime of aluminide coating under high temperature oxidation and corrosion environment. However, they can be controlled by aluminizing process parameters such as temperature, pressure, gas flows and ratios, chlorinator temperature, and aluminum activity.

Aluminide coating lifetime, also, can be improved by the addition of reactive (e.g. Zr, Y, Hf, Ce, or La, etc.) [6] and/or alloying (e.g. Cr or Co, etc.) elements to the coating [7]. Reactive elements mainly improve scale adherence to coating surface by preventing detrimental effect of sulfur, while alloying elements promotes protective scale formation such as α-Al_2O_3 or Cr_2O_3 at component surface. By the addition of such elements to aluminide coating, the lifetime of coating/substrate system can be improved.

In this study, the effect of CVD process parameters and substrate properties (surface condition, composition, and thickness) on aluminide coating formation were investigated to optimize the aluminizing process. Also, co-deposition of reactive or alloying elements (Hf, Y, Zr, Cr and Co) together with aluminum were studied to incorporate such elements to aluminide coating homogeneously. Then, the influence

of ternary elements (Cr, Cr/Y, Y, Zr, Hf) on the hot corrosion resistance of aluminide coatings was investigated by comparative analysis of hot corrosion.

1.2 Literature Review

1.2.1 History of Gas Turbines

Development of combustion type gas turbines was started in the 18th century. John Barber was the pioneer of gas turbines who patented combustion turbine in 1791 [8]. Although the concept of gas turbines has a great potential, progress in technological improvements was limited due to lack of associated materials technology. Power generation by early versions of gas turbines was not efficient because generated combustion power was not sufficient to operate the turbine compressors [9]. To improve the efficiency of gas turbines, it was compulsory to increase combustion and inlet temperatures with the utilization of advanced materials. However, no remarkable improvement in gas turbine materials was achieved until the middle of the 20th century [10]. Due to World War II, governments started to fund research and development programs for jet turbines and advancements were transferred to industrial gas turbines for power generation [11].

German Junkers and British Rolls-Royce were the first companies that started the commercial production of combustion turbines [12]. Later, the agreement between British Power Jets Ltd. and American GE Company led to rapid technological improvement in land, sea, and air based gas turbines. Then, Solar Turbines Inc. also emerged manufacturing high temperature materials for turbine manifold applications. After World War II, American Pratt & Whitney Company became a powerful developer of turbine engines [13]. On the other hand, Germans Siemens could not start to develop commercial gas turbine engines until 1952 [14].

Gas turbines started to be used commercially for power generation in the early 1960s with improvements in advanced high temperature materials and design of turbines, which permitted to increase combustion and rotor inlet temperatures [15]. Figure 1.1 shows typical gas turbine engine belong to GE Company used for power generation.

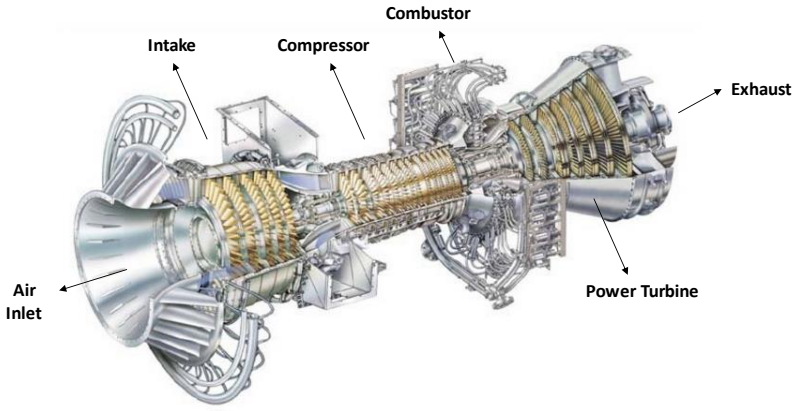

Figure 1.1 Typical industrial gas turbine engine diagram [16].

In Turkey, the first industrial gas turbine was started to be operated in 1987 at Trakya Natural Gas Combined Cycle Power Plant [17]. Over the years, the dependence of gas turbines for power generation increased with growing energy demand as a result of developing industry and growing economy. The number of power plants operates industrial gas turbines increased remarkably in 30 years. In 2015, 37.8 % of Turkey`s total electricity was generated by using natural gas in gas turbines [18].

Over the years, industrial gas turbine efficiency has also been increased remarkably with development in high temperature materials and turbine designs. For example, the maximum operating temperature was 550 °C in the 1940s and increased to 1200 °C in 2000s resulted in the production of more efficient gas turbines [19]. The new generation combined cycle industrial gas turbines reaches 58 % overall efficiency at 1425 °C combustion temperature [20]. Figure 1.2 shows temperature ranges for different high temperature production and energy generation processes. It can be seen that modern industrial gas turbines work in the temperature range of 600 – 1200 °C, and material selection for gas turbine engines is important design criteria to provide required reliability and durability of components at this temperatures.

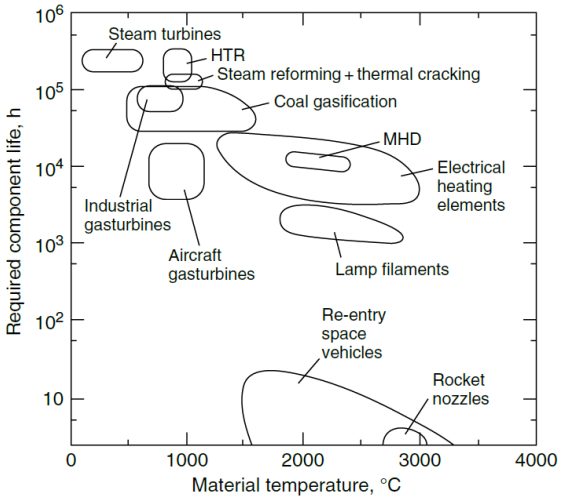

Figure 1.2 High-temperature processes with component temperatures and required lives [21].

1.2.2 Materials

Gas turbines consist of several parts, mainly air inlet, intake, compressor, combustor, power turbine and exhaust as shown in Figure 1.1. Power turbine part, which consists rotor and stator turbine blades, operates under extreme environmental conditions than any other parts of a turbine engine. Turbine blades are not only exposed to direct stress but also experiences high temperature with corrosive gasses. Due to the combination of such stress and temperature, creep resistance become essential for blade materials. In addition to creep, blades are exposed to highly corrosive exhaust gasses including chlorides, sulfides, and vanadium which causes hot corrosion.

Requirements for high strength creep resistant materials led to the development of advanced alloys such as nickel or cobalt based superalloys and titanium alloys. Figure 1.3 shows that temperature capabilities of these materials with their strength ranges. Although titanium alloys are mostly used as compressor blades that operate relatively lower temperatures, nickel based superalloys required for parts that operate over 500 °C temperatures such as turbine blades [22].

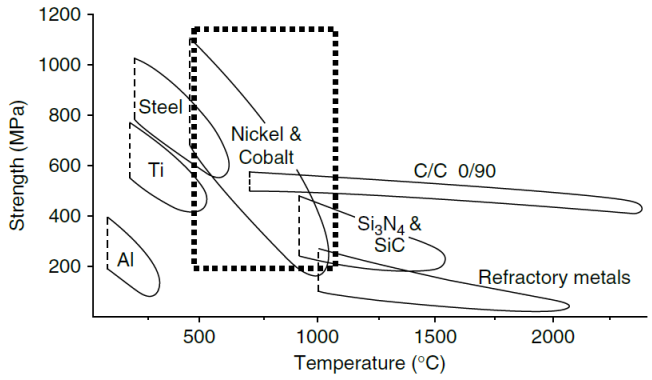

Figure 1.3 Temperature capabilities of classes of materials [23].

The trend of the materials used in gas turbines has changed over the years as shown in Figure 1.4. It can be claimed that steels and aluminum alloys mostly employed in early turbines. Only the nickel based superalloys meet the required properties for turbine blades because of their high capability to keep mechanical properties such as strength, creep and fatigue resistance even at elevated temperatures [24]. Therefore, usage of nickel based superalloys for various turbine components have started to increase.

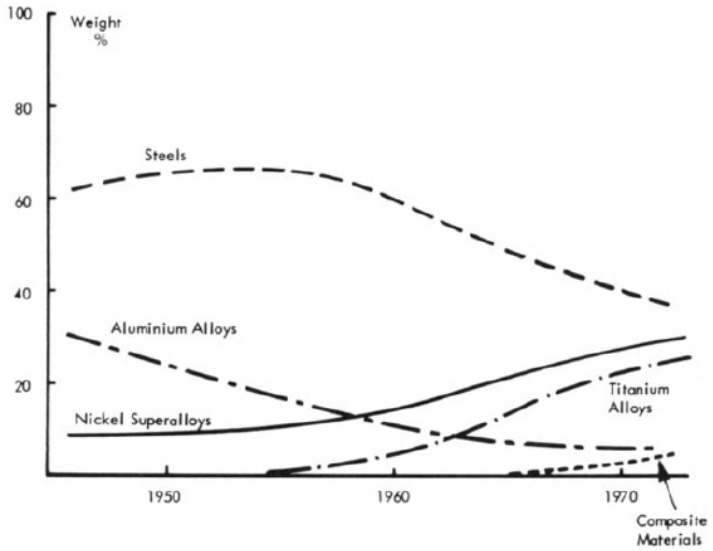

Figure 1.4 Trends in gas turbine materials usage over the years [25].

1.2.2.1 Nickel Based Superalloys

Nickel based superalloys are widely used in gas turbine engines as turbine blade material due to their excellent mechanical properties at a wide range of temperatures [26,27]. Nickel containing superalloys was first developed in the 1940s as simple nickel-chromium matrix alloys, and they evolved to a multi-element and multi-phase system. These alloys have face-centered cubic (FCC) crystal structure and have the capability to maintain its strength and creep resistance at 0.8 T_m (melting point of alloy) operating temperature [28].

1.2.2.1.1 Strengthening Mechanism

There are several strengthening mechanisms as shown Table 1.1 which provide required mechanical properties to superalloys.

Table 1.1 Strengthening mechanisms for superalloys [1].

Mechanisms	Effective Temperature
Solid-solution strengthening	High temperature
Precipitation (or age) strengthening	High temperature
Grain size control	Moderate temperature
ODS	Moderate temperature
Martensitic transformation strengthening	For specific metals and at low temperature
Work hardening	Low temperature

Among these mechanisms, main strengthening mechanisms for nickel based superalloys are solid solution strengthening, precipitation strengthening by carbides and γ` precipitates. These are shortly described below:

1- Solid solution strengthening:

Nickel based superalloys matrix consist of γ-Ni phase. When metallic elements such as Al, Cr, Co, Mo, Fe, Ta, W, Re, etc. dissolved in γ matrix, these alloying element atoms randomly replace the matrix atoms as shown in Figure 1.5. Atomic size difference between alloying atoms and Ni matrix atoms create stress field which slows dislocation movement; hence, strength increases with dissolving larger size alloying element atoms.

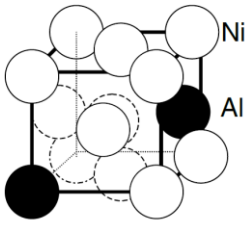

Figure 1.5 Schematic of substitutional solid solution (Al dissolved in Ni) [1].

2- Precipitation strengthening by carbides:

Several types of carbides are present in nickel based superalloys as MC, $M_{23}C_6$ and M_6C. MC carbides (with Ti, Ta, Mo, W, Nb), $M_{23}C_6$ carbides (with Cr, W, Mo) and M_6C carbides (with Mo, W, Nb) can be formed with different morphologies (Fig. 1.6) in superalloys depending on casting, heat treatment, and service conditions. The principal strengthening mechanism of carbides is obstructing dislocation movement within grains and pinning grain boundary movement; thereby increasing strength.

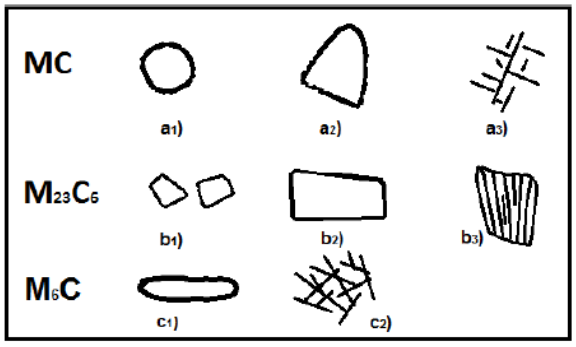

Figure 1.6 Image a_1) shows a typical MC carbide, a_2) and a_3) respectively, blocky and script morphologies. b_1) represent discontinuous blocky particles, b_2) plate and b_3) cellular type carbides. Image c_1) represents a blocky form of M_6C and c_2) represents Widmanstätten morphology [29].

3- Precipitation strengthening by γ` precipitates:

Precipitates of intermetallic compound γ`- Ni_3Al, also known as gamma prime, is the primary strengthening mechanism for nickel based superalloys, while solid solution and carbide precipitates provide additional (secondary) strengthening. Figure 1.7 represents a microstructure of nickel based superalloy (IN 738 LC) showing primary and secondary γ`- $Ni_3Al$ precipitates taken by colleague graduate student Mustafa Tarık Boyraz. γ` precipitates have a coherent interface with the γ-matrix. Ni atoms may be replaced by Cr, Co, and/or Mo atoms, and Al atoms may be replaced by Ti and Nb atoms in the crystal structure of γ`- $Ni_3Al$. Fine distributed γ` precipitates block the dislocation motion, resulting in a remarkable increase in strength of nickel based superalloys. Creep and fatigue resistance of the superalloys are affected by the size, distribution and the volume fraction of γ`- Ni_3Al along the matrix. These parameters can be controlled by not only Al and Ti content of the alloy but also the manufacturing conditions such as casting, hot isostatic pressing, solutionizing, CVD and aging parameters.

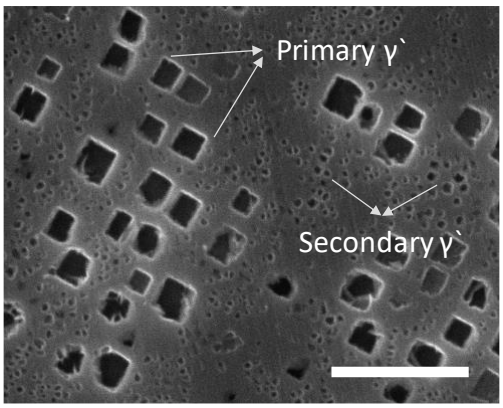

Figure 1.7 SEM microstructure image of nickel based superalloys includes γ`- Ni_3Al precipitates (The scale bar = 2 μm). Courtesy of Mustafa Tarık Boyraz.

1.2.2.1.2 Grain Type and Orientation Effect

Another important factor that affects the creep behavior of superalloys is grain orientation. Creep resistance can be improved significantly for polycrystalline alloys by annihilating transverse grains and obtaining columnar grains which are aligned to turbine blade axis. Further improvements can be achieved by eliminating grain

structure by forming single crystal alloy. Figure 1.8 represents rotor turbine blades showing these three different grain structures manufactured by Pratt & Whitney.

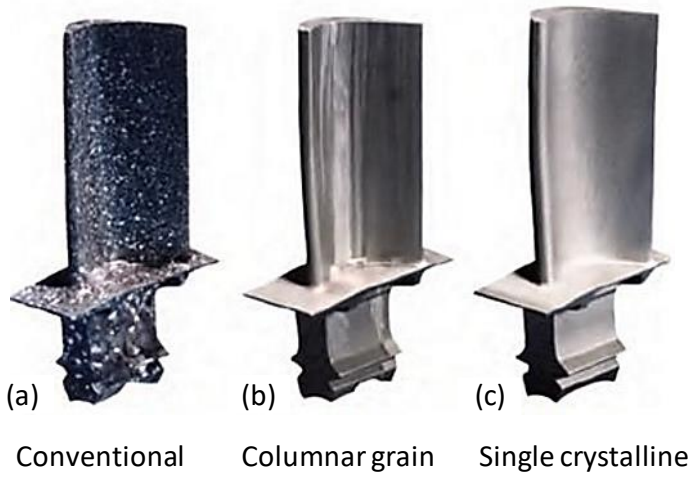

Figure 1.8 Turbine blades made of nickel base alloys with various grain structures [30].

The primary function of superalloys is to provide high strength and ductility at elevated temperatures. Alloy composition was rearranged over the years to increase this high temperature mechanical properties but resulted in degraded oxidation and hot corrosion resistance. Although increasing amount of Al and Cr promotes oxidation and hot corrosion behavior of these alloys, creep resistance significantly deteriorates above a certain level of Al and Cr. It is not possible to provide strength and creep resistance together with oxidation and hot corrosion resistance at the same time. Therefore, mechanical strength and creep resistance were maintained by keeping Al and Cr level in alloy composition low. Oxidation and hot corrosion resistance provided by a separate coating layer.

In this research, Inconel 738 LC widely used in rotor blades, was utilized as substrate material for aluminizing experiments. IN 738 LC consists of more than ten alloying elements and its composition is given in Table 1.2. In addition to IN 738 LC, IN 939 substrate material was used to study the effect of substrate composition on aluminide coatings. The composition of IN939 alloy is also given in Table 1.3.

Table 1.2 Composition of alloy IN738LC [31].

	Composition of IN738 LC, weight percent	
Element	Range	Nominal
Carbon	0.09-0.13	0.11
Cobalt	3.00-9.00	8.50
Chromium	15.70-16.30	16.00
Molybdenum	1.50-2.00	1.75
Tungsten	2.40-2.80	2.60
Tantalum	1.5-2.0	1.75
Niobium	0.60-1.10	0.90
Aluminum	3.20-3.70	3.40
Titanium	3.20-3.70	3.40
Aluminum + Titanium	6.50-7.20	6.80
Boron	0.007-.0.012	0.010
Zirconium	0.03-0.08	0.05
Iron	0.05 max	LAP †
Manganese	0.02 max	LAP
Silicon	0.30 max	LAP
Sulfur	0.015 max	LAP
Nickel	Balance	Balance (61)

† Low as possible

Table 1.3 Composition of alloy IN939 [32].

	Composition of IN939, weight percent
Element	Nominal
Carbon	0.15
Cobalt	19.00
Chromium	22.40
Tungsten	1.60
Tantalum	1.40
Niobium	1.00
Aluminum	1.90
Titanium	3.70
Boron	0.010
Zirconium	0.1
Iron	LAP †
Manganese	LAP
Silicon	LAP
Sulfur	LAP
Nickel	Balance

† Low as possible

1.2.3 High Temperature Coatings

Surface degradation by oxidation and hot corrosion reduces the load bearing capacity of nickel based superalloys used in turbine blades, eventually limiting their lifetime. Therefore, environmental protection of superalloys has to be provided by additional metallic coatings applied to surfaces. The idea of applying protective coatings on nickel based superalloys was first practiced in the 1960s and have been started to be used in gas turbine engines [4]. Protection mechanism of such coatings relies on stable oxide formation on coating surface that limits diffusion of oxygen and corrosive compounds through the substrate material. Hancock and Nicholls (1994) suggested several requirements for oxidation and corrosion resistant coatings described in Table 1.4.

Table 1.4 Desirable properties of oxidation and corrosion resistant coatings [33,34].

Coating Property	Requirements
Oxidation & Corrosion Resistance	• Thermodynamically stable oxide formation • Slow growth rate of protective surface scale • Adherent surface scale • High concentration of scale former
Stability	• No undesired phase changes within the coating • Low diffusion rate across interface at use temperature • Adequate compositional stability across interface • Minimized brittle phase formation
Adhesion	• Good adherence of coating to substrate • Matched coating/substrate properties to reduce thermal stress • Optimized surface conditions
Structural Properties	• Withstand all stresses including creep, fatigue and impact loading generated at component surface during service

Diffusion (aluminide) and overlay (MCrAlY) coatings are two main types of protective coatings that are employed against high temperature oxidation and corrosion [35]. Depending on turbine service conditions such as temperature range, thermal cycles, gas atmosphere and turbine blade geometry both coatings have several advantages and disadvantages in terms of coating stability, lifetime and application techniques. Table 1.5 shows a basic comparison of diffusion and overlay coatings.

Table 1.5 Advantages and disadvantages of coatings used for turbine engines [36].

Coating Type	Advantages	Disadvantages
Overlay Coatings	• Better corrosion resistance • Less interaction with substrate materials than diffusion coatings • More flexibility in coating compositions compared to diffusion coatings • Coated parts can be repaired/recoated easily than diffusion coatings	• Coating adherence not as good as diffusion coatings
Diffusion Coatings	• Numerous techniques can be used to deposit coatings • Excellent adhesion • Better surface properties such as roughness	• Significant interaction with substrate can eventually decrease mechanical properties of substrate

1.2.3.1 Overlay Coatings

The overlay coatings consist of Cr and Al within MCrAlX system, where M represents Ni, Co or Fe and X symbolizes reactive elements such as Si, Hf, Zr, Y, etc. For example, in NiCrAlX system β-NiAl phase forms in γ-Ni matrix of overlay coating which contains Cr as solid solution. By controlling the initial composition of NiCrAlX system, resultant phases and their ratios can be determined. Consequently, the formation of undesirable phases such as α-Cr and γ`-Ni_3Al can be prevented.

Overlay coatings commonly applied by physical vapor deposition (PVD) or plasma spray. Formation of overlay coatings does not require any interaction with the substrate material. Interdiffusion of the overlay coating and the substrate elements occurs only when coating and substrate are exposed to heat during heat treatment or high temperature service conditions. Subsequent interdiffusion occurs at limited depth from the surface. On the other hand, diffusion coatings are applied at high process temperatures, and it allows the interdiffusion of the coating and the substrate elements during the formation of coating. Therefore, surface adherence of overlay coatings is weaker compared to diffusion coatings.

1.2.3.2 Diffusion Coatings

Diffusion coatings are formed by enrichment of substrate surface with Al, Si or Cr elements which are stable oxide formers. By exposing the substrate surfaces to these elements, intermetallic phases form at substrate surface depending on their compositions. Since diffusion coatings are formed by solid state diffusion of deposited elements with substrate elements, excellent coating/substrate adhesion is obtained. Aluminide coating is the most favored diffusion coating type compared to siliconized and chromized coatings which are not suitable for operating temperatures above ~950 °C due to the formation of volatile oxides. Therefore, aluminide coatings are widely preferred for the protection of turbine blades as oxide species of aluminum is durable even if elevated service temperatures.

1.2.3.2.1 Aluminide Coatings

The main function of aluminide coating is to protect superalloy by forming a thin and dense layer of aluminum oxide (Al_2O_3) at coating surface when exposed to high temperatures. Such oxides are called as thermally grown oxide (TGO). Figure 1.9 shows an illustration of typical aluminide coating system.

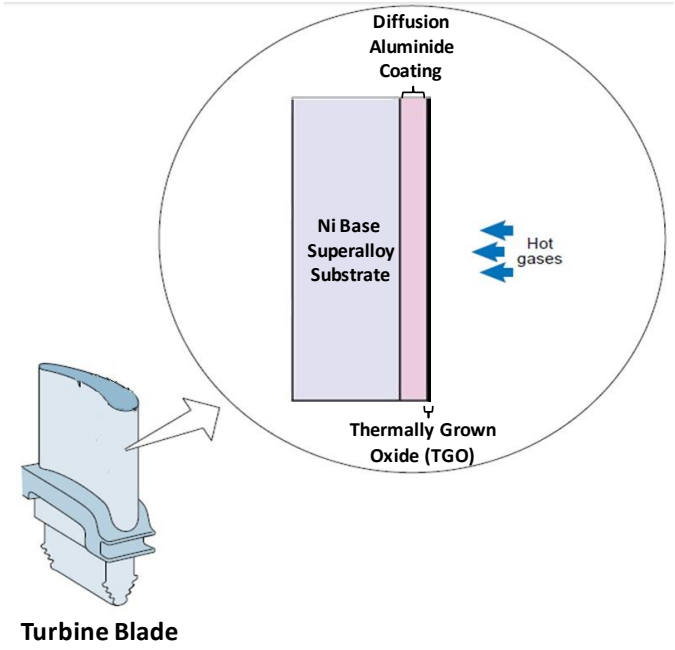

Figure 1.9 A typical aluminide coating system of nickel base superalloys [37].

Alumina is one of the most stable oxide at high temperatures (Fig. 1.10) and protects the superalloy from oxidation and corrosion by preventing oxygen diffusion through the substrate. α - Al_2O_3 is the most stable and dense oxide phase than other meta stable Al_2O_3 phases. Aluminide coating acts as an aluminum reservoir for the formation of Al_2O_3. When Al composition of aluminide coating drops to a critical level by oxide formation or inward diffusion of Al through the substrate, less protective oxides start to form, thereby shortening the component life. Depending on the substrate material, less protective oxides such as NiO, CoO, TiO_2, etc. could form at surface together with Al_2O_3.

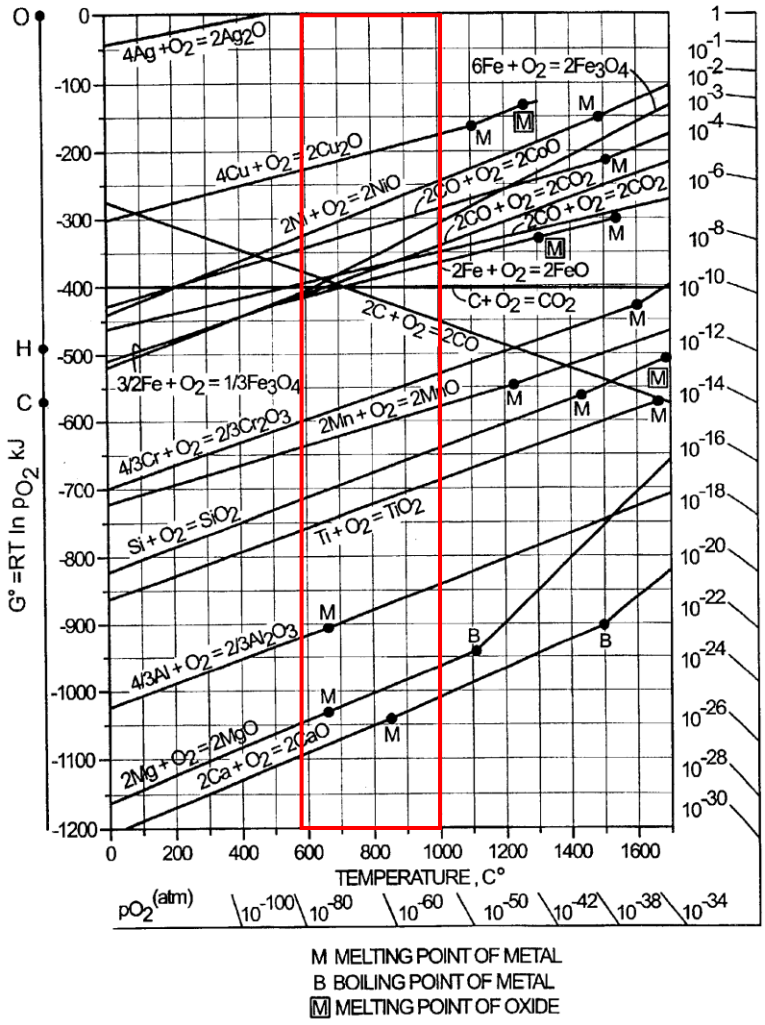

Figure 1.10 Ellingham diagram of free energy of formation of oxides as a function of temperature, red frame shows service temperature range of industrial gas turbine blades [38].

Aluminide coatings can be applied by several coating methods. Regardless of the coating method, process is called “aluminizing”. Aluminizing of high temperature alloys was first applied in 1911 by Van Aller [39] followed by Allison and Hawkins [40] in 1914, all from General Electric Research Laboratory. The process was originally developed for aluminizing of Fe wires or ribbons as heating elements and Cu tubes for steam turbines. Then, aluminized steels were used for combustion chambers in 1942 by Anselm Franz from Germany [41]. However, application and development of aluminide coatings were not documented well until it started to be

used for turbine blade (cobalt base superalloy) protection in 1957 [42]. Aluminide coating was first used for nickel based superalloys in 1963 by Pratt and Whitney [43].

Aluminizing of nickel based superalloys for turbine blades relies on surface enrichment with aluminum which forms binary Ni – Al phases. β-NiAl is the most preferred phase for protective aluminide coatings rather than Ni_3Al or Ni_2Al_3 phases shown in shaded region of Figure 1.11. High Al content of β-NiAl phase supplies aluminum to surface for the formation of Al_2O_3. Other NiAl phases are not preferred because low Al content of Ni_3Al causes unstable oxide formation and, Ni_2Al_3 phase has brittle behavior [44]. β-NiAl as the main phase of aluminide coating provides enhanced oxidation and corrosion resistance, hence prolong the service life of superalloy [45].

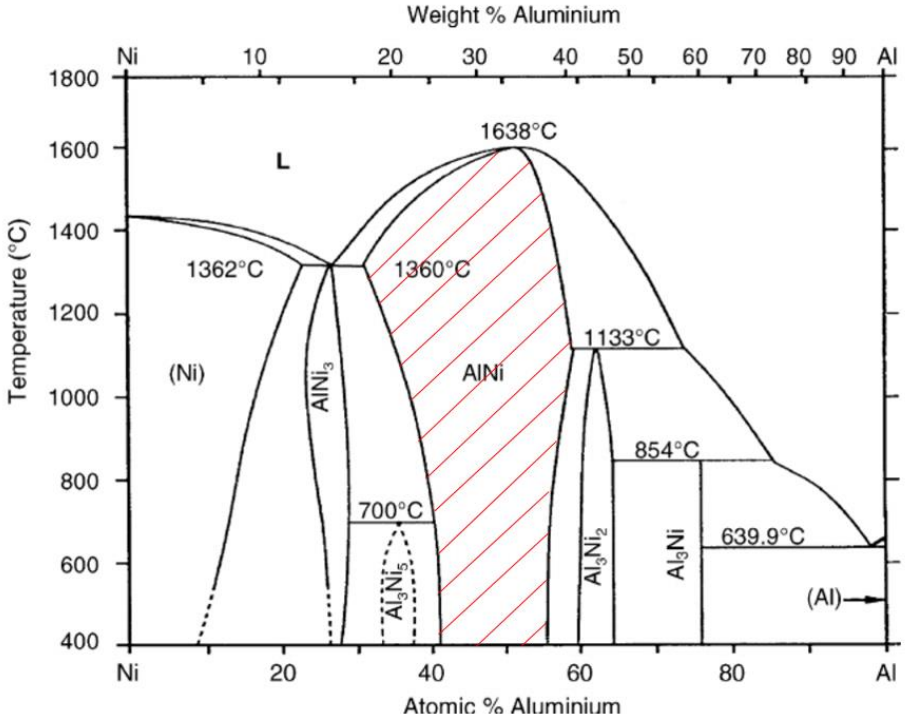

Figure 1.11 Binary phase diagram of Ni – Al system [46].

Field of β-NiAl phase in binary Ni – Al system has wide composition range, thereby β phase forms in a wide range of Al composition (40 – 55 at. % at 400 °C). Aluminide coatings have typically Al composition lower than 45 at. % in hypo-stoichiometric composition. If aluminum content is higher, bluish tint β phase forms and called as "blue beta".

Aluminide coatings generally have a two-layer structure which consists of the outer coating layer (β-NiAl) and interdiffusion zone (IDZ) as shown in Figure 1.12. Between outer β-NiAl layer and substrate, IDZ forms by gradually adjusting the concentration difference of the aluminide coating and substrate elements by diffusion. While these species are diffusing, substrate elements such as Cr, Ni, Ti, Nb, etc. precipitate along this zone due to their low solubility in various region of aluminide coating.

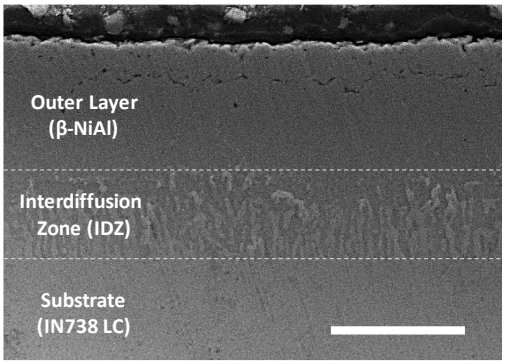

Figure 1.12 Typical microstructure of two-zone aluminide coating applied on IN 738 LC superalloy substrate. (The scale bar = 50 µm)

1.2.4 Aluminide Coating Production Methods

There are several thermochemical coating methods to apply aluminide coatings on nickel based superalloys such as pack process, above the pack process or chemical vapor deposition (CVD) [47]. Figure 1.13 shows different coating processes for ceramic and metallic materials including aluminide coatings.

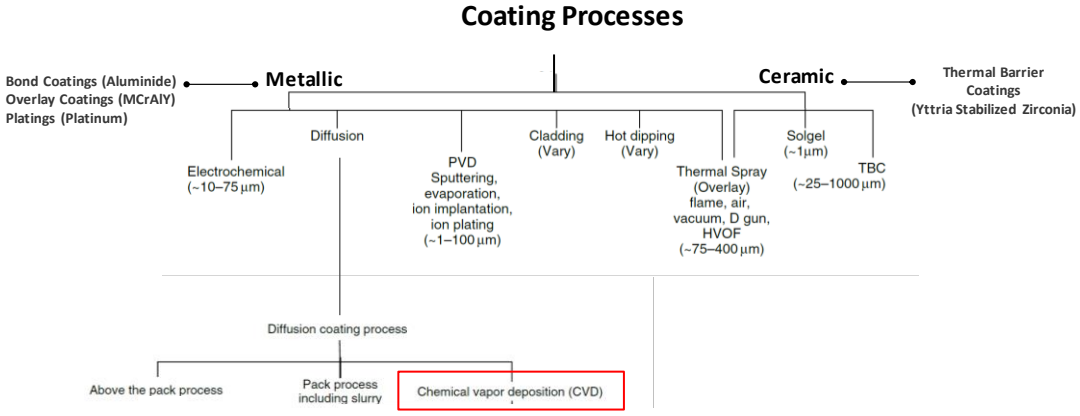

Figure 1.13 Types of different coating processes for turbine components [1], red frame shows coating method used in this study.

The basic principle of all three diffusion coating processes relies on the generation of aluminum containing halide vapors to deposit aluminum on the substrate surface. Main difference is the way of halide vapor generation and transportation of halides to surface. In pack and above the pack processes, halide vapors are formed in heated coating reactor by using powder mixture. Powder mixture is in contact with component in the pack process [48]. On the other hand, component is placed above the powder in above the pack process and halide vapors are transferred to surface of component [49]. In the CVD method, halide vapors are externally generated in a heated chamber and transferred to heated coating reactor by using Ar or H_2 as a carrier gas [50].

Each aluminide coating processes have some advantages and disadvantages in terms of coating quality, setup, operating costs, etc. which is shown in Table 1.6.

Table 1.6 Advantages and disadvantages of different aluminizing processes.

Coating Type	Advantages	Disadvantages
Pack Process	• Relatively inexpensive process • simple process • relatively higher deposition rates	• Difficult to coat internal cooling channels • Homogeneity and purity cannot be obtained easily • Difficult for Co-deposition of reactive or alloying elements
Above the pack process	• Relatively inexpensive process • Relatively simple process	• Difficult for Co-deposition of reactive or alloying elements
Chemical Vapor Deposition (CVD)	• Has an ability to coat parts with complex geometries • Internal cooling channels can be coated without any blockage • Homogeneous and high purity coatings are obtained	• Expensive process • Low pressures required • Difficult to optimize process parameters • Low deposition rates

1.2.4.1 Pack Process and Above the Pack Process

Pack process which is defined as in-situ CVD process has been used for the production of oxidation and corrosion resistant coatings for over 75 years [40]. In the pack process, also called as pack cementation, components are buried into a powder mixture which mostly consists of source material (Al or Al alloys for aluminide coating), activator (NH_4Cl, NaF, NaCl, etc.) and inert constituent like alumina powder. Activator reacts with aluminum and forms halide vapors. Alumina powder is used to avoid sintering of pack powder at high process temperatures. Figure 1.14 shows a schematic illustration for pack and above the pack processes. For the aluminizing by pack process, component embedded into powder mixture are placed in a retort and heated to elevated temperatures (e.g. 700 – 1100 °C) depending on process conditions. Source material (Al or Al alloys) reacts with activator and forms aluminum halide vapors. By the reduction reactions of aluminum halides, Al is deposited on the component surface, and nickel aluminide phases are formed by solid state diffusion of Al and Ni. The advantages of the pack cementation are the reproducibility of coating, low production costs, and simplicity of the process. However, entrapment of pack powder particles in the coating zone decreases coating life by preventing the formation of continuous alumina formation on the surface. Also, coating the components which have complex geometry and internal cooling channels is difficult in pack process because the component is in contact with powder mixture. To prevent detrimental effect of pack process, above the pack (also named “out of pack”) process was developed by physically separating the component from the powder mixture. In this way, aluminum halide vapors can reach to not only external but also internal surfaces of components. The advantage of out of pack process is the ability to obtain uniform coating at internal cooling channels of turbine blades. Also, cleaner coatings can be obtained by preventing entrapment of powder particles in the coating zone [51]. Nevertheless, controlling the process parameter is still limited in above the pack method compared to chemical vapor deposition (CVD) method.

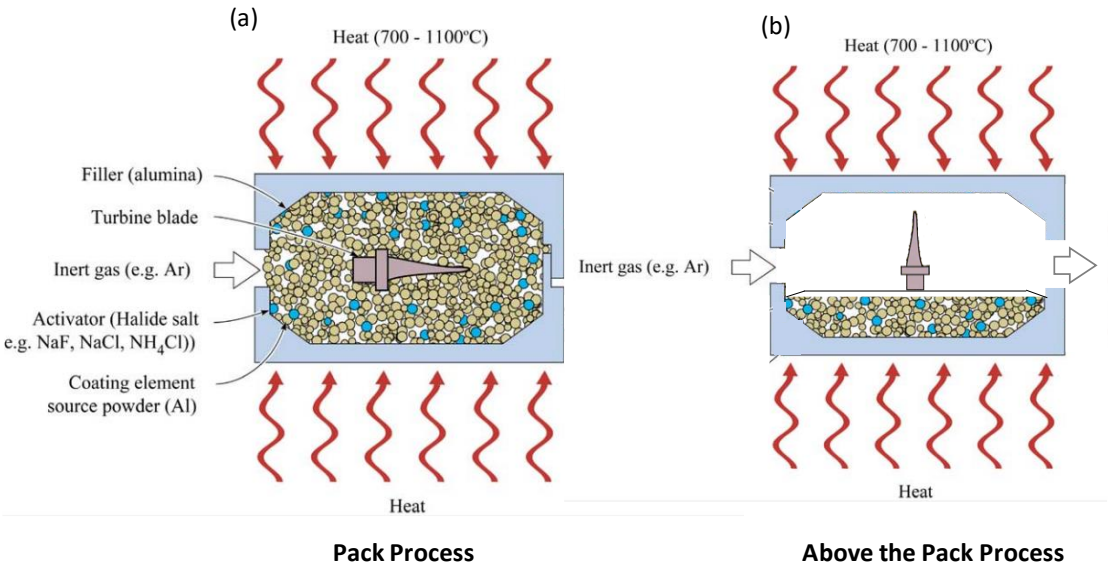

Figure 1.14 A schematic illustration of the (a) pack cementation process [52], (b) above the pack process.

1.2.4.2 Chemical Vapor Deposition (CVD)

Chemical vapor deposition (CVD) is the most advanced technique used for aluminizing of nickel based superalloy components. CVD aluminizing is recently developed while pack processes are used industrially since the 1970s. Figure 1.15 shows a schematic illustration of the CVD aluminizing system. In the CVD process, halide vapors of aluminum are generated at external generator rather than coating reactor. Mostly chloride (Cl_2) or hydrogen chloride (HCl) gas is used as activator and $AlCl_3$ is formed by passing Cl or HCl gas over aluminum pellets at external generator between 300 - 400 °C. Aluminum chloride vapors are transferred to coating furnace by using an inert gas (H_2 or Ar) as a carrier. Also, additional Al source can be placed into coating chamber to increase the activity of aluminum and partial pressures of aluminum sub-chloride gases. The components to be coated are also placed in a coating furnace at the temperature range of 950 – 1100 °C. By the reduction reactions of aluminum sub-chloride gases ($AlCl_2$ and AlCl) on nickel based substrate surface, β-NiAl phase forms [50]. CVD aluminizing was patented by Howmet company in 2001 and used in industrial turbine blade coatings [53].

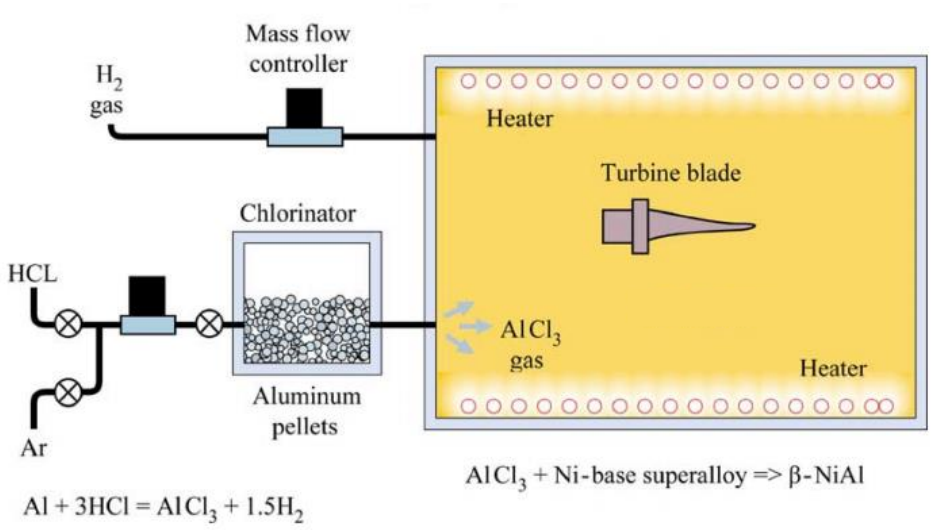

Figure 1.15 A schematic illustration of the CVD aluminizing process.

The main advantages of CVD system over pack and above the pack process is its ability to control process variables, thereby growth rate and coating microstructure. Uniformly distributed clean coatings could be easily obtained for components with complex geometries and internal cooling channels. Also, simultaneous deposition of reactive or alloying elements with aluminum is possible by CVD and the composition of those co-deposited elements can be controlled.

The major process variables of CVD system are furnace temperature, chlorinator temperature, pressure, gas flows and ratios, aluminum activity and process time. However, it is complex to optimize all these parameters to obtain aluminide coating with high growth rates. Figure 1.16 illustrates the relation between CVD parameters and aluminide coating formation.

The growth of aluminide coating is mainly controlled by the combination of aluminum deposition rate on the surface and solid state diffusion rate [54] as shown in Figure 1.16. Temperature, pressure, gas flow rates and ratios, chlorinator temperature and aluminum activity affect the partial pressures of aluminum chloride gases and control the surface reactions and aluminum deposition rate.

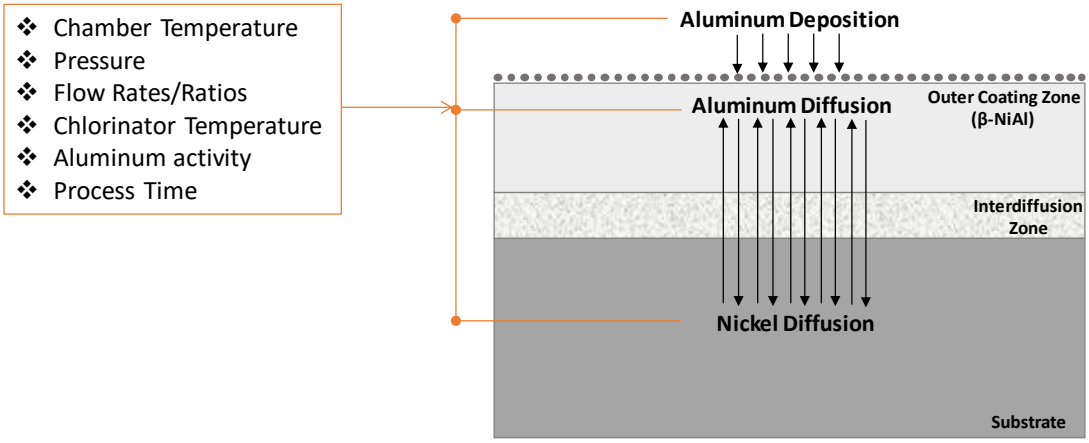

Figure 1.16 The effect of CVD process parameters on the formation of aluminide coatings.

Solid state diffusion rate can be defined by following diffusion based relation [1].

$$x^2 \approx Dt \qquad (1)$$

where x is the thickness of the coating, D is diffusion coefficient of relevant element, and t is aluminizing duration. The coating thickness increases as a square root of process time and follows parabolic rate law. The diffusion coefficients are strongly affected by temperature and the composition of substrate alloy. Therefore, the growth rate can be increased by increasing process temperature. However, phases formed at IDZ can melt at high process temperature (above 1100 °C) and degrade the strength of the coating.

In this study, our criteria are to maximize;

1- β-NiAl growth rate
2- Outer layer (β-NiAl) / IDZ thickness ratio

at the same time by satisfying required coating properties (preventing formation of undesirable NiAl phases "Ni_2Al_3, Ni_3Al, etc." and obtaining homogeneous thickness along the coating layer).

The CVD process variables affect not only the aluminum deposition rate on the substrate surface but also the diffusion coefficients of Al and Ni at the surface. Therefore, the optimization of CVD parameters is a significant challenge to obtain

uniform coating with high coating growth rate and the outer layer/IDZ ratio while preventing the formation of undesirable NiAl phases.

Formation of aluminide coating involves three main steps which are gas phase diffusion, surface reaction and solid state diffusion for the pack processes [55]. Seigle et al. (1978) assumed that aluminide coating growth by pack processes is controlled by gaseous diffusion and solid state diffusion due to surface reactions are rapid [56]. However, the formation of aluminide coating in CVD is mainly controlled by surface reaction and solid state diffusion assuming gas phase diffusion is rapid. The formation mechanism of aluminide coatings on nickel substrates was first examined by Goward and Boone (1971) [57] and following research is published by Pichoir (1978) [58]. They asserted that NiAl stoichiometry in aluminide coatings controls diffusion coefficient of Ni (D_{Ni}) and Al (D_{Al}), hence coating formation mechanism. In nickel rich NiAl (Al $\leq$ 50 at. %), D_{Ni}/D_{Al} ratio is almost 3.0. However, in Al rich NiAl (Al = 51.5 at. %), the diffusion rate of Al greatly increases and D_{Ni}/D_{Al} ratio decreases below to 0.3. Therefore, aluminum activity which has a critical role in diffusion rates of species controls aluminide coating formation together with coating temperature. Depending on the aluminum activity, the coating process is described as low activity or high activity.

Low Activity Process:

In low activity process, aluminide coatings are formed by outward diffusion of Ni from the substrate through the aluminide surface where coating being developed. At surface following reaction takes place:

$$3AlX_{(g)} + 2Ni_{(s)} \rightarrow 2NiAl_{(s)} + AlX_{3(g)}$$

Outwardly diffused Ni combines with Al and forms β-NiAl phase which has very low solubility for many alloying elements of nickel based superalloys. Thus, alloying elements of the substrate, mostly Cr, precipitate at the NiAl/substrate interface which called as interdiffusion zone (IDZ). Low activity coatings have the two-layer structure: external β-NiAl and IDZ. Low activity coatings are usually applied at high deposition temperatures in the range of 1000 – 1100 °C.

High Activity Process:

In high activity process, aluminide coatings are formed by inward diffusion of Al from the growing coating surface to substrate. Different from low activity process; coating forms through the substrate and original substrate surface becomes external surface of the coating, since inward Al diffusion is greater than outward Ni diffusion. Also, high activity coatings are usually applied at temperatures below 1000 °C. At substrate surface following reaction takes place:

$$9AlX_{(g)} + 4Ni_{(s)} \rightarrow 2Ni_2Al_{3(s)} + 3AlX_{3(g)}$$

Depending on Al activity, only Ni_2Al_3 phase or a combination of Ni_2Al_3 and β-NiAl can be obtained in coating zone.

- Very high activity of Al causes δ-Ni_2Al_3 phase formation.
- High activity of Al results in outer δ-Ni_2Al_3 and inner β-NiAl formation.
- Moderate activity of Al forms hyper-stoichiometric β-NiAl phase.

Figure 1.17 shows microstructures of low and high activity aluminide coatings with Al and Ni diffusivity change by the composition of Al.

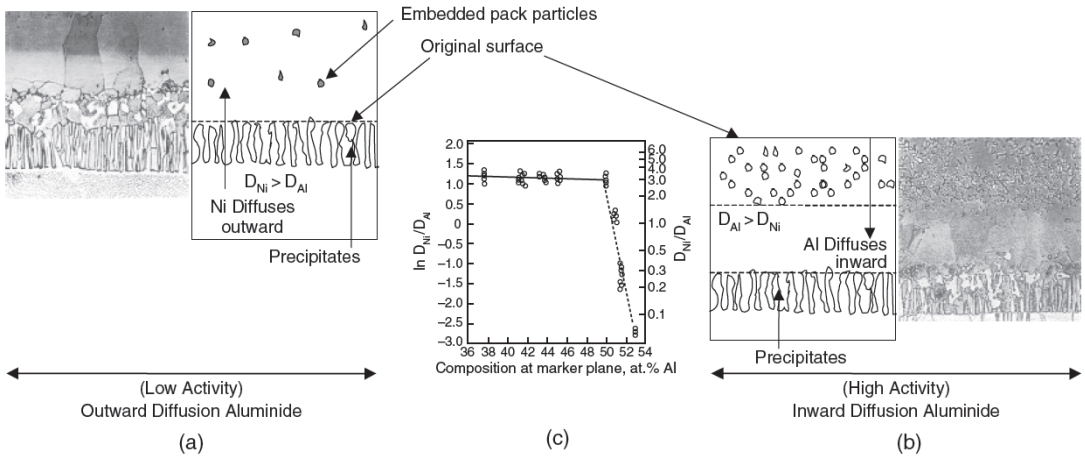

Figure 1.17 Microstructure of (a) low- and (b) high-activity aluminide coatings [59], (c) dependence of Ni and Al diffusivities as a function of NiAl composition [60]

Coatings include δ-Ni_2Al_3 phase require post-heat treatment process to transform brittle δ-Ni_2Al_3 phase to β-NiAl phase. The heat treatment process is generally applied for several hours close to 1100 °C [61]. Inward diffusion of Al and outward diffusion of Ni takes place during post heat treatment. Hence aluminum content of δ-Ni_2Al_3 phase decreases until it totally transferred to (Al rich) β-NiAl phase [42]. Both low activity and high activity coatings have β-NiAl as main coating phase, but β-NiAl is obtained in two steps (coating + heat treatment) by high activity process.

1.2.4.2.1 Reactive or Alloying Elements Addition to Aluminide Coatings

The addition of reactive (RE) or alloying elements increases the oxidation and hot corrosion resistance of aluminide coatings mostly by improving scale adhesion and decreasing the growth rate of alumina scale; therefore, prevents spallation of continuous alumina layer above the coating [62]. Although both REs and alloying elements have beneficial effects on aluminide coating lifetime, their roles in preventing coating failure are different.

Role of Reactive Elements:

The addition of reactive elements to aluminide coatings prolongs the service life of components at high service temperature. Elements such as Zr, Y, Hf, Si, La, Ce, etc. are known as oxygen reactive elements because they form more stable oxides than alloying elements of many alloys. A small concentration of REs on aluminide coatings increases adherence of protective scale to coating surface [63]. There are several explanations related to the mechanism of reactive element effect [1].

- Reactive elements form oxide pegs at oxide/coating interface and mechanically increase the adherence of oxide layer to the coating surface.
- Reactive elements suppress void formation at oxide/coating interface.
- Reactive elements prevent sulfur segregation to interfaces and boundaries; thereby increases the bonding strength of oxide to the coating surface.
- Reactive elements reduce residual stress of oxide layer by altering the growth mechanism of alumina from the combination of outward diffusion of Al and inward diffusion of oxygen to particularly inward diffusion of oxygen.

Effect of different reactive elements on aluminide coating is not the same. Therefore, each element may play a different role and affect oxidation and corrosion resistance of coating at a different level. Hafnium, yttrium, and zirconium are the most promising REs which improve aluminide coating lifetime.

Although the addition of REs to aluminide coating is promising, it is difficult to incorporate REs homogeneously to aluminide coating at ppm levels. Also, their solubility in β-NiAl phase is limited; therefore, their content in coating have to be controlled precisely.

Role of Alloying Elements:

The addition of alloying elements such as Cr, Co, Pt, etc. have a beneficial effect on aluminide coating service life. Although the influence of alloying elements is similar with REs, predominant mechanisms are different. Pt is the most promising alloying element which significantly increases oxide adherence and reduces Al depletion under service conditions; however, it is far more expensive than Cr and Co.

Under oxidizing environment, metastable Al_2O_3 phases rapidly form compared to more protective α-Al_2O_3. However, the addition of Cr promotes the formation of more stable, slower growing α-Al_2O_3 scale [64]. This mechanism is explained as transient Cr_2O_3 is isostructural with α-Al_2O_3 and it provides nucleation sites for α-Al_2O_3. Hence, fine grain α-Al_2O_3 grows faster with the presence of Cr than α-Al_2O_3 formed on binary β-NiAl phase [65]. Nevertheless, if the amount of Cr exceeds solubility level in β-NiAl (~10 at. % depending on phase composition), it precipitates as α-Cr which decrease beneficial effect of Cr on hot corrosion behavior [66]. Similar with Cr, it is reported that presence of Co in aluminide coating promotes the formation of Al_2O_3 at lower Al concentrations [67].

1.2.5 Failure Mechanisms

Mechanical and thermal stresses on turbine blades cause several types of failures such as creep, fatigue, oxidation, and corrosion. Nickel based superalloys provide excellent creep and fatigue resistance to turbine blades under extreme operating conditions. Additionally, to enhance the high temperature oxidation resistance of these alloys, aluminide coatings are widely applied to turbine blade surfaces. The formation of stable, dense and continuous alumina scale on aluminide coating surfaces improves oxidation resistance of superalloys. Therefore, the durability of coating/substrate system is mainly limited by hot corrosion. The mechanisms governing hot corrosion is given below.

1.2.5.1 Hot Corrosion

When metals or alloys are exposed to oxygen containing gasses at elevated temperatures, oxygen reacts with metals and forms their oxides. This phenomenon is called as oxidation. As a result of oxidation, adherent protective oxides can form at metal/alloy surfaces which prevent further oxidation. However, industrial gas turbine blades are not only exposed to oxygen but also other gasses like CO_2, SO_2, SO_3 and corrosive compounds like chlorides (NaCl), and sulfates (Na_2SO_4). When fuel oil is used, blades are also exposed to oxides such as V_2O_5. Exposure to such corrosive environment at elevated service temperatures causes hot corrosion of substrate/coating system [68]. Figure 1.18 shows an example of corroded turbine blade used in the industrial gas turbine.

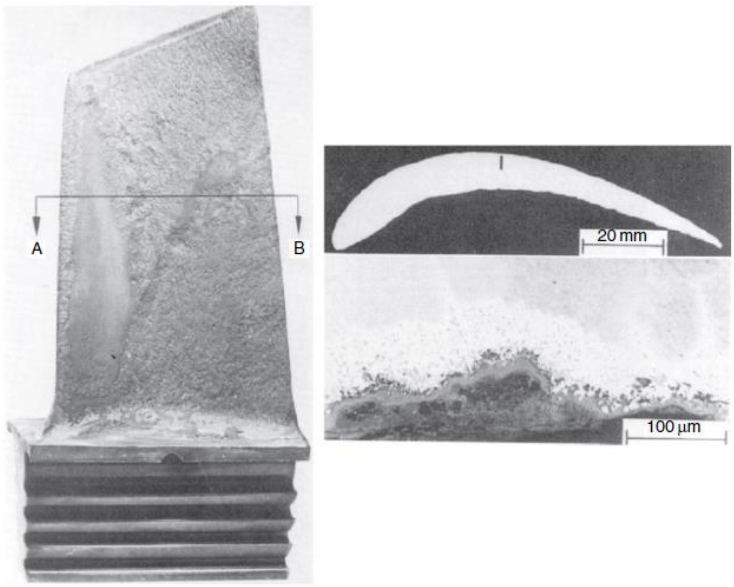

Figure 1.18 Turbine blade of Ni base superalloy after 27,293 hours service at 750 °C in a natural gas burning industrial gas turbine engine [69].

The term of "hot corrosion" can be defined as accelerated oxidation and corrosion occurred when corrosive molten constituents deposited at substrate surface at temperatures between 700 – 925 °C. Hot corrosion is mostly divided into two as Type I (high temperature hot corrosion) and Type II (low temperature hot corrosion) depending on temperature, alloy composition, corroding constituents, flux rate, etc.

1.2.5.2 Type I Hot Corrosion

Type I hot corrosion, also called as HTHC, is mainly observed at the temperature range of 850 – 950 °C [70]. By the condensation of fused alkali salts on the substrate surface, protective oxide scales start to degrade as a result of subsequent chemical reactions. Depletion of protective oxide formers such as Al or Cr from the substrate or coating surfaces causes oxidation of base material elements which causes the formation of non-protective oxides. Most influential salt of Type I hot corrosion is Na_2SO_4 which has high thermodynamic stability at high temperatures. Na_2SO_4 can be present in fuel as well as can be formed during the combustion by sodium and sulfur. Another corrosive contaminant is vanadium which also can be present in certain fuels. The presence of vanadium causes accelerated hot corrosion of components. Also, very corrosive phases

of vanadium can form at relatively low temperatures (~535 °C) [71]. A mixture of Na_2SO_4 and V containing phases considerably increases the solubility of protective oxides and decreases the lifetime of coating/substrate system [72].

1.2.5.3 Type II Hot Corrosion

Type II hot corrosion, also called as LTHC, is mainly observed at the temperature range of 650 – 800 °C which is below the melting point of Na_2SO_4 [73]. To LTHC reactions occur, SO_3 is required in the gas phase with high partial pressure, while HTHC is observed in air or pure oxygen atmosphere [70]. Type II hot corrosion mainly occurs with local corrosion attacks and results in local scale failures.

Depending on the service condition of gas turbines, turbine blades can be exposed to Type I or Type II hot corrosion. In this thesis, hot corrosion test of aluminide coatings was performed at 900 °C (Type I) in the presence of Na_2SO_4 and V_2O_5.

1.3 Thesis Overview

The main objective of this study is to develop and apply aluminide coatings to turbine blades with CVD to improve their lifetime.

Chapter 2 covers optimization of CVD aluminizing process to obtain high coating growth rate and high outer layer/IDZ ratio. The effect of CVD variables as chamber temperature, pressure, chlorinator temperature, aluminum activity, gas flow rates and ratios on simple aluminide coatings were presented in details. Additionally, the influence of sample thickness on the growth of aluminide coating and surface roughness on coating microstructure were studied to optimize aluminizing process and final microstructure. Also, the effect of different substrates on aluminide coating was compared by simultaneous aluminizing of IN 738 LC and IN 939 materials.

Chapter 3 involves the addition of reactive (REs) or alloying elements to aluminide coatings by CVD. Process details and chemical analysis by WDS are presented for Cr, Co, Y and Zr co-deposited aluminide coatings.

Chapter 4 includes comparative analysis for hot corrosion behavior of aluminide coatings with the addition of ternary elements. Hot corrosion test was performed for simple, Cr, Zr, Hf, Y and Cr/Y modified aluminide coatings. After hot corrosion test, weight gain and weight change measurements of simple, Cr, Zr, Hf, Y and Cr/Y modified aluminide coatings are presented along with microstructure and phase analysis.

Chapter 5 covers the future recommendations for the production and development of aluminide coatings.

CHAPTER 2

SIMPLE ALUMINIDE COATING OPTIMIZATION BY CVD

2.1 Introduction

In this chapter, optimization of simple aluminide coating process by CVD was studied to maximize 1) Growth rate, and 2) Outer layer/IDZ ratio of aluminide coating at the same time. Main variables of CVD aluminizing system that affect growth rate and coating properties are chamber temperature, system pressure, gas flow rates and ratios, chlorinator temperature, aluminum activity and process time. The effect of each variable on aluminide coating was studied to obtain optimum process parameters, and then the range of parameters was defined to obtain expected coating properties and high growth rate. Moreover, the effect of surface roughness on aluminide coating homogeneity in terms of thickness and composition were investigated to optimize surface preparation processes. The effect of substrate thickness was also studied because aluminizing process is controlled not only by aluminum deposition but also by solid state diffusion, In addition, the effect of substrate composition on aluminide coating formation and final microstructure were investigated by coating IN 738 LC and IN 939 substrates simultaneously.

2.2 Experimental Details

2.2.1 Substrate and Sample Preparation

Inconel 738 LC Superalloy was used as a substrate material for the development of simple aluminide coating by CVD. The chemical composition of alloy IN 738 LC is given in Table 1.2. Also to study the effect of substrate material on aluminide coating, IN 939 substrate material is used and its composition is shown in Table 1.3.

Turbine blades were inductively melted in a vacuum chamber and cast by investment casting method in Tübitak Marmara Research Center and Gür Metal. After casting of turbine blades, hot isostatic pressing (HIP) was applied (1200 °C, 150 MPa, 10 hours) to decrease porosity amount of cast turbine blades. To remove any residual oxides formed during HIP, sand blasting was applied to the surface of turbine blades. After sand blasting, turbine blades were cut by electrical discharge machining (EDM) in 20 x 20 mm dimensions to obtain IN738 LC pieces as shown in Figure 2.1. All pieces were categorized with regard to their original position on the turbine blade. Prior to CVD process, all the substrates were labeled to track process date, substrate location on turbine blade, material type and history of material such as applied heat treatments and hot isostatic pressing.

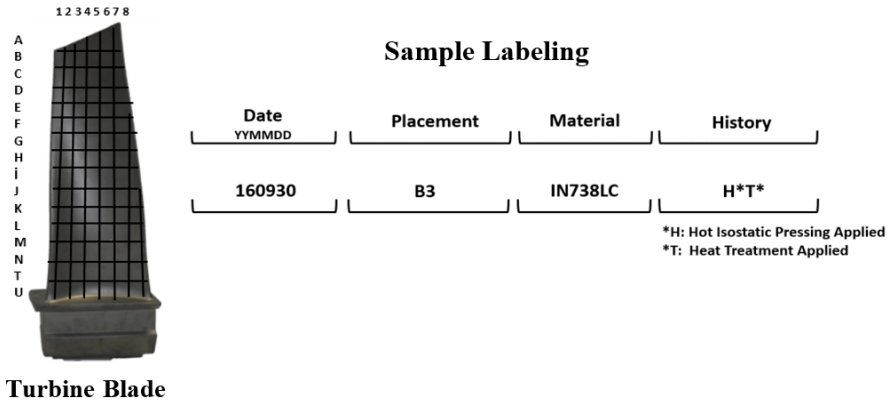

Figure 2.1 Sample preparation by cutting of rotor turbine blade and sample labeling procedure.

Due to the complex geometry of turbine blade, all pieces had different thickness. Therefore, all turbine blade pieces were sliced by abrasive cutter in 5 mm thickness to obtain samples in 20 x 20 x 5 mm dimensions.

Prior to aluminizing, all samples were heat treated in Heat Treatment Furnace (VAKSİS). Table 2.1 shows heat treatment process parameters.

Table 2.1 Heat Treatment Process Parameters.

Heat Treatment Type	Temperature	Pressure	Cooling Rate	Process Time
Solutionizing	1120 °C	10^{-5} Torr	140˚C/min	2 hour

Samples were ground by 120, 220, 400 grit size SiC emery paper to obtain clean and oxide-free coating surface. After grinding, the surface roughness of samples in terms of Ra (arithmetic average) and Rz (mean roughness depth) was measured by Mahr M300 Linear Profilometer with 5.6 mm profile length (L_t). In each surface, five measurements were taken in different directions as shown in Figure 2.2. After that, average surface roughness values were calculated. For all samples, lower than 0.14 µm Ra value and lower than 1.2 µm Rz value were aimed.

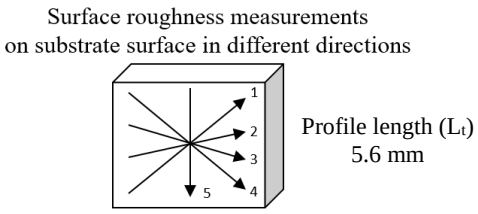

Figure 2.2 Illustration of surface roughness measurement on substrate surface in different directions.

To clean the surface of samples prior to aluminizing, all samples were cleaned by acetone (99.5%) and isopropyl alcohol (99.8%) in an ultrasonic cleaner for 10 minutes, separately. After that, washed under isopropyl alcohol (99.8%), deionized water for 30 seconds and dried by nitrogen gas.

2.2.2 Aluminide Coating Process

Aluminizing processes were performed by Laboratory Design Hot Wall Chemical Vapor Deposition System (Archer Technicoat). CVD System consists of seven main units which are electrical cabinet, gas cabinet, chlorination unit, coating chamber, chiller, scrubber unit and HCl Cabinet. Process control system is based on an Omron PLC for all digital, control, and analog functions. PLC unit is controlled by the user interface on desktop PC. Diagram of CVD System is given in Figure 2.3.

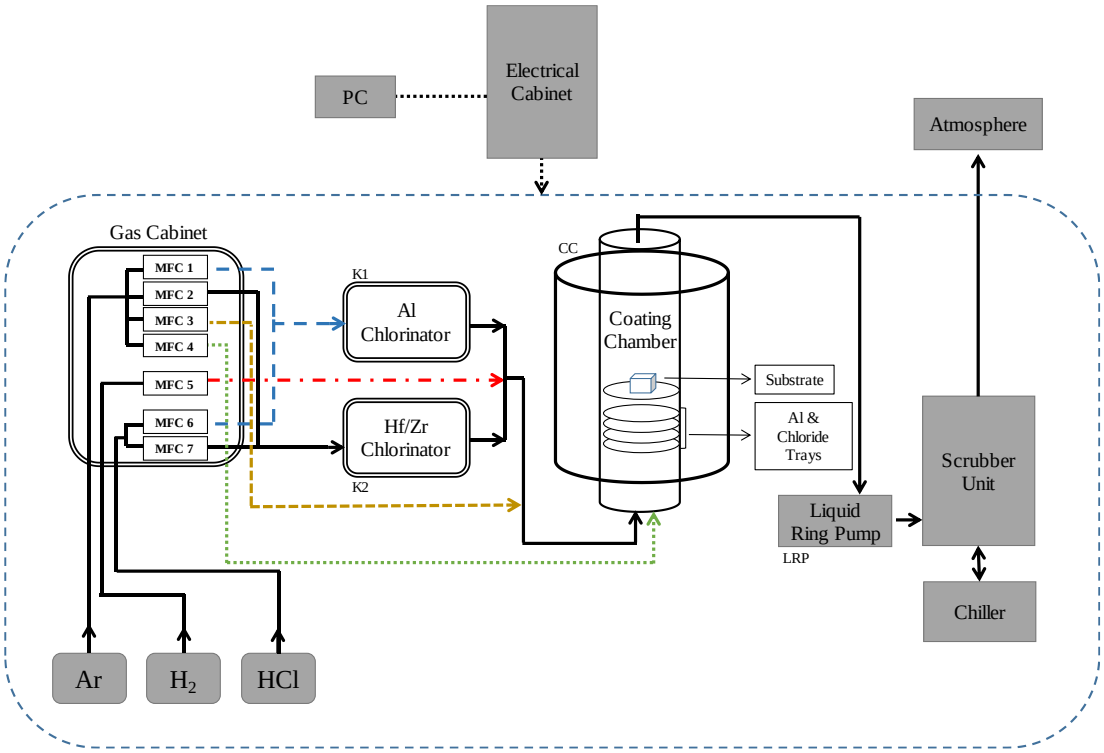

Figure 2.3 Diagram of CVD System including main units and gas piping.

Aluminum chlorinator was filled with 2 kg of pure aluminum pellets (99.99 %) for the aluminizing process. External chlorinator was not used in simple aluminide coating processes. Four internal trays were designed and placed into the coating chamber to increase the activity of aluminum in the gas phase. Three of internal trays were filled with 100 g of pure aluminum pellets (99.99 %), 70 g of Aluminum-Chromium (50/50 wt., 99.9 %), 70 g of Aluminum-Chromium (70/30 wt., 99.9 %) or left empty depending on the aluminizing process. High purity HCl gas (99.999 %) was used to form aluminum chlorides at chlorinator unit. Argon (99.999 %) was used to dilute HCl gas and to transfer aluminum chlorides to coating chamber as a carrier gas. Hydrogen (99.9995 %) gas was added to gas mixture comes from chlorinator to promote coating growth rate.

To place the samples and internal trays, graphite liners were used inside the ceramic tube coating chamber. Internal trays and coating tray were settled into 200 mm uniform coating zone coinciding with center of the ceramic tube. The samples to be coated were placed into the coating tray which was the 50 mm tray of the 200 mm tray stack.

Gas pipe line between chlorinator unit and coating chamber was heated to 300 °C to prevent any blockage due to sudden sublimation of $AlCl_x$ gases. Similarly, exhaust pipe line through scrubber system was heated to 200 °C to avoid sublimation of excess process gases. A water cooled trap was used to collect $AlCl_x$ waste before it was transferred to scrubber tank filled with sodium hydroxide alkaline solution. After neutralization, harmless exhaust gases were released to the atmosphere.

Coating processes were performed in three steps as heating, aluminizing and cooling. The heating rate of coating chamber was set to maximum 5 °C/min up to 1000 °C (using 82.5 % power output) and decreased to 3 °C/min for any temperatures above 1000 °C. Similarly, while cooling, 3 °C/min cooling rate was set for process temperatures above 1000 °C to prevent any possible thermal damage to the ceramic tube. Below 1000 °C, heaters were turned off, and samples were cooled naturally to room temperature in the coating chamber. During heating segment, the system was continuously purged with argon gas at 2000 sccm. During cooling segment, the system was purged with argon gas at 2000 sccm until chamber temperature dropped to 900 °C. When chamber temperature reached to 900 °C, the system pressurized with argon to atmospheric pressure.

2.2.3 Coating Characterization

2.2.3.1 Metallographic Sample Preparation

Prior to SEM analysis, all coated samples were sectioned by Buehler IsoMet 5000 Precision Saw. After that, samples were molded by Metkon EcoPress 100 into Bakelite. Each sample was ground by 220, 400, 800, 1200 and 2000 grit SiC emery paper, respectively. 6 µm and 1 µm diamond polish was applied to polish cross section surface of samples. After cleaning by spraying ethanol (99.5%), samples were etched for 15 seconds by Marble's Reagent Etchant. The composition of the etchant is shown in Table 2.2.

Table 2.2 Composition of Marble's Reagent [74].

Etchant Name	Composition	Method
Marble's Reagent	4g $CuSO_4$ + 20ml HCl + 20ml H_2O	Immersion

2.2.3.2 Scanning Electron Microscopy (SEM)

Aluminide coating thickness and microstructure were analyzed by Field-Emission Scanning Electron Microscopy (FEI Nova NanoSEM 430) operated at 20 kV accelerating voltage. Aluminide coating thickness was measured on cross section SEM images at ten different points by ImageJ Software and average values were calculated as shown in Figure 2.4.

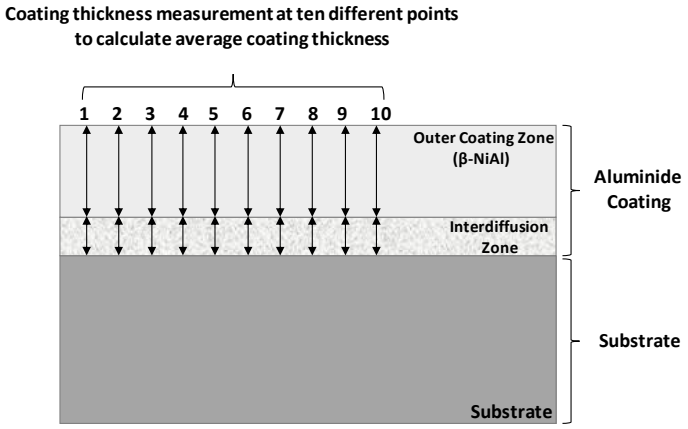

Figure 2.4 Aluminide coating thickness measurement at ten different points to calculate the average value by ImageJ.

After the thickness measurements, standard deviation for varying thicknesses were calculated as shown in Figure 2.5. It was observed that for all coatings standard deviation is changing in the range of 0.5 µm to 2 µm.

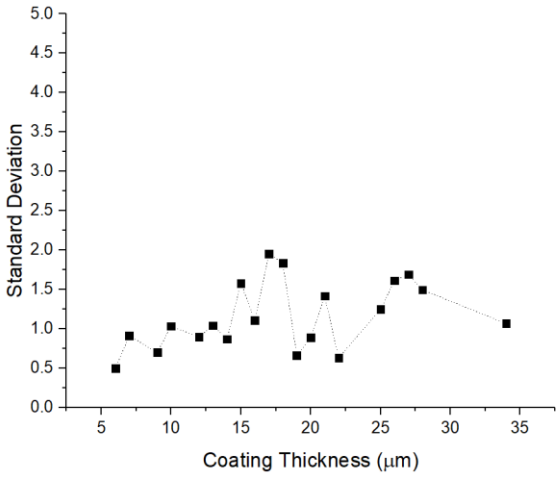

Figure 2.5 Standard deviation for different coating thicknesses.

2.2.3.3 Energy Dispersive Spectroscopy (EDS)

Elemental composition of aluminide coating from the surface through the substrate was analyzed by energy dispersive spectroscopy detector belong to SEM equipment. Compositional changes along the aluminide coating were obtained and used to identify coating phases.

The accuracy of EDS detector:

Energy dispersive spectroscopy is mainly used for qualitative compositional analysis. For quantitative analysis, other methods such as wavelength dispersive spectroscopy are commonly preferred due to high resolution and accuracy of the technique.

In this study, EDS is used for compositional linear analysis of simple aluminide coatings. It is found that EDS detector has an error for aluminum content compared to WDS analysis. Figure 2.6 shows comparison of EDS and WDS aluminum composition analysis. The error is in the range of 15 at. % for cross-section linear analysis (500 ms. for each point) and in the range of 5 at. % for long duration (60 sec.) point analysis. However, SEM-EDS is more practical method than EPMA-WDS, linear compositional analysis of simple aluminide coatings was performed by EDS. Only

compositional analysis of reactive or alloying element modified aluminide coatings was conducted by WDS as mentioned in Chapter 3 and 4.

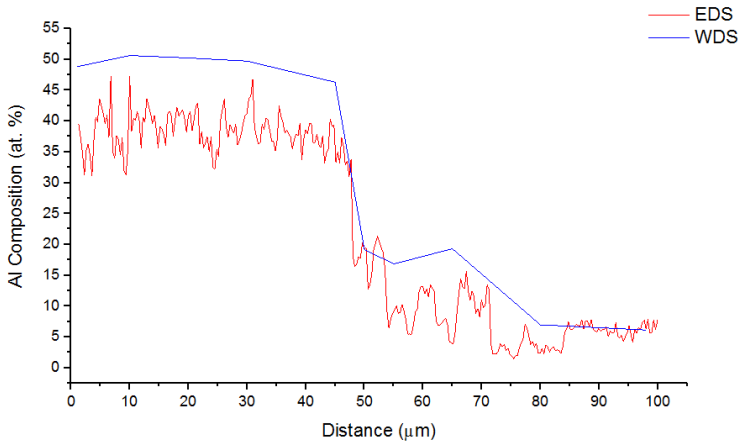

Figure 2.6 Comparison of EDS and WDS chemical analysis for aluminum at the cross section of aluminide coated sample.

2.2.3.4 X-ray Diffraction (XRD) Analysis

X-ray diffraction (XRD) analysis was used to identify coating phases at the substrate surface. Bruker D8 Advance XRD was employed using Cu-Kα radiation (λ=1.5406 Å) with 40 kV and 40 mA at 2°/min scanning rate. Two aluminide coated sample were analyzed by XRD at 0.1 °/min and 2°/min scanning rate to ensure higher scanning rate is suitable to observe all possible coating phases. In both analysis, same phases were observed at substrate surface. Only difference was peak intensities (a.u.) as expected. Therefore, all XRD analysis were performed at 2°/min scanning rate.

2.3 Results and Discussions

2.3.1 Effect of CVD Process Parameters on Aluminide Coating

Aluminide coatings can be applied by different coating processes such as pack cementation, above the pack processes or CVD. Although pack processes are simpler and easier technique, CVD provides the largest possibility to control process variables. These process variables are mainly chamber temperature, chlorinator temperature, system pressure, gas flows/ratios, aluminum activity and process time. In this section, the effect of CVD parameters on aluminide coating growth rate, outer layer/IDZ thickness ratio, microstructure, and phase formations were studied. In each coating experiment, only one CVD process parameter was changed and all other variables were kept constant to examine the effects of a single variable on aluminide coating physical and chemical properties. However, the biggest challenges in the CVD method is that each process variable is associated with other variables as illustrated in Figure 2.7. For example, the effects of different gas flows and ratios on the coating would exhibit a different behavior when the system pressure or chamber temperature is changed. Univariate experiments, however, are remarkably crucial in understanding the effect of CVD parameters on coating formation and creates guidelines for optimization studies.

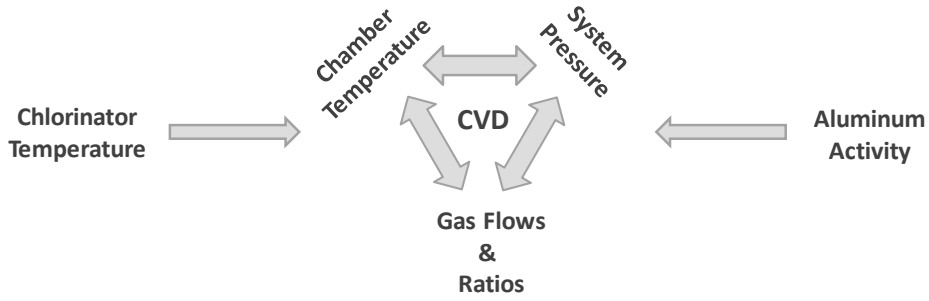

Figure 2.7 Relationship of CVD process parameters.

Thermodynamic Calculations:

Many chemical reactions take place during aluminizing process at chlorinator and coating chamber. To better understand the formation of aluminide coating, thermodynamic calculations have been made for all chemical reactions that could occur at different locations within the CVD system. The ΔG and ΔH values of possible reactions were calculated at different temperatures to observe the effects of chlorinator and coating chamber temperature on these reactions.

ΔG and ΔH of formation reactions occur in the aluminum chlorinator were calculated by Thermocalc computer software and are shown in Figure 2.8.

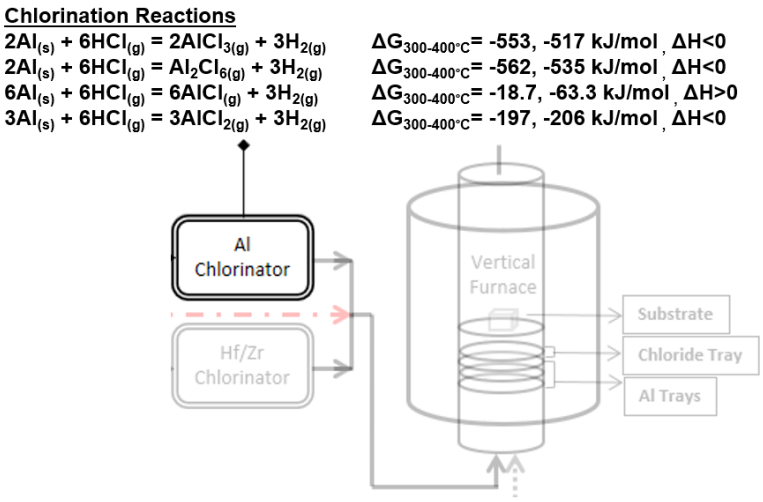

Figure 2.8 ΔG and ΔH calculations of chemical reactions occurred at aluminum chlorinator unit; calculations were obtained by Thermocalc Software.

Aluminum in the chlorinator reacts with HCl gas to form $AlCl_3$ and Al_2Cl_6 gases. Also, thermodynamic calculations show that small amount of AlCl and $AlCl_2$ form in the chlorinator ($\Delta G < 0$). These gases are transferred from the chlorination unit to the coating furnace by argon gas. The increase in chlorinator temperature from 300 °C to 400 °C, results increase in ΔG of $AlCl_3$ and Al_2Cl_6 formation means driving force to form aluminum chlorides decreases. On the other hand, ΔG of AlCl and $AlCl_2$ formation decreases with temperature which means driving force to form aluminum sub-chlorides increases. Therefore, the effect of chlorinator temperature on the formation of aluminide coating was studied in the temperature range of 300 – 400 °C.

400 °C is decided as maximum temperature limit to prevent local melting of aluminum pellet because both reactions are exothermic.

In addition to chlorinator, the possible chemical reactions and their ΔG - ΔH values that occurred at coating chamber are shown in Figure 2.9. Reactions were divided into two group as internal tray reactions and surface deposition reactions.

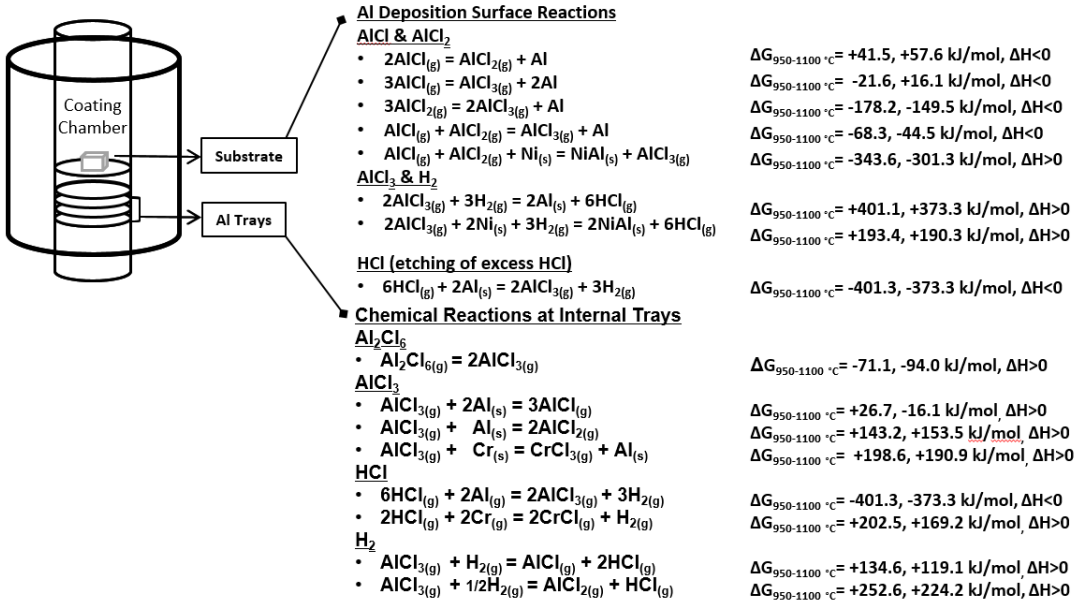

Figure 2.9 ΔG and ΔH calculations of chemical reactions occurred at coating chamber; calculations were obtained by Thermocalc Software.

Chemical Reactions at Internal Trays:

Thermodynamic calculations showed that Al_2Cl_6 which forms at chlorinator decomposes to $AlCl_3$ at coating chamber. ΔG of reaction gets more negative when temperature increases from 950 °C (-71.1 kJ/mol) to 1100 °C (-94.0 kJ/mol). It is assumed that Al deposition rate rises with increasing temperature because $AlCl_3$ is the main source of AlCl which is responsible for Al deposition [75].

AlCl gas does not form at 950 °C due to positive ΔG value (+26.7 kJ/mol), but when the temperature rises to about 1050 °C reaction takes place in the direction of AlCl

formation (ΔG = -16.1 kJ/mol). $AlCl_2$ formation is not favorable in relevant temperature range ($\Delta G > 0$).

In addition, unreacted HCl transferred from chlorinator reacts with aluminum source at internal trays and forms $AlCl_3$. When temperature increases, ΔG of reaction slightly rises from – 401.3 kJ/mol (950 °C) to – 373.3 kJ/mol (1100 °C). However, the amount of HCl at coating chamber is negligible, assuming HCl is completely consumed at chlorinator. Also, HCl and $AlCl_3$ do not react with chromium in the Al-Cr alloy placed to the internal tray ($\Delta G > 0$). Chromium chlorides do not form; therefore, chromium does not deposit together with aluminum.

Moreover, thermodynamic calculations showed that H_2 gas does not affect the formation of aluminum sub-chloride gases due to positive ΔG of related reactions.

Al Deposition Surface Reactions:

There is no direct reduction reaction of aluminum chlorides by H_2 at the substrate surface ($\Delta G > 0$). Aluminum deposition occurs by the reduction of aluminum sub-chloride gases ($\Delta G < 0$). The increase in temperature causes a slight increase in ΔG of deposition reactions which could mean decrease in driving force, assuming that aluminum activity at substrate surface is not changing. Although, ΔG of Al deposition reactions increases, the amount of aluminum sub-chloride gases rises with temperature.

As a result, thermodynamic calculations show that increasing chlorinator and process temperature promotes the formation of aluminum sub-chloride gases which are responsible for Al deposition. However, driving force for surface deposition reactions slightly decreases with temperature. It is assumed that the effect of temperature on the formation of aluminum sub-chloride gases is more dominant than Al deposition reactions due to higher driving force of deposition reactions. Therefore, it can conclude that higher process temperature promotes the coating growth rate. Nevertheless, aluminide coating formation is also solid state diffusion controlled process. Temperature directly affects the diffusibility of species; therefore, increasing temperature could negatively affect coating microstructure and composition.

Coating Growth Rate:

Aluminide coating growth is mainly controlled by surface reactions and solid state diffusion. Therefore, coating growth rate is not constant during the aluminizing process. However, to compare aluminide coating growth rates depending on CVD process parameters, average growth rates were calculated in µm/sec unit by dividing total coating thickness to process time.

2.3.1.1 Chamber Temperature

The chamber temperature of the CVD system affects aluminide growth rate, IDZ thickness and resulting phases such as β-NiAl or Ni_2Al_3 formation. CVD aluminide coatings are usually carried out in the temperature range of 950 - 1100 ˚C. Above 1100 ˚C, IDZ region could locally melt depending on present phases. To observe the effect of chamber temperature on aluminide coating, aluminizing experiments were carried out at four different coating temperatures which are 950 ˚C, 1000 ˚C, 1050 ˚C and 1100 ˚C. Table 2.3 shows CVD parameters used for chamber temperature effect study.

Table 2.3 CVD process parameters of chamber temperature experiments conducted at 950 ˚C, 1000 ˚C, 1050 ˚C and 1100 ˚C chamber temperature.

Temperature	Pressure	HCl Flow	H_2 Flow	HCl:H_2	Ar Flow	HCl:Ar	Internal Trays	Time
950 °C	100 mbar	125 sccm	1000 sccm	1:8	250 sccm	1:2	Al-Cr (50/50)	4 h
1000 °C	100 mbar	125 sccm	1000 sccm	1:8	250 sccm	1:2	Al-Cr (50/50)	4 h
1050 °C	100 mbar	125 sccm	1000 sccm	1:8	250 sccm	1:2	Al-Cr (50/50)	4 h
1100 °C	100 mbar	125 sccm	1000 sccm	1:8	250 sccm	1:2	Al-Cr (50/50)	4 h

Figure 2.10 shows SEM cross-section analysis, EDS chemical analysis and XRD phase analysis of aluminide coatings. Also, the coating thickness and outer layer/IDZ ratio change depending on process temperature is shown in Figure 2.11.

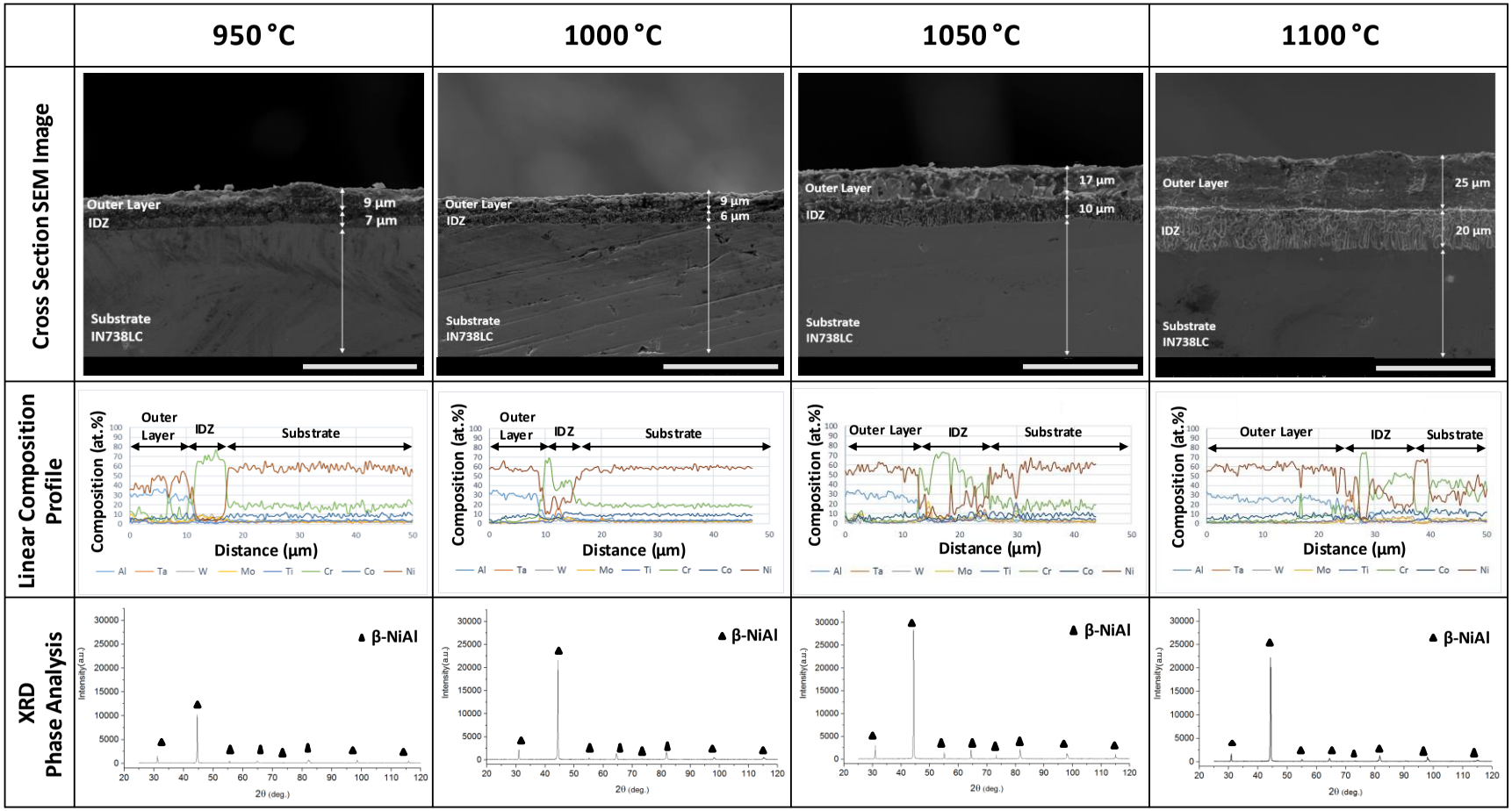

Figure 2.10 Cross section SEM images (The scale bar = 50 µm), linear composition profile and XRD pattern of aluminide coatings conducted at 950, 1000, 1050, 1100 °C.

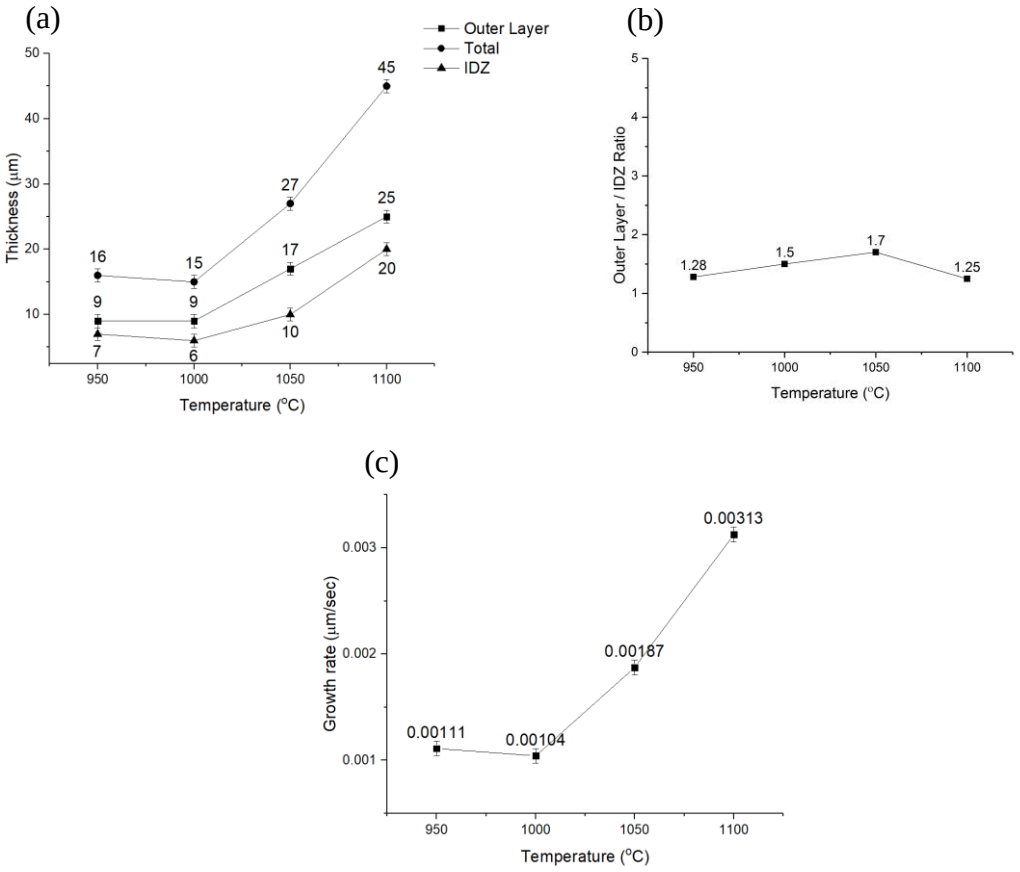

Figure 2.11 (a) Outer layer, IDZ and total aluminide coating thickness change, (b) outer layer/ IDZ ratio, (c) growth rate change depending on CVD chamber temperature.

After aluminizing processes, coating thicknesses were measured by SEM. For the coatings applied at 950 °C and 1000 °C, 9 μm outer layer thickness were obtained. Similar with outer layer thickness, IDZ thickness were almost identical and 7 μm at 950 ° C, 6 μm at 1000 ° C was obtained. Coating thicknesses began to increase when the temperature exceeded 1000 °C. In the coating applied at 1050 ° C, 17 μm outer layer and 10 μm IDZ thickness (27 μm total) were obtained. By increasing the temperature, coating thickness continued to increase and average 25 μm outer coating and 20 μm IDZ thickness (45 μm total) were obtained at 1100 °C. It is obvious that higher aluminizing temperature promotes growth rate of the coating (Fig. 2.11 (c)). Similarly, Rafiee et al. (2010) found that coating thickness increases more than twice when coating temperature was increased from 950 °C to 1050 °C for both low activity and high activity aluminizing processes [76].

According to the linear composition analysis results by EDS, it was found that approximately 30 - 40 at. % aluminum present at the outer layer of all coatings. Composition analyses conducted by EDS show approximate value ranges and are not as sensitive as WDS method. The XRD phase analyses show that β - NiAl phase was obtained at the surface between 30 – 40 at. % aluminum content. At the interface between the outer layer and IDZ, the amount of aluminum falls to 6 at. % which is the Al composition of the IN738LC alloy. Composition and phase analyses show that the β - NiAl phase is completely formed in the outer zone. In the IDZ region, it was observed that the amount of chromium increased up to 70 at. % and fluctuates between 40 – 70 at. % range. Cr atoms in the substrate and the coating (β-NiAl) replace by Ni atoms due to their similar atomic radius. When β-NiAl forms at the substrate surface, amount of Ni sites in the crystal structure decreases, thereby decreasing Cr solubility. Since the solubility of chromium in the β - NiAl phase is low compared to the substrate, the chromium concentrates in IDZ region and precipitates.

In the CVD aluminizing, the kinetics of aluminizing process is controlled by the combination of solid state diffusion and surface reactions (Fig. 1.16). By controlling and optimizing the rate of solid state diffusion and surface reactions, it is possible to maximize 1) Coating growth rate, and 2) Outer (β-NiAl) layer/IDZ ratio. Thermodynamic calculations showed that formation of AlCl which is main reactant responsible for aluminum deposition become favorable ($\Delta G < 0$) at higher chamber temperatures (above 1000 °C). Kikuchi et al. (1964) and Masset et al. (2012) suggested that partial pressure of AlCl increases with rising aluminizing temperature [77,78]. As a result of higher AlCl partial pressure, the growth rate significantly increases. Also, nickel diffusion to surface become dominant above 1000 °C which promotes NiAl phase formation, thereby increases the growth rate [79]. At higher temperatures, not only the surface reaction rates but also diffusibility of main coating species increase significantly. Therefore, more Al incorporates with nickel to form β-NiAl due to both higher surface reaction rate and solid state diffusion rate. The growth rate and the outer coating thickness significantly increase in direct proportion to the temperature. However, the outer layer (β-NiAl)/IDZ ratio decreased with increasing solid state diffusion rates of substrate elements above 1050 °C. Experimental results also confirm

that temperature does not affect growth rate below 1000 °C due to lower surface reaction and diffusion rates. Despite the increase in coating thickness with increasing temperature, no CVD coating was performed above 1100 °C chamber temperature. Exceeding 1100 °C may result in the melting of phases with a low melting temperature in the IDZ region, which affects the aluminide coating properties negatively [2]. Also, the standard solutionizing temperature of IN738 LC given by the manufacturer is 1120 °C; hence, microstructure could be destroyed above 1100 °C chamber temperature.

CVD System Notes:

CVD system which is used in this study has a maximum furnace temperature limit as 1200 °C defined by the manufacturer. However, it was observed that furnace is only suitable to work at 1200 °C for a limited time. For long time aluminizing processes, 1100 °C is maximum operating temperature that CVD aluminizing process can be performed. Although furnace can be operated at any temperature below 1100 °C, it was observed that aluminide growth rate is very limited under 1000 °C.

2.3.1.2 System Pressure

Another parameter that affects the aluminide coating formation is the system pressure. Pressure affects the diffusion of the gases present in the pressurized medium and the partial pressures of the coating gases. Two separate aluminizing studies were carried out at different pressures. When first experiment set was performed, CVD system could not be operated above 180 mbar due to technical issues. After problems are fixed, second experiment set was conducted to observe the effect of pressure on aluminide coating. Also, maximum operating pressure of CVD system was specified. Table 2.4 shows the CVD process parameters of first experiment set.

Table 2.4 CVD process parameters conducted at 50, 100, and 180 mbar system pressure.

Pressure	Temperature	HCl Flow	H_2 Flow	HCl : H_2	Ar Flow	Internal Trays	Time
50 mbar	1050 °C	125 sccm	1000 sccm	1:8	250 sccm	Al-Cr (50/50)	4 h
100 mbar	1050 °C	125 sccm	1000 sccm	1:8	250 sccm	Al-Cr (50/50)	4 h
180 mbar	1050 °C	125 sccm	1000 sccm	1:8	250 sccm	Al-Cr (50/50)	4 h

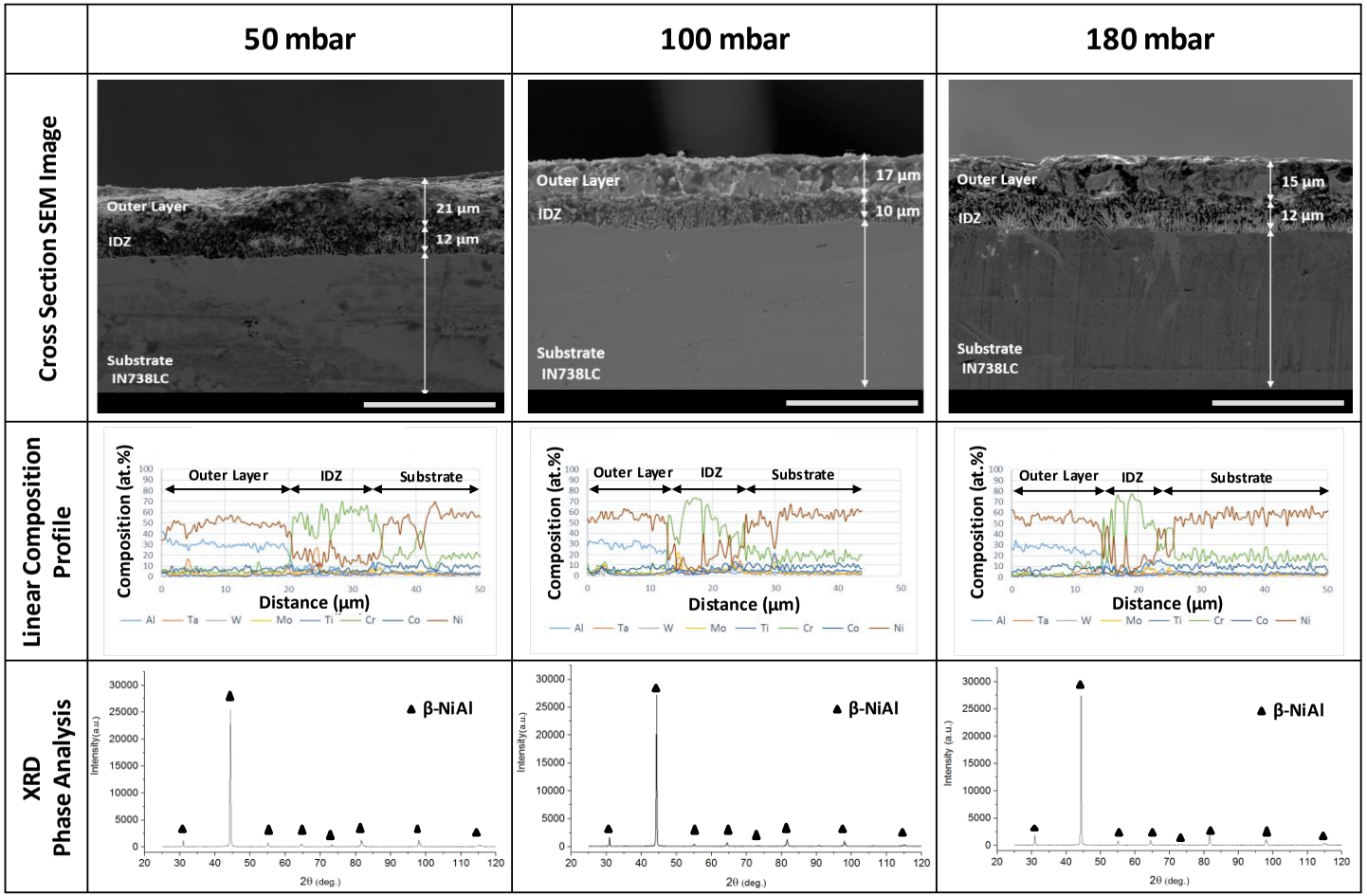

Figure 2.12 Cross section SEM images (The scale bar = 50 µm), linear composition profile and XRD pattern of aluminide coatings conducted at 50, 100, 180 mbar.

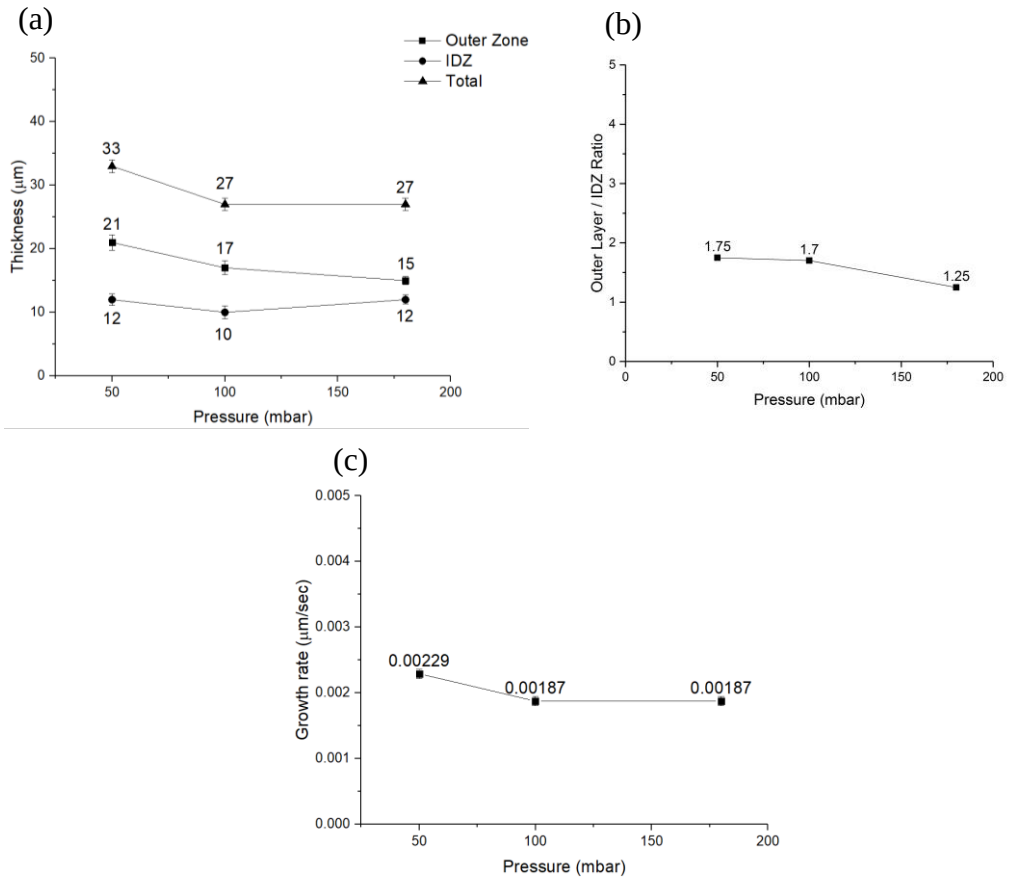

Figure 2.13 (a) Outer layer, IDZ and total aluminide coating thickness change, (b) outer layer/ IDZ ratio change (c) growth rate change depending on CVD system pressure.

Cross-sectional analyzes by SEM shows that 21 µm outer coating zone and 12 IDZ thickness (total 33 µm) were observed at 50 mbar (Fig. 2.12). When the pressure was increased to 100 mbar, outer layer thickness decreased to 17 µm and IDZ thickness decreased to 10 µm. When the system pressure rises to 180 mbar, 15 µm outer coating and a 12 µm IDZ thickness was obtained. By increasing pressure, outer layer/IDZ ratio slightly decreased from 1.75 to 1.25 as shown in Figure 2.13 (b).

The increase in system pressure suppresses aluminide growth rate; as a result, β-NiAl thickness decreases together with outer layer/IDZ ratio. The growth rate and the resulting coating thicknesses were not significantly changed when the pressure was increased above 100 mbar, but when the pressure was reduced below 100 mbar, an increase in coating thickness was observed (Fig. 2.13 (c)).

After pressure control problem of CVD system had solved, another experiment set was conducted at 100, 200 and 300 mbar. The only difference between first set and second set is $HCl:H_2$ ratio decreased from 1:8 to 1:2. Although growth rates were changed by altering $HCl:H_2$ ratio, the effect of system pressure on growth rate and outer layer/IDZ ratio was observed. Table 2.5 shows CVD process parameters used for pressure limit determination experiments.

Table 2.5 CVD process parameters of pressure limit determination experiments conducted at 100, 200 and 300 mbar system pressure.

Pressure	Temperature	HCl Flow	H_2 Flow	HCl : H_2	Ar Flow	HCl:Ar	Internal Trays	Time
100 mbar	1050 °C	125 sccm	250 sccm	1:2	250 sccm	1:2	Al-Cr (50/50)	4 h
200 mbar	1050 °C	125 sccm	250 sccm	1:2	250 sccm	1:2	Al-Cr (50/50)	4 h
300 mbar	1050 °C	125 sccm	250 sccm	1:2	250 sccm	1:2	Al-Cr (50/50)	4 h

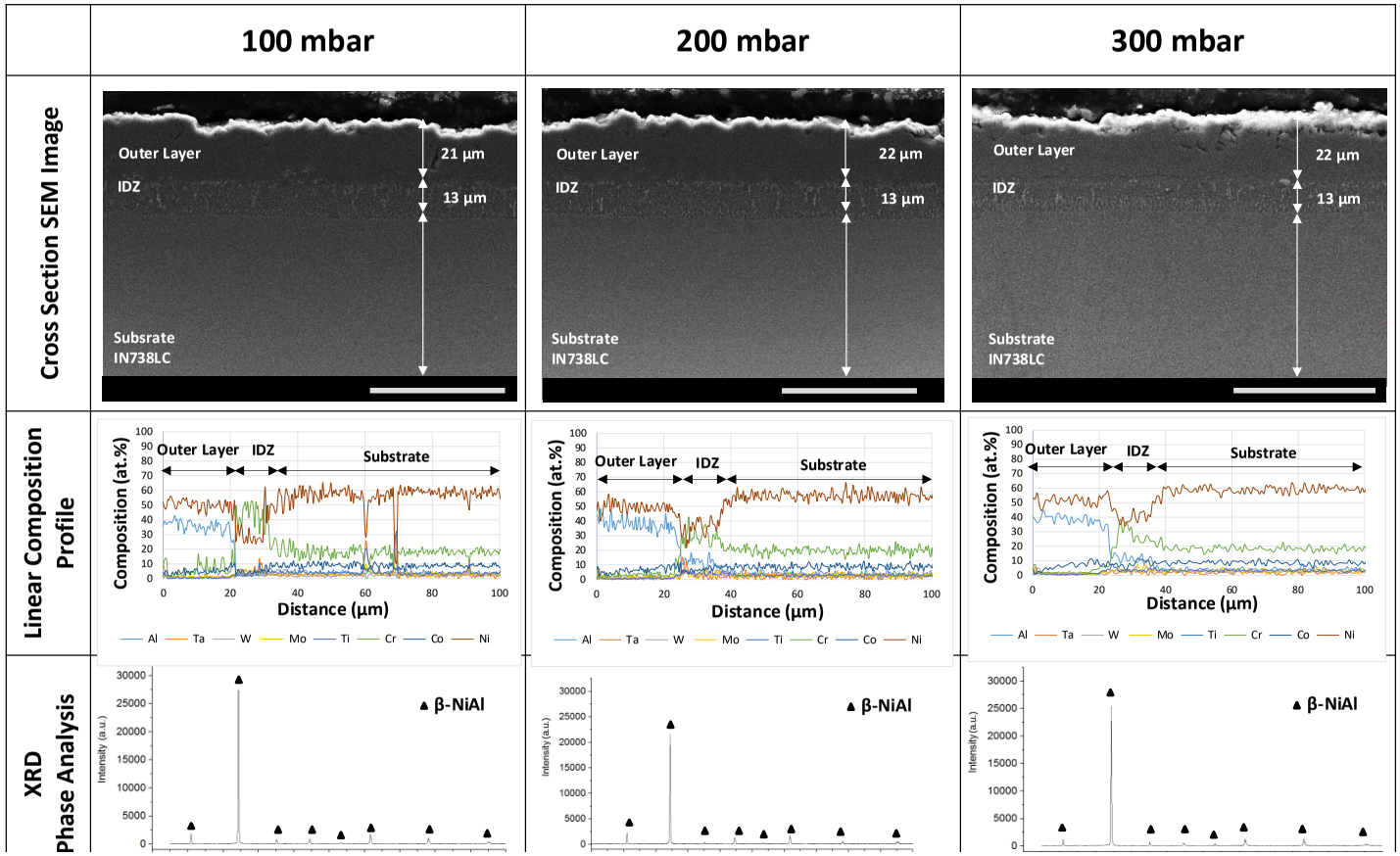

Figure 2.14 Cross section SEM images (The scale bar = 50 µm), linear composition profile and XRD phase analysis results of aluminide coatings conducted at 100, 200, and 300 mbar pressure.

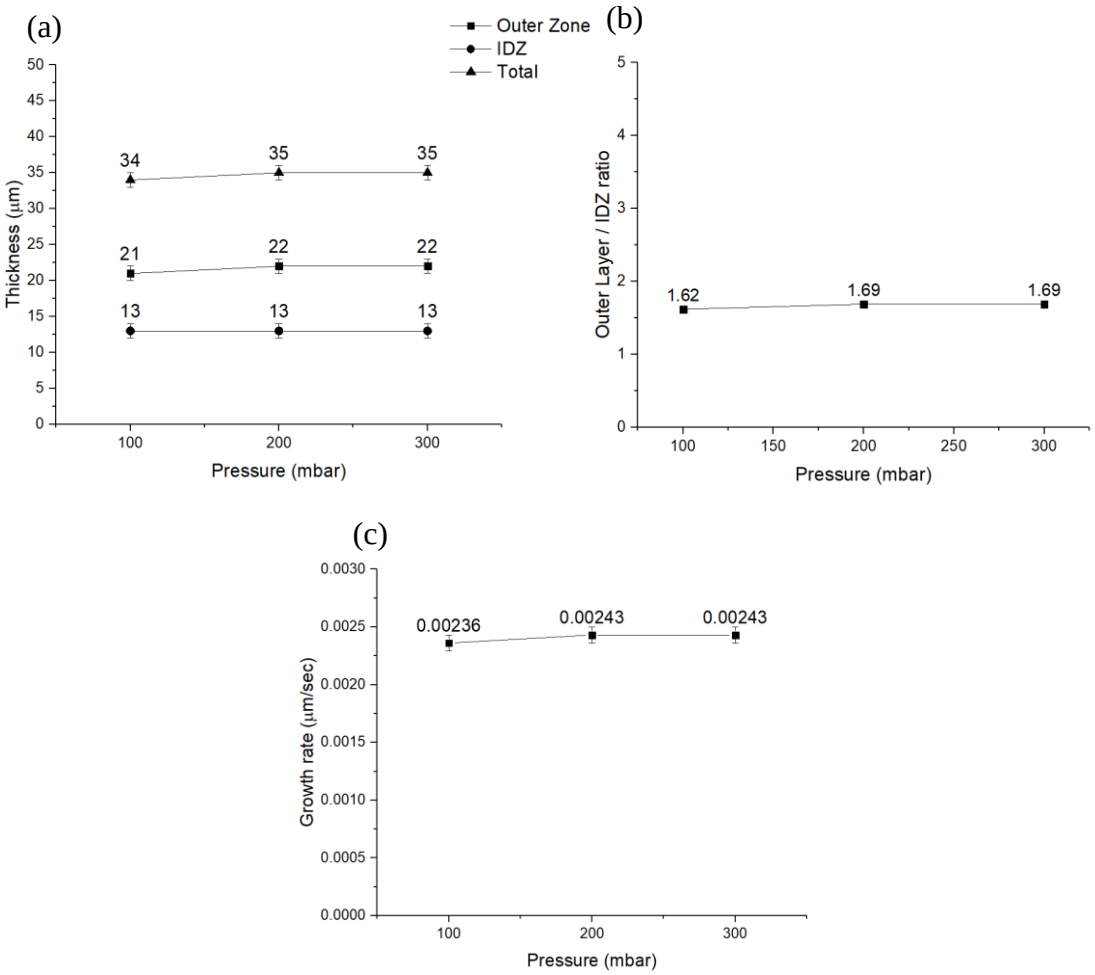

Figure 2.15 (a) Outer layer, IDZ and total aluminide coating thickness change, (b) outer layer to IDZ ratio, (c) growth rate change depending on CVD system pressure.

Aluminide coatings applied at different system pressures were compared (Fig. 2.14). For all coating runs at 100, 200 and 300 mbar, average 21-22 µm outer layer and 13 µm IDZ thickness were obtained. Linear compositional analysis showed that aluminum content is altering between 30 - 45 at. % at outer layer and XRD phase analysis proved that only β-NiAl phase present at the substrate surface. Experiments showed that pressure has no effect on aluminide coating growth rate above 100 mbar with this specific temperature, gas flows/ratios (Fig. 2.15), while previous experiments showed that growth rate slightly increased when the pressure was decreased to 50 mbar. Similarly, Nowotnik et al. (2012) performed CVD aluminizing on Re 80 superalloy at 100, 150 and 350 mbar pressure. They found that at 100 mbar coating

thickness slightly increased compared to 150 and 350 mbar (Fig. 2.16). They implied that pressure has a small influence on aluminide growth rate [80].

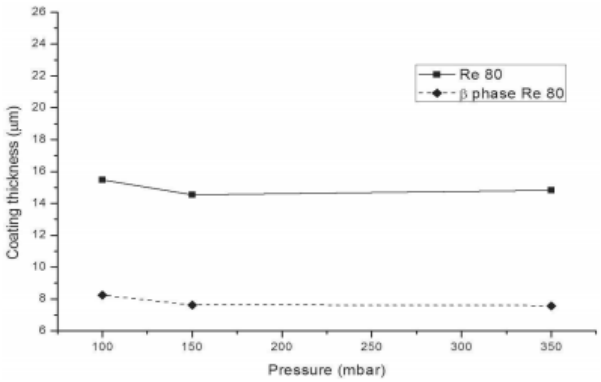

Figure 2.16 The influence of pressure in retort on the thickness of aluminide coating obtained on Re 80 superalloy by CVD method [80].

When the system pressure decreases, the diffusibility of gasses increases which is inversely related to system pressure. However, at low operating pressure, the influence of mass transfer is less significant than at higher pressure (e.g. atmospheric pressure) and rate limiting step is the surface reactions rather than mass transport [81]. Therefore, the effect of pressure on aluminide growth rate is insignificant compared to aluminizing temperature. However, partial pressures of reactants such as AlCl, $AlCl_2$ and $AlCl_3$ determine the kinetic rate, aluminide growth rate could be notably influenced by pressure at different gas flows and ratios, aluminum activity and temperatures.

CVD System Notes:

METU CVD system has pressure range specified as 20 – 200 mbar by the manufacturer (Archer Technicoat). High speed pressure throttle valve which is connected to pressure transducer controls system pressure and keeps it constant during the aluminizing process. However, it is observed that above 50 mbar pressure, liquid ring pump (LRP) of CVD system is excessively powerful; therefore, pressure throttle valve cannot maintain pressures above 50 mbar. It is found out that an excess air flow through LRP by using anti-cavitation valve decreases the efficiency of the pump and it is possible to obtain higher system pressures during aluminizing. As a result of step

by step experiments, it is observed that CVD system can be operated at 300 mbar pressure by increasing air flow through LRP by the anti-cavitation valve. Depending on process gas flows and air flow rate through LRP, pressure can be maintained up to 350 mbar. Although the effect of pressure on growth rate and outer layer/IDZ ratio is limited, high operating pressures may need to optimize co-deposition of reactive or alloying elements which is discussed in Chapter 3.

2.3.1.3 HCl, H_2 and Argon Flow Rates

The gas flow rates are another major CVD process parameters that affect the coating growth rate; hence, microstructure and the phases present. Partial pressures of chloride gases formed in chlorinator and coating chamber are directly influenced by gas flow rates. HCl, H_2 and Ar are used as process gas in our CVD system. HCl could be defined as the main process gas responsible for the aluminide coating process. HCl gas is passed through the aluminum metal pellets and by the reaction of HCl with aluminum metal results in the formation of $AlCl_x$ gases. The main chemical reactions of HCl occurred in chlorinator and coating chamber are given in Figure 2.17.

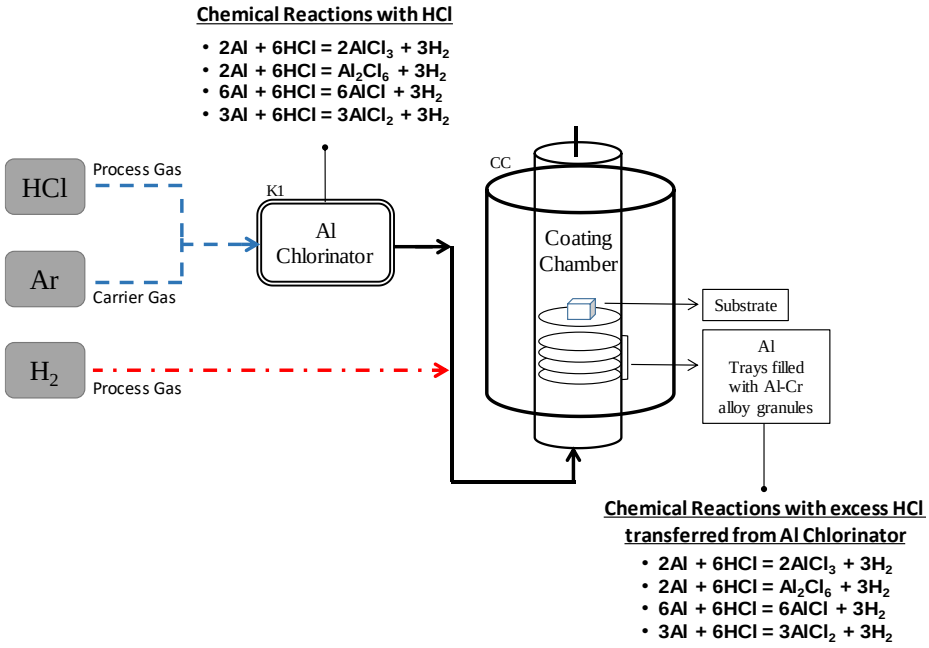

Figure 2.17 A basic illustration of CVD system showing chemical reactions at Al chlorinator (K1) and coating chamber (CC) that HCl gas involved.

HCl gas reacts with aluminum present in chlorinator and forms aluminum chloride gases. Unreacted HCl is transferred to coating chamber and reacts with Al in Al-Cr alloy present in chamber trays. By changing the HCl flow, $AlCl_x$ formation rate can be controlled to increase aluminum deposition rate at the substrate surface. Argon gas is used to transfer aluminum chloride gases from the chlorinator to coating chamber as a carrier gas. Also, argon dilutes the HCl gas in the chlorinator depending on HCl:Ar ratio. On the other hand, H_2 is used to decrease partial pressure of oxygen present in coating chamber. No influence of H_2 was observed on Al deposition reactions according to thermodynamic calculations. However, both HCl:Ar and HCl:H_2 ratio affect the partial pressure of aluminum chloride gases, thereby affecting the coating growth rate. For that reason, HCl:Ar and HCl:H_2 ratio were kept constant during the effect of HCl flow rate experiments.

To observe the influence of HCl flow rate on aluminizing process, experiments were carried out by using 125 sccm, 250 sccm and 500 sccm HCl flow by keeping HCl to H_2 (1:8) and Ar (1:2) ratio constant. Table 2.6 shows CVD process parameters used for the effect of gas flow rate experiments.

Table 2.6 CVD process parameters of HCl flow rate experiments conducted by using 125, 250, and 500 sccm HCl flow.

HCl Flow	Temperature	Pressure	H_2 Flow	HCl : H_2	Ar Flow	HCl : Ar	Internal Trays	Time
125 sccm	1050 °C	100 mbar	1000 sccm	1:8	250 sccm	1:2	Al-Cr (50/50)	4 h
250 sccm	1050 °C	100 mbar	2000 sccm	1:8	500 sccm	1:2	Al-Cr (50/50)	4 h
500 sccm	1050 °C	100 mbar	4000 sccm	1:8	1000 sccm	1:2	Al-Cr (50/50)	4 h

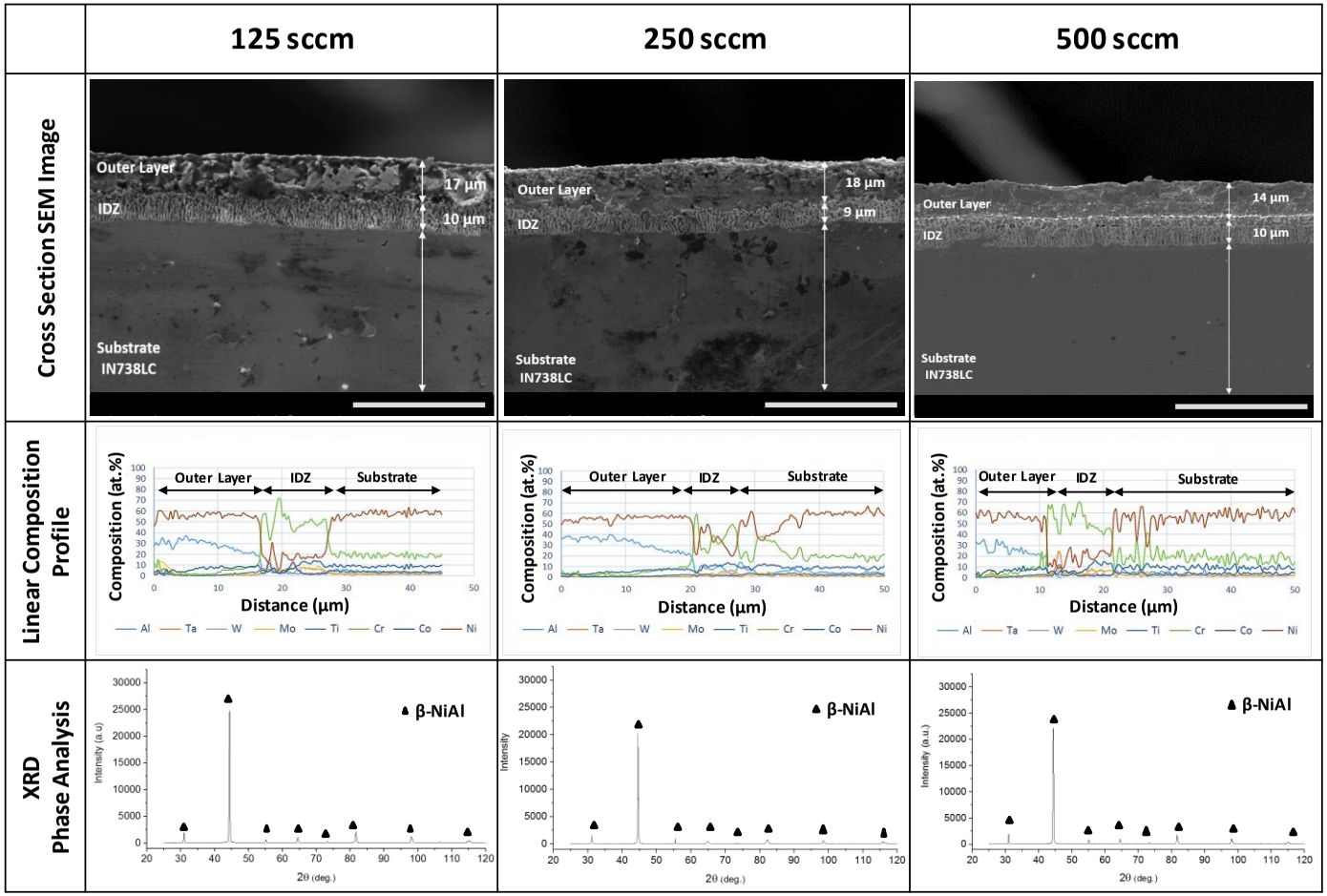

Figure 2.18 Cross section SEM images (The scale bar = 50 µm), linear composition profile and XRD pattern of aluminide coatings conducted by using 125, 250 and 500 sccm HCl flow by keeping HCl:H_2 = 1:8 and HCl:Ar = 1:2 ratio constant.

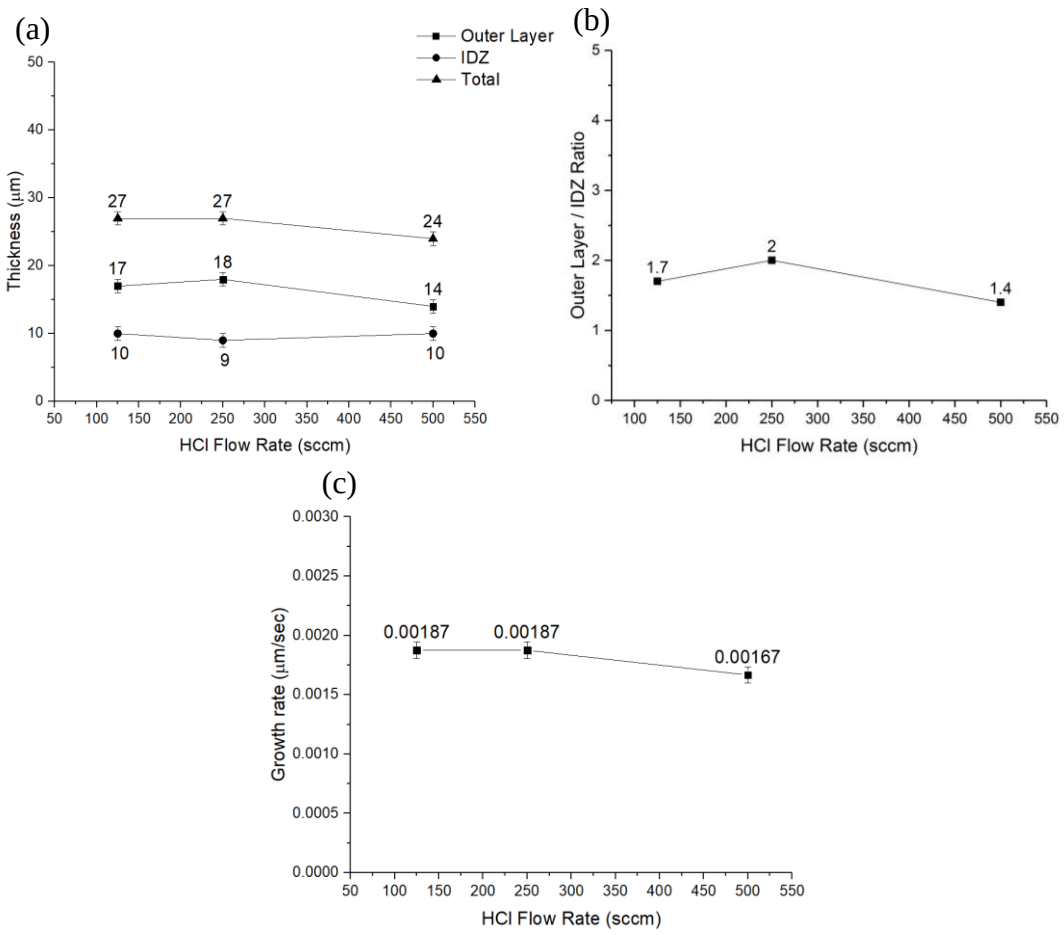

Figure 2.19 (a) Outer layer, IDZ and total thickness change, (b) outer layer/IDZ ratio, (c) growth rate change depending on HCl flow rate by keeping HCl:H_2 (1:8) and HCl:Ar (1:2) ratio constant.

After SEM and EDS analyses (Fig. 2.18), it was observed that coatings applied by 125 and 250 sccm HCl flow had identical coating thicknesses. 18 µm outer coating and 9 µm IDZ thickness were obtained at 250 sccm HCl flow and 17 µm outer coating and a 10 µm IDZ thickness at 125 sccm HCl flow. However, when the HCl flow was increased to 500 sccm, it was observed that there was a decrease in the outer layer thickness from 18 to 14 µm but IDZ thickness was not affected. Results indicate that IDZ thickness is not affected by the Al deposition rate while aluminizing temperature is constant. The diffusibility of substrate and coating species governs the IDZ formation. At constant temperature, similar IDZ thicknesses were obtained because solid state diffusion rates of substrate elements did not change. Besides IDZ thickness, outer coating layer thickness decreased with increasing HCl flow. The amount of aluminum chloride formed in the chlorinator is limited by the surface area of the metal

particles. As the amount of HCl sent to the system increases, excess HCl gas which could not react with aluminum in the chlorinator due to limited surface area transferred to the coating chamber. During aluminum deposition, unreacted HCl gas present in the coating chamber reacts with the aluminum on the coating surface to form $AlCl_x$ gases. As a result, the growth rate decreases due to etching effect of HCl gas [75]. Therefore, increase in HCl flow does not mean that the aluminum deposition rate would increase. Similarly, decrease in the HCl flow could greatly affect the aluminide growth rate, since the amount of aluminum chlorides formed in the chlorinator would be reduced (Fig. 2.19 (c)). For this reason, coating studies should be carried out using the optimum HCl flow range. By using those specific CVD parameters, higher growth rate and outer layer/ IDZ ratio were obtained between 125 to 250 sccm HCl flow. Higher HCl flow decreases the growth rate and outer layer/IDZ ratio as shown in Figure 2.19 (b).

CVD System Notes:

In CVD system, process gas flows are physically limited by the type of mass flow controllers (MFCs). In our CVD System, Bronkhorst El-Flow Base mass flow controllers are used. The full range of H_2 and Argon MFCs are specified as 0-5000 sccm, while full range of HCl MFCs is 0-1000 sccm. However, mass flow controllers cannot be operated at maximum and minimum limits specified by the producer. Although MFCs on our CVD system have an accuracy of ±1%, it should be operated in the 2 to 98 % of full scale for best accuracy. That means H_2 and Argon MFCs could be operated in the range of 100 – 4900 sccm and 20 – 980 sccm for HCl MFCs.

Depending on HCl:H_2 and HCl:Ar ratio of the process, HCl flow rate is limited not only by HCl MFCs but also H_2 and Ar MFCs. For instance, if HCl:H_2 ratio is set to 1:8, maximum HCl flow could set to 612 sccm due to H_2 MFC is limited by 4900 sccm.

2.3.1.4 HCl:H_2 gas ratio

The effects of hydrogen gas flow and thus the ratio of HCl: H_2 gas on the aluminide coating formation were investigated by three aluminizing experiments which were carried out by changing H_2 flow rates. 250, 500, 1000 sccm H_2 flows were used and 1:2, 1:4 and 1:8 HCl:H_2 ratio were obtained by keeping HCl gas flow and other CVD parameters constant.

Table 2.7 CVD process parameters of HCl:H_2 gas ratio experiments conducted by using 1:2, 1:4, 1:8 ratio.

HCl:H_2	Temperature	Pressure	HCl Flow	H_2 Flow	Ar Flow	HCl:Ar	Internal Trays	Time
1:2	1050 °C	100 mbar	125 sccm	250 sccm	250 sccm	1:2	Al-Cr (50/50)	4 h
1:4	1050 °C	100 mbar	125 sccm	500 sccm	250 sccm	1:2	Al-Cr (50/50)	4 h
1:8	1050 °C	100 mbar	125 sccm	1000	250 sccm	1:2	Al-Cr (50/50)	4 h

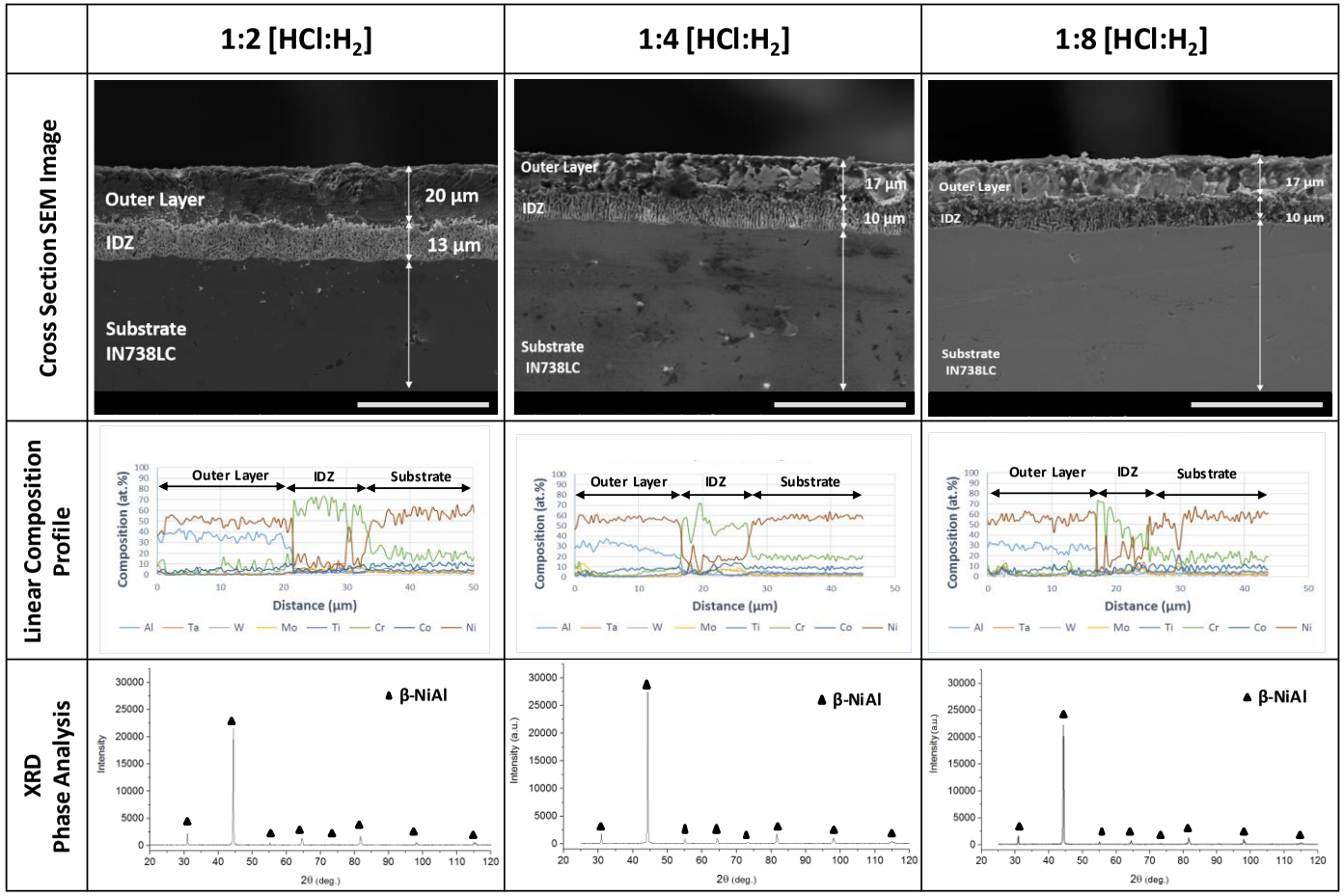

Figure 2.20 Cross section SEM images (The scale bar = 50 µm), linear composition profile and XRD pattern of aluminide coatings conducted with 1:2, 1:4 and 1:8 [HCl:H_2] gas ratio by keeping HCl flow (125 sccm) and HCl:H_2 (1:2) ratio constant.

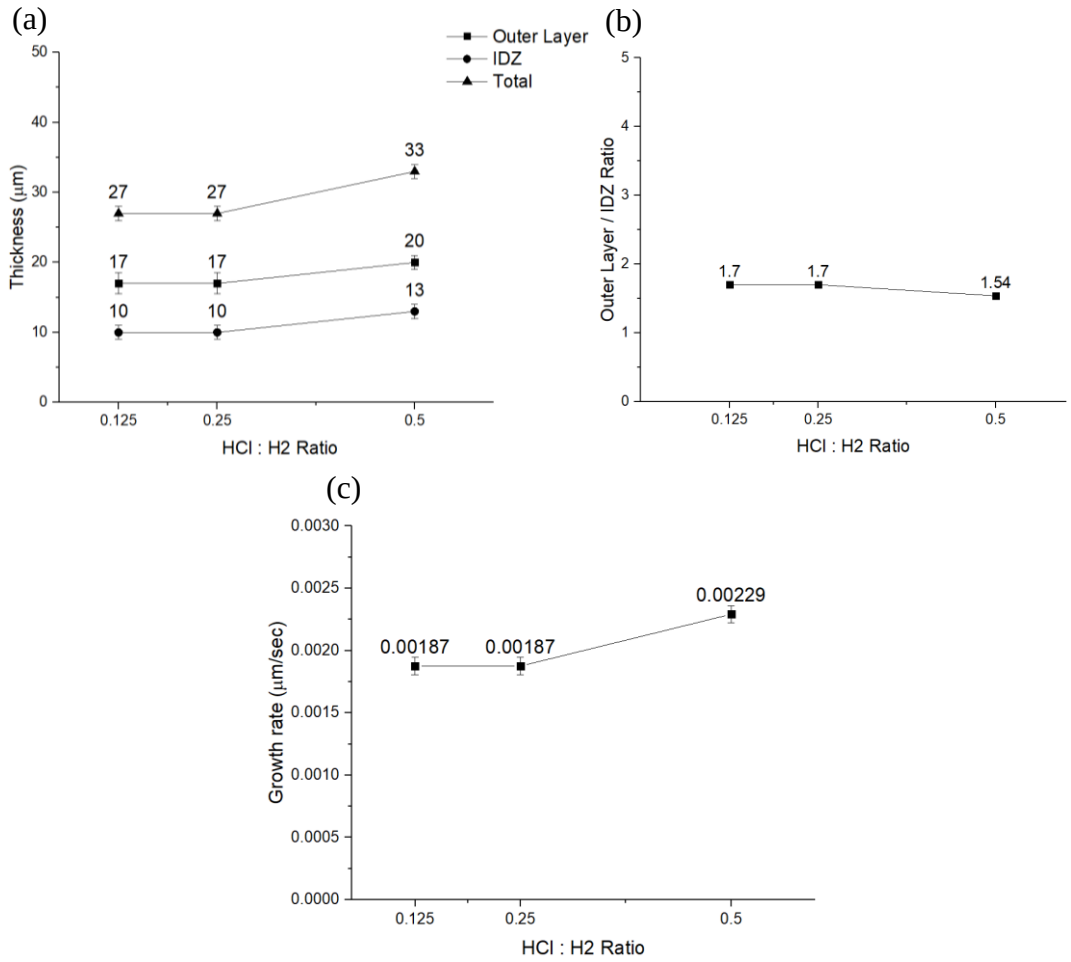

Figure 2.21 (a) Outer layer, IDZ and total aluminide coating thickness change, (b) outer layer/ IDZ ratio, (c) growth rate change depending on HCl : H_2 gas ratio.

Masset et al. (2012) suggested that as the HCl: H_2 ratio decreases, the growth rate increases due to increasing partial pressures of AlCl and $AlCl_2$ gasses according to thermodynamic calculations. They also mentioned that lower HCl:H_2 (<0.1) ratio favors single phase β-NiAl formation rather than β-NiAl + γ'-Ni_3Al at outer coating layer [77]. However, experiments showed that higher HCl:H_2 ratio favors the growth rate which is opposite to Masset et al.'s results. When HCl:H_2 ratio increased from 1:8 to 1:4, no difference was observed on the aluminide growth rate and microstructure as shown in Figure 2.20 and 2.21. However, when hydrogen flow was reduced to 250 sccm (HCl:H_2 = 1:2 ratio), an increase in the growth rate was observed. In comparison with other studies on H_2 flow, thermodynamic calculations proved that hydrogen does not have a direct role in the reduction reactions of aluminum deposition. When the flow of hydrogen was reduced, an increase in the growth rate was observed because

partial pressures of aluminum sub-chlorides were increased and resulted in increased growth rate. Although the coating thickness increased as H_2 flow decreased, the outer layer/IDZ ratio slightly decreased from 1.7 to 1.54. For all H_2 flow rates, the β-NiAl phase at coating surface was obtained at 30 – 40 at. % aluminum composition.

CVD System Notes:

As explained in previous topic, H_2 and Argon MFCs could be operated in the range of 100 – 4900 sccm and 20 – 980 sccm for HCl MFCs. Experiments showed that lower HCl to H_2 ratio favors the growth rate of aluminide coating. While H_2 MFC could be operated at 100 sccm as a minimum value, the minimum HCl flow is 50 sccm which is greater than 20 sccm (equipment limitation).

2.3.1.5 Chlorinator Temperature

Aluminum chloride gases are formed in the chlorinator by the reaction of HCl and aluminum. Chemical reactions occur in aluminum chlorinator is given below.

- $2Al + 6HCl = 2AlCl_3 + 3H_2$ $\quad \Delta G_{300\text{-}400°C}$= -553, -517 kJ/mol , $\Delta H<0$
- $2Al + 6HCl = Al_2Cl_6 + 3H_2$ $\quad \Delta G_{300\text{-}400°C}$= -562, -535 kJ/mol , $\Delta H<0$
- $6Al + 6HCl = 6AlCl + 3H_2$ $\quad \Delta G_{300\text{-}400°C}$= -18.7, -63.3 kJ/mol , $\Delta H>0$
- $3Al + 6HCl = 3AlCl_2 + 3H_2$ $\quad \Delta G_{300\text{-}400°C}$= -197, -206 kJ/mol , $\Delta H<0$

Aluminum deposition rate is significantly influenced by partial pressures of aluminum chloride gases. Thermodynamic calculations show that ΔG of $AlCl_3$ and Al_2Cl_6 formation increase when the chlorinator temperature increases from 300 °C to 400 °C. That means driving force to form aluminum chlorides decreases. On the other hand, ΔG of AlCl and $AlCl_2$ formation reactions decreases with temperature which means driving force to form aluminum sub-chlorides increases. It is obvious that chlorinator temperature affects the formation rates of chlorinator reactions. Therefore, coating experiments were carried out at three different chlorinator temperatures at 300, 350 and 400 °C to investigate the effects of increasing chlorinator temperature on aluminide coating formation. CVD process parameters are shown in Table 2.8.

Table 2.8 CVD process parameters of chlorinator temperature experiments conducted at 300 ˚C, 350 ˚C, and 400 ˚C chlorinator temperature.

Chlorinator Temperature	Temperature	Pressure	HCl Flow	H_2 Flow	HCl : H_2	Ar Flow	Internal Trays	Time
300 ˚C	1100 ˚C	100 mbar	125 sccm	1000 sccm	1:8	250 sccm	Al-Cr (50/50)	4 h
350 ˚C	1100 ˚C	100 mbar	125 sccm	1000 sccm	1:8	250 sccm	Al-Cr (50/50)	4 h
400 ˚C	1100 ˚C	100 mbar	125 sccm	1000 sccm	1:8	250 sccm	Al-Cr (50/50)	4 h

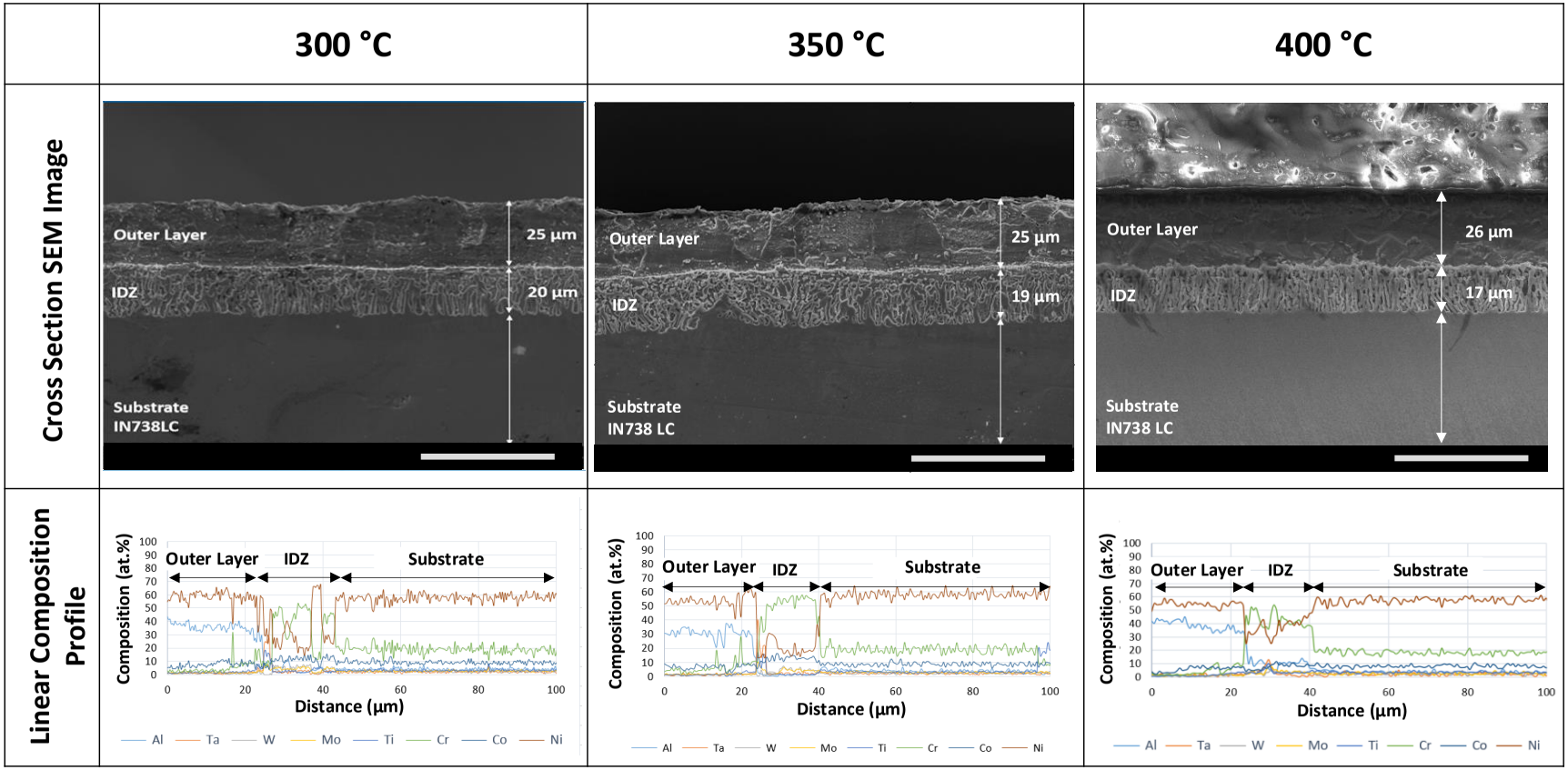

Figure 2.22 Cross section SEM images (The scale bar = 50 µm), linear composition profile aluminide coatings conducted by using 300, 350, 400 °C aluminum chlorinator temperature.

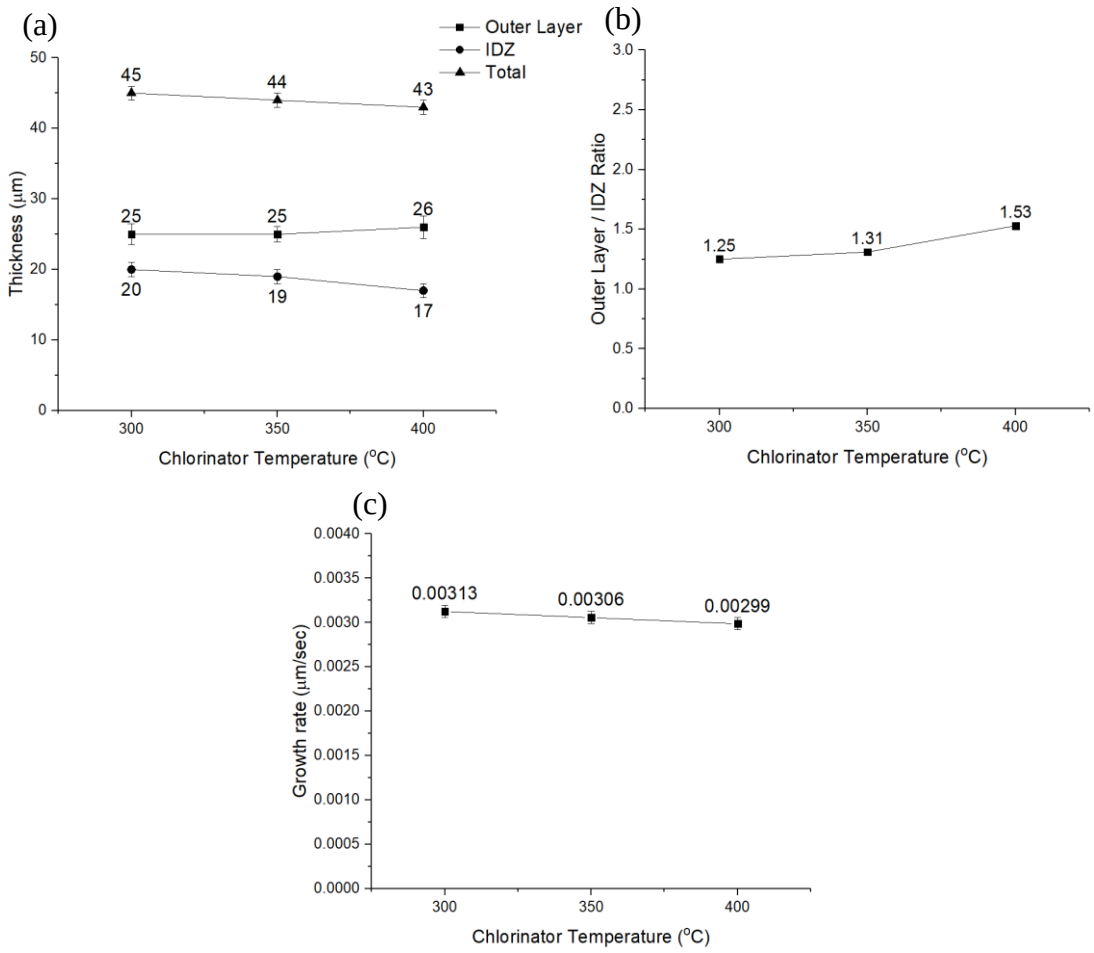

Figure 2.23 (a) Outer layer, IDZ and total aluminide coating thickness change, (b) outer layer/ IDZ ratio, (c) growth rate change depending on chlorinator temperature.

It has been observed that there is not any change in the coating thicknesses obtained at chlorinator temperature of 300 and 350 °C as shown in Figure 2.22 and 2.23. In the experiments performed at 300 and 350 °C, 25 µm outer coating thickness and 19-20 µm IDZ thickness were obtained. When the chlorinator temperature was increased to 400 °C, it was observed that outer layer thickness increased from 25 µm to 26 µm and IDZ thickness decreased to 16 µm but total coating thickness decreased 3 µm. Despite the decrease in total coating thickness, the outer layer / IDZ ratio has increased from 1.25 to 1.53. It is assumed that the partial pressure of aluminum sub-chloride gases slightly increases with increasing chlorinator temperature. However, an increase in the chlorinator temperature had only small effect on growth rate (Fig. 2.23 (c)).

CVD System Notes:

Since the reactions occur at chlorinator are exothermic, the unexpected temperature increase due to chemical reactions may cause local melting of the aluminum (T_m = 660.3 °C) pellets above 400 °C. In the event of such melting, chlorinator gas inlet could be possibly blocked by aluminum and damage the equipment. For that reason, 400 °C was decided as a maximum temperature limit of aluminum chlorinator, while both chlorinators have a capability to operate at 800 °C.

2.3.1.6 Aluminum Activity

In gas phase aluminizing, aluminum chloride gas is generated at external chamber which is aluminum chlorinator unit in our CVD system. However, aluminum sub-chlorides are mainly formed at coating chamber by the reduction of $AlCl_3$ to $AlCl_2$ and AlCl. The reduction reaction of $AlCl_3$ is described by the following [82]:

$$AlCl_{3(g)} + Al \rightarrow AlCl_{(g)} + AlCl_{2(g)}$$

Although 50/50 wt.% Al-Cr granules are typically used to increase the aluminum activity of gas mixture at coating chamber, the influence of Al concentration of Al-Cr alloy was studied by using 70/30 wt.% Al-Cr granules at internal trays. Aluminide coating process was carried out by using CVD process parameters given in Table 2.9.

Table 2.9 CVD Process parameters for experiments conducted with 50/50 and 70/30 wt. % Al-Cr alloy at internal trays.

Temperature	Pressure	HCl Flow	H_2 Flow	HCl : H_2	Ar Flow	HCl:Ar	Internal Trays	Time
1100 °C	100 mbar	125 sccm	250 sccm	1:2	250 sccm	1:2	**Al-Cr (50/50)**	4 h
1100 °C	100 mbar	125 sccm	250 sccm	1:2	250 sccm	1:2	**Al-Cr (70/30)**	4 h

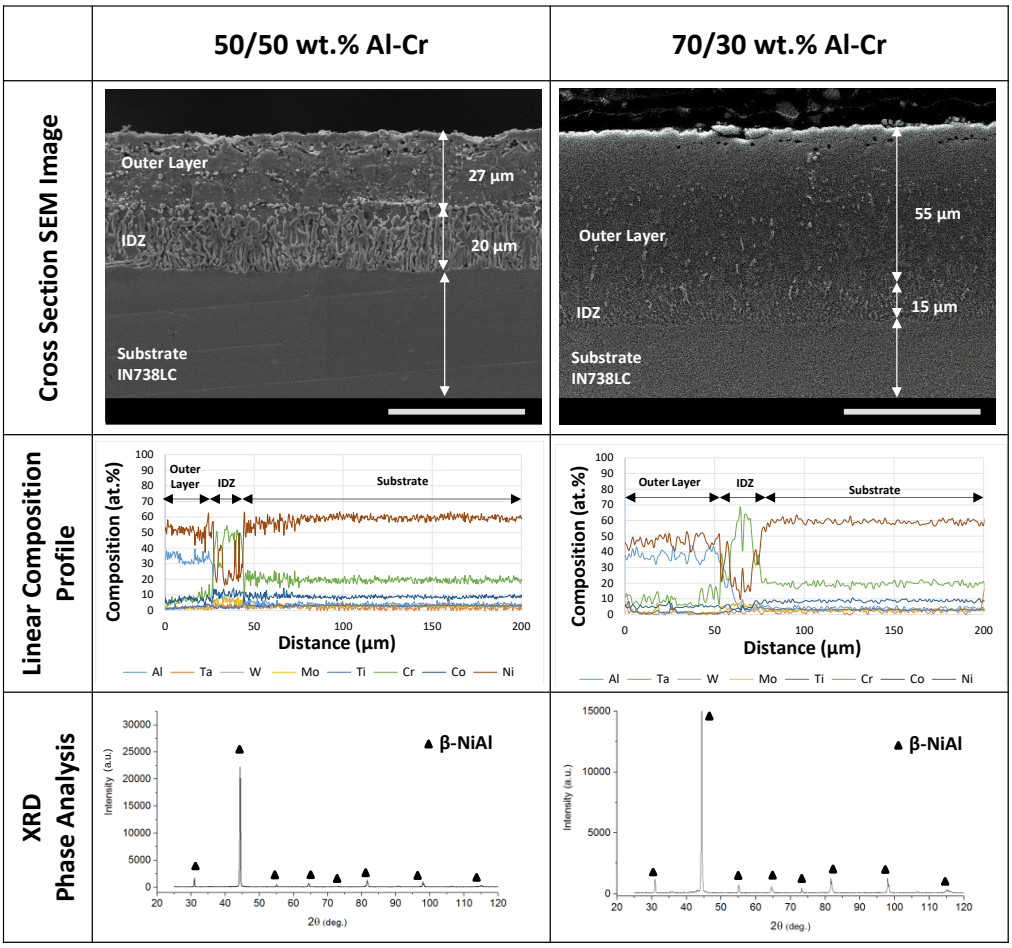

Figure 2.24 Cross section SEM images (The scale bar = 50 µm), linear composition profile and XRD pattern of aluminide coatings applied by using 50/50 and 70/30 wt. % Al-Cr alloy.

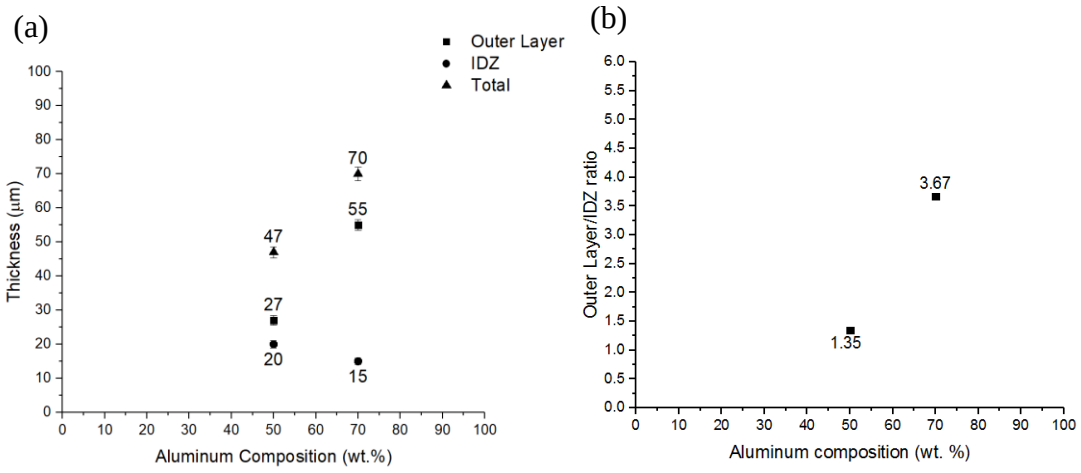

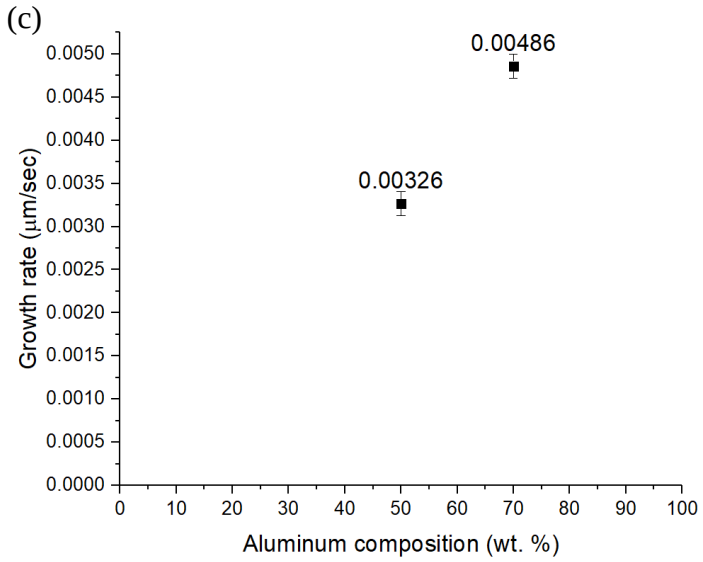

Figure 2.25 (a) Outer layer, IDZ and total aluminide coating thickness change, (b) outer layer/ IDZ ratio, (c) growth rate change depending on aluminum composition of Al-Cr alloy.

Effect of 70/30 Al-Cr alloy on aluminide coating formation was compared to the previous experiment which was conducted by using same CVD parameters with 50/50 wt.% Al-Cr alloy. By using 50/50 wt.% Al-Cr alloy, 27 µm outer coating thickness and 20 µm IDZ thickness (47 µm total) were obtained. Increasing the aluminum content from 50 to 70 wt.% in Al-Cr alloy promoted aluminum deposition rate. Outer coating thickness increased from 55 µm and the IDZ thickness decreased to 15 µm. By increasing outer layer thickness and decreasing IDZ thickness, outer coating / IDZ ratio increased from 1.35 to 3.67. At the outer coating layer, fine distributed Cr rich precipitates were observed in high activity process.

Results demonstrate that growth rate and outer layer/IDZ ratio are significantly affected by aluminum activity (Fig. 2.25). As mentioned before, the kinetics of aluminizing process is controlled by the combination of solid state diffusion and surface reactions. When the aluminum composition in the Al-Cr alloy was raised from 50 wt.% to 70 wt.%, the aluminum activity increased. It is assumed that partial pressures of aluminum chloride gases increased with increasing aluminum activity. Higher aluminum chloride partial pressures promoted the Al deposition surface reactions. Also, by increasing the aluminum activity, not only Al deposition rate but

also diffusivity of aluminum in the coating layer was affected. It is assumed that inward diffusion of Al through the substrate became more dominant than outward diffusion of Ni and aluminide coating was mainly formed by inward diffusion of Al. However, inward formation of aluminide coating resulted in precipitation of substrate elements along the outer coating layer rather than IDZ due to their relatively lower diffusion rates compared to aluminum. Since aluminum diffuses through the substrate faster than substrate elements, these substrate elements gradually precipitate in the outer coating layer and IDZ thickness significantly decreased.

While higher Al content of Al-Cr alloy enhanced aluminide coating growth rate, there could be possible disadvantages of high aluminum activity. Possible advantages and disadvantages of using 50/50 wt.% or 70/30 wt.% Al-Cr alloy were listed in Table 2.10.

Table 2.10 Possible advantages and disadvantages of using 50/50 and 70/30 wt. % Al-Cr alloy on aluminide coating properties.

	Composition of Al-Cr Alloy	
	50/50 wt.%	70/30 wt.%
Advantages	• Homogeneous β-NiAl phase formation at outer coating layer.	• Aluminide coating growth rate is high even if low chamber temperatures. • Low IDZ thickness and high outer IDZ ratio are obtained. • Due to high growth rate, short process time even if low chamber temperatures are possible.
Disadvantages	• Aluminide coating growth rate is relatively low. • Low outer layer/IDZ ratio is obtained. • Coating process time is too long due to low growth rates.	• High growth rate by high Al activity causes precipitation of chromium at outer coating region. Effect of Cr precipitates on oxidation and corrosion behavior is unknown. • Due to high Al activity, coating mainly forms by inward diffusion of aluminum through the substrate. Therefore, substrate carbides present at outer layer and their effects are unknown to oxidation and corrosion behavior.

It is obvious that aluminum activity has a great impact on the aluminide growth rate. However, using high Al-containing alloys at internal trays has potential disadvantages. For this reason, to understand the influence of the aluminum activity on aluminide formation, aluminizing experiments by using alloys containing different Al and Cr compositions (such as 20/80, 30/70, 40/60, 50/50, 60/40, 70/30, 80/20 wt.%) is needed to study as a future work.

- **Issues with pure aluminum at internal trays**

Pure aluminum at internal trays was not included to aluminum activity work plan. At the beginning of this study, an aluminizing experiment was conducted by using pure aluminum pellets at internal trays and faced with some troubles. After several experiments to solve issues, it was decided that using 50/50 Al-Cr alloy at internal trays. Following experiments were performed by using pure aluminum at internal trays and Table 2.11 shows CVD process parameters.

Table 2.11 CVD Process parameters for experiments conducted by using pure aluminum in internal trays.

Exp No	Temperature	Pressure	HCl Flow	H_2 Flow	HCl : H_2	Ar Flow	HCl :Ar	Internal Trays	Time
1	1050 °C	50 mbar	250 sccm	1000 sccm	1:4	500 sccm	1:2	**Pure Al**	4 h
2	950 °C	50 mbar	250 sccm	1000 sccm	1:4	500 sccm	1:2	**Pure Al**	4 h

The first experiment was conducted at 1050 °C chamber temperature and 50 mbar pressure. Relatively high HCl flow (500 sccm) was used by keeping HCl to Ar and H_2 ratio at 1:2 and 1:4, respectively. After 4 hours CVD aluminizing, average 21 µm outer layer and 14 µm IDZ thickness (total = 35 µm) were obtained as shown in Figure 2.26.

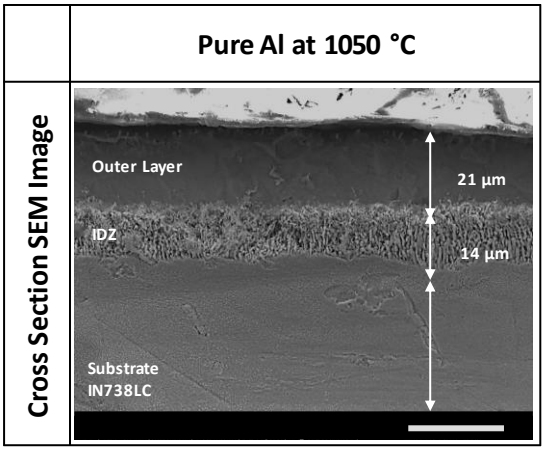

Figure 2.26 Cross-section SEM image of aluminizing sample applied at 1050 °C by using pure Al at internal trays.

Although aluminide coating distribution was homogeneous along the surface, there were local surface deformations at substrate surface caused by free fall of aluminum droplets to surface. After a detailed investigation, aluminum droplets at upper trays were observed and by free fall of these droplets caused surface deformation of samples. Also, it is found that there was a blockage at exhaust graphite insulators because of deposited and liquefied aluminum. Also, the holes of middle graphite insulator were completely obstructed by aluminum as shown in Figure 2.27.

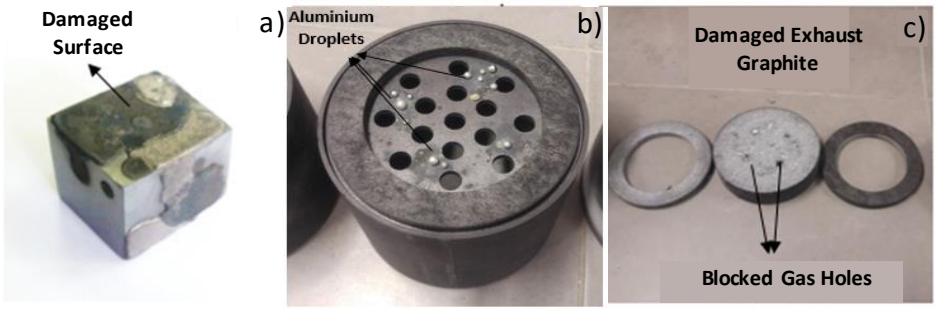

Figure 2.27 Image of surface damaged specimen (a), aluminum droplets formed at graphite trays (b) and blocked gas holes of exhaust insulation graphite due to aluminizing process.

Using pure aluminum pellets at internal trays increased gas phase aluminum activity and caused oversaturation of process gases. As a result of oversaturation, exhaust graphite blocked and sample surface damaged due to Al droplets.

In the second experiment, chamber temperature was decreased from 1050 °C to 950 °C by keeping all CVD parameters constant to decrease aluminum saturation of process gases. At 950 °C, average 14 µm outer layer and 7 µm IDZ thickness (total = 21 µm) were obtained as shown in Figure 2.28. 100 °C decrease in chamber temperature caused 14 µm decrease in total aluminide coating thickness due to lower aluminum saturation of process gases.

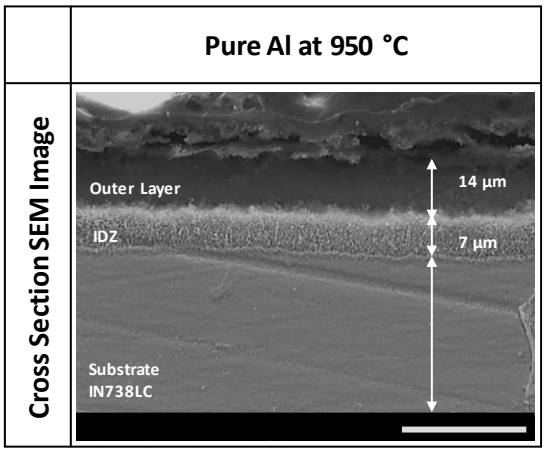

Figure 2.28 Cross-section SEM image of aluminizing sample applied at 950 °C by using pure Al at internal trays.

However, exhaust graphite insulators were partially blocked and sample surfaces were locally damaged. Because of the low melting point of pure aluminum (660.37 °C) [83], aluminum pellets loaded to internal trays melts at process temperatures and caused oversaturation of process gases. Therefore, internal trays were left empty in following experiments to prevent surface deformation and exhaust blockage problem by lowering oversaturation of process gases. Following two experiments were conducted with empty internal trays by using CVD parameters shown in Table 2.12.

Table 2.12 CVD Process parameters for experiments conducted with empty internal trays.

Exp No	Temperature	Pressure	HCl Flow	H_2 Flow	HCl : H_2	Ar Flow	HCl: Ar	Internal Trays	Time
3	1050 °C	50 mbar	250 sccm	1000 sccm	1:4	500 sccm	1:2	**Empty**	4 h
4	1050 °C	50 mbar	125 sccm	500 sccm	1:4	250 sccm	1:2	**Empty**	4 h

The third experiment was conducted by using similar CVD parameters in the first experiment. The only difference was internal trays not loaded by aluminum source and only aluminum chloride generator was used to form aluminum chloride gases. After aluminizing, SEM analysis showed that aluminum was not deposited at surfaces and there was no sign of aluminide coating as shown in Figure 2.29.

However, by using same CVD parameters with pure aluminum pellets at internal trays, 35 µm total aluminide thickness was obtained in experiment 1. One of the reasons of loading internal trays by aluminum source is to decrease the amount of excess HCl gas at coating chamber because unreacted HCl transferred from aluminum chloride generator acts as etchant and etches the substrate surface during aluminizing process. Therefore, in experiment 4, to decrease the amount of unreacted HCl at coating chamber, HCl gas flow was decreased from 250 sccm to 125 sccm by keeping HCl:Ar and HCl:H_2 ratio constant. After SEM analysis, no aluminide coating was observed at substrate surface similar to experiment 3.

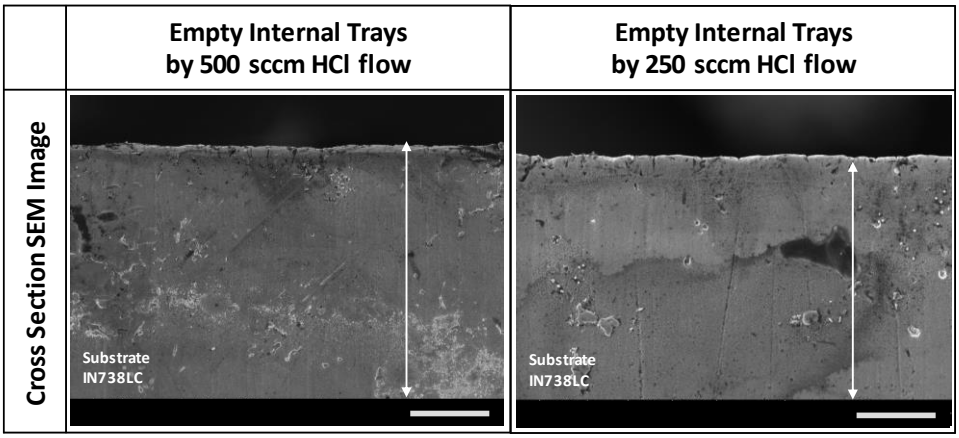

Figure 2.29 Cross-section SEM image of aluminizing sample applied at 1050 °C with empty internal trays.

Results showed that aluminum deposition did not occur without using aluminum source at internal trays. Two possible reasons are indicated below:

1 - Unreacted HCl transferred from aluminum chloride generator to coating chamber etches substrate surfaces faster than aluminum deposition rate.

2- Partial pressures of aluminum sub-chloride gases is too low for deposition of aluminum at substrate surface due to low aluminum activity in the gas phase.

Both possible reasons indicate that net reaction rate in the chlorinator is not sufficient to consume HCl gas completely. To analyze the reaction efficiency, Al consumption in the chlorinator was calculated by following equation, and results were compared to actual Al consumption in the chlorinator.

$$\frac{HCl\ Flow\ Rate\left(\frac{\mathrm{L}}{min}\right) x\ Process\ Time(min)}{Molar\ Volume\ of\ Gas\ (L/mol)}\ x\ \frac{Moler\ Mass\ of\ Aluminum\ (g)}{\substack{HCl\ mole\ for\ per\ mole\ of\ Aluminum \\ (according\ to\ related\ chemical\ reaction)}} \quad (1)$$

According to following chemical reaction, per mole of HCl reacts with 1/3 mole of aluminum in the chlorinator when aluminum sub-chloride formation reactions are ignored due to lower driving force.

- $Al + 3HCl = AlCl_3 + 3/2H_2$

For the comparison of actual Al consumption with calculated value, weight of aluminum pellets in the chlorinator was measured before long term usage (50 h). After 50 hours aluminizing process (total), weight of the aluminum pellets left in the chlorinator was measured again and actual Al consumption was calculated. Weight analysis showed that almost 55 g. excess aluminum was present in the chlorinator for 50 hours operation. Results demonstrate that HCl did not react with aluminum completely. Therefore, small amount of unreacted HCl is transferred to coating chamber which adversely affects Al deposition rate in the absence of aluminum source at internal trays.

To eliminate problems mentioned above, internal trays must be loaded by aluminum source; however, pure aluminum pellets causes surface deformation and exhaust

blockage. Therefore, in experiment 5, Al-Cr (50/50 wt.%) alloy pieces were used increase not only partial pressure of aluminum sub-chloride gases but also prevent surface damage and exhaust blockage. Aluminizing was performed by using same CVD parameters (Table 2.13) with experiment 2.

Table 2.13 CVD Process parameters for experiments conducted with Al-Cr alloy (50/50 wt. %) at internal trays.

Exp No	Temperature	Pressure	HCl Flow	H_2 Flow	HCl : H_2	Ar Flow	HCl: Ar	Internal Trays	Time
5	950 °C	50 mbar	250 sccm	1000 sccm	1:4	500 sccm	1:2	**Al-Cr**	4 h

SEM analysis after aluminizing showed that 9 µm outer layer and 7 µm IDZ thickness (total = 16 µm) were obtained by using Al-Cr pieces at internal trays as shown in Figure 2.30. Coating growth rate relatively decreased by using Al-Cr pieces than pure aluminum pellets. Although lower deposition rate was obtained by Al-Cr pieces, exhaust blockage problem was completely prevented. Small surface damages caused by free fall of Al droplets from upper trays were noticed. Detailed investigation showed that only few Al droplets deposited and liquefied at upper graphite trays. To inhibit surface destruction completely, a carbon filter was placed between sample and upper trays and control experiment showed that surface damage of substrates was fully prohibited.

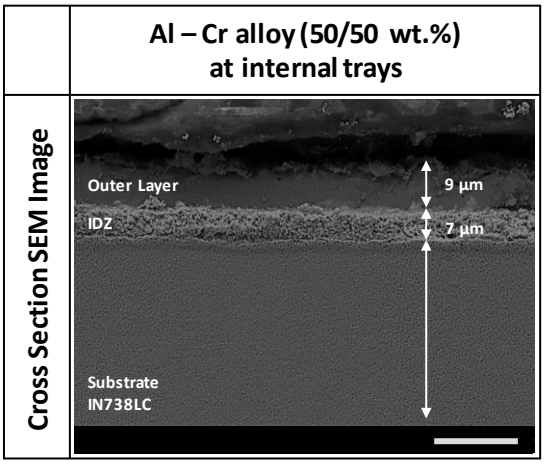

Figure 2.30 Cross-section SEM image of aluminizing sample applied at 950 °C by using 50/50 wt. % Al-Cr alloy at internal trays.

Using the 50/50 wt. % Al-Cr alloy was decided in consideration of issues faced by using pure aluminum at internal trays. In this study, therefore, 50/50 wt. % Al-Cr alloy was used in all aluminizing processes except aluminum activity experiments. To observe the influence of aluminum activity on coating formation, 70/30 wt.% Al-Cr alloy was used at internal trays and no exhaust graphite blockage or surface deformation observed. Following 3 experiment set was performed to investigate effect chamber temperature, gas flows and system pressure on aluminide coating when using 70/30 wt.% Al-Cr alloy at internal trays.

2.3.1.6.1 Effect of Temperature

In previous studies, the effect of chamber temperature on aluminide formation has been studied by using 50/50 wt.% Al-Cr alloy at internal trays. However, when Al content of Al-Cr alloy was increased to 70 wt.%, a significant increase in aluminide coating growth rate have been obtained. Accordingly, it is possible to achieve high growth rate at lower chamber temperatures by using 70/30 wt.% Al-Cr alloy. Therefore, the influence of coating chamber temperature on aluminide coating growth rate has been investigated to decrease aluminizing process temperature by keeping growth rate relatively high. The CVD coating parameters for the experiments are shown in Table 2.14.

Table 2.14 CVD Process parameters for experiments conducted with 70/30 wt. % Al-Cr alloy at 1000, 1050 and 1100 °C chamber temperature.

Temperature	Pressure	HCl Flow	H_2 Flow	HCl : H_2	Ar Flow	HCl:Ar	Internal Trays	Time
1100 °C	100 mbar	125 sccm	250 sccm	1:2	250 sccm	1:2	**Al-Cr (70/30)**	4 h
1050 °C	100 mbar	125 sccm	250 sccm	1:2	250 sccm	1:2	**Al-Cr (70/30)**	4 h
1000 °C	100 mbar	125 sccm	250 sccm	1:2	250 sccm	1:2	**Al-Cr (70/30)**	4 h

The aim of the study was to reduce the aluminizing process temperature. Thus the adverse effect of the high temperature CVD process on the IN738 LC microstructure and mechanical properties could be minimized. The effects of different aluminizing process temperatures on the IN738 LC microstructure were studied by colleague graduate student Mustafa Tarık Boyraz and it is observed that 1100 °C chamber temperature is too high to obtain desired microstructure. In this context, two different aluminizing experiments have been carried out at 1050 °C and 1000 °C chamber temperature by keeping other process parameters constant.

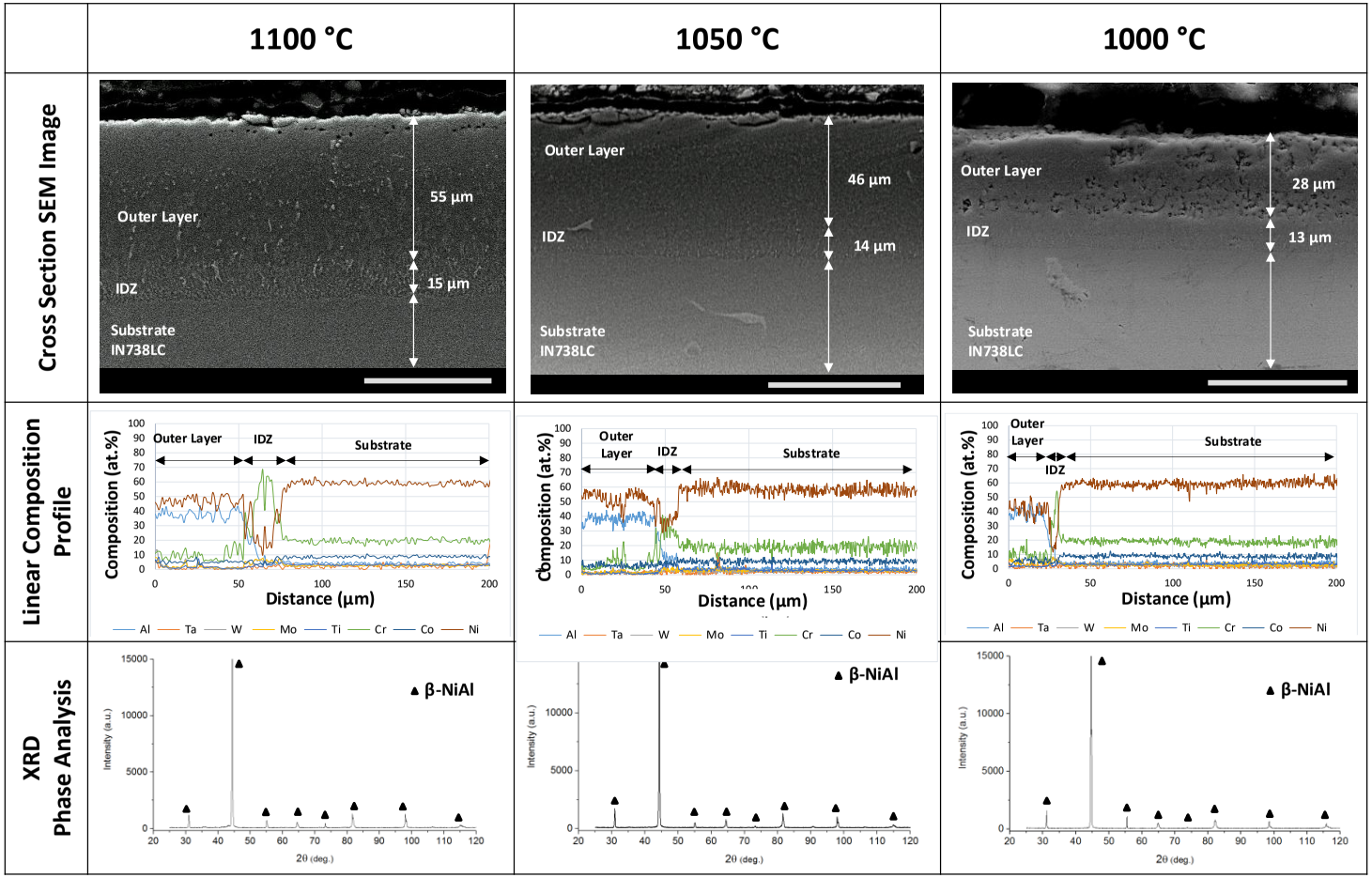

Figure 2.31 Cross section SEM images (The scale bar = 50 µm), linear composition profile and XRD pattern of aluminide coatings applied by using 70/30 wt. % Al-Cr alloy at 1000, 1050 and 1100 °C chamber temperature.

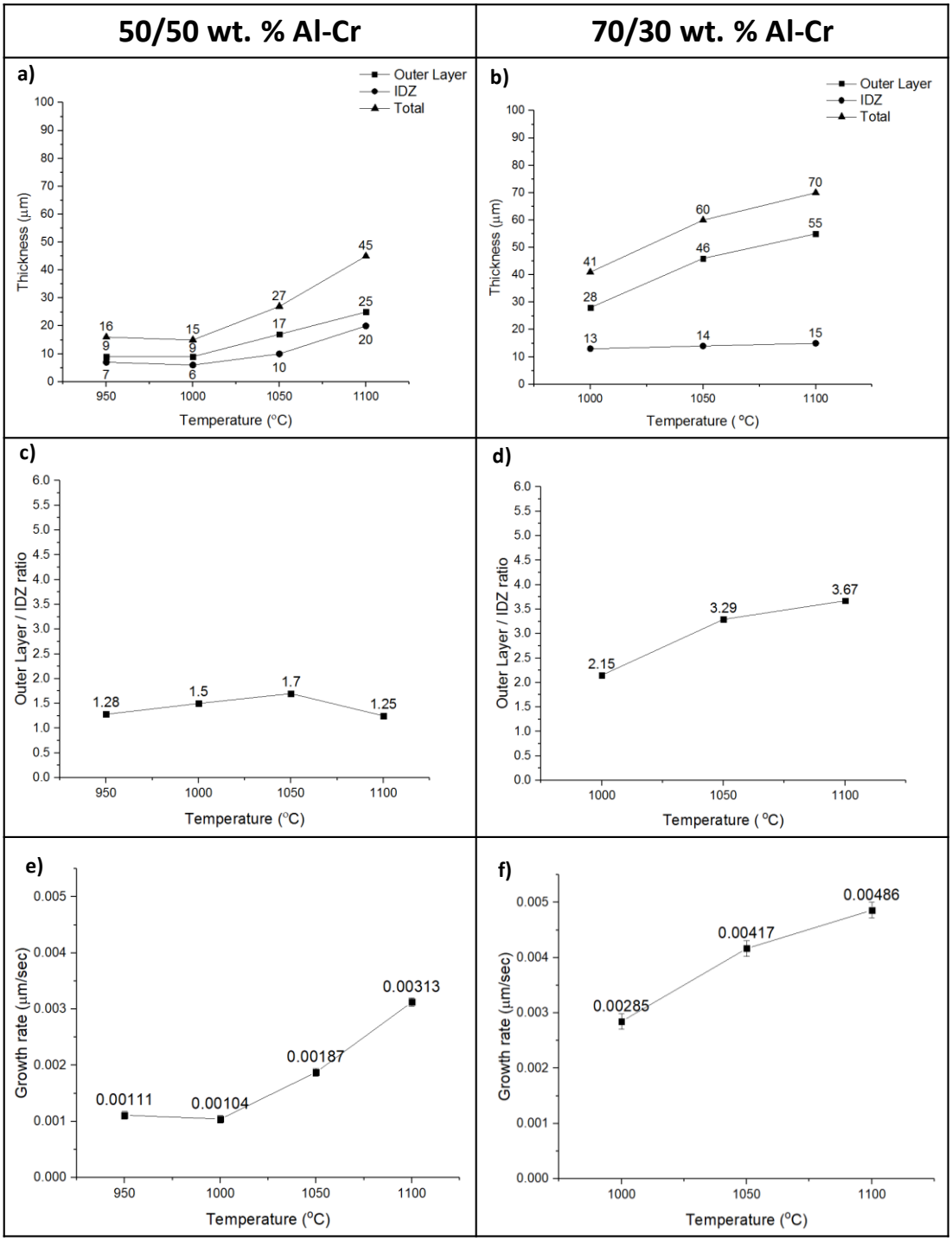

Figure 2.32 (a) Outer layer, IDZ and total aluminide coating thickness change by 50/50 wt. %, (b) 70/30 wt. % Al-Cr alloy, (c) outer layer/IDZ ratio change by 50/50 wt. %, (d) 70/30 wt. % Al-Cr alloy, (e) growth rate change by 50/50 wt. %, (f) 70/30 wt. % Al-Cr alloy; depending on chamber temperature.

When the chamber temperature is reduced from 1100 ° C to 1050 ° C, the thickness of the outer coating layer decreased from 55 μm to 46 μm (Fig. 2.31 and 2.32). However, no significant change in IDZ thickness was observed and it decreased from 15 μm to 14 μm. The outer layer / IDZ ratio decreased from 3.67 to 3.29. When the furnace temperature is reduced to 1000 °C, 28 μm outer coating and 13 μm IDZ thickness was obtained. The outer coating / IDZ ratio decreased to 2.15. It is seen that the aluminide coating growth rate and the outer coating / IDZ ratio are noticeably high even at 1000 °C when 70/30 wt.% alloy was used at internal trays (Fig. 2.32). Because by using 50/50 wt.% Al-Cr, similar coating thickness was only achieved at 1100 °C.

The compositional analysis showed that there is 33-45% aluminum along outer coating layer independent of chamber temperature. When the microstructure of the coating was examined more closely, it was observed that homogeneously dispersed Cr precipitates were present in the outer coating region near to IDZ interface. The high temperature oxidation and corrosion resistance of aluminide coatings obtained by using 70/30 wt. % Al-Cr is not known yet. However, great progress has been achieved with respect to the 50/50 wt.% Al-Cr alloy in terms of aluminide coating growth rate and the outer coating/IDZ ratio.

2.3.1.6.2 Effect of Gas Flows

Because of high partial pressures of aluminum sub-chloride gasses were obtained by 70/30 Al-Cr alloy, the effect of higher HCl gas flow was investigated by doubled up HCl gas flow together with H_2 and Ar gas flows at 1050 ° C (100 mbar). It is aimed to increase the growth rate by increasing partial pressures of $AlCl_3$, $AlCl_2$ and AlCl gasses in the coating chamber by increasing HCl amount. Table 2.15 shows CVD aluminizing parameters for experiments conducted with 70/30 wt. % Al-Cr alloy by 125, 250 and 500 sccm HCl flow.

Table 2.15 CVD Process parameters for experiments conducted with 70/30 wt. % Al-Cr alloy by 125, 250 and 500 sccm HCl flow.

Temperature	Pressure	HCl Flow	H_2 Flow	HCl : H_2	Ar Flow	HCl:Ar	Internal Trays	Time
1050 °C	100 mbar	125 sccm	250 sccm	1:2	250 sccm	1:2	**Al-Cr (70/30)**	4 h
1050 °C	100 mbar	250 sccm	500 sccm	1:2	500 sccm	1:2	**Al-Cr (70/30)**	4 h
1050 °C	100 mbar	500 sccm	1000 sccm	1:2	1000 sccm	1:2	**Al-Cr (70/30)**	4 h

As a result of the aluminizing experiments, the outer coating increased from 46 μm to 65 μm and IDZ thickness decreased from 14 μm to 12 μm when HCl gas flow increased from 125 sccm to 250 sccm as shown in Figure 2.33. Higher growth rates and outer layer/IDZ ratios were obtained with the aluminizing carried out at 1050 °C with 250 sccm HCl flow than at 1100 ° C with 125 sccm HCl flow.

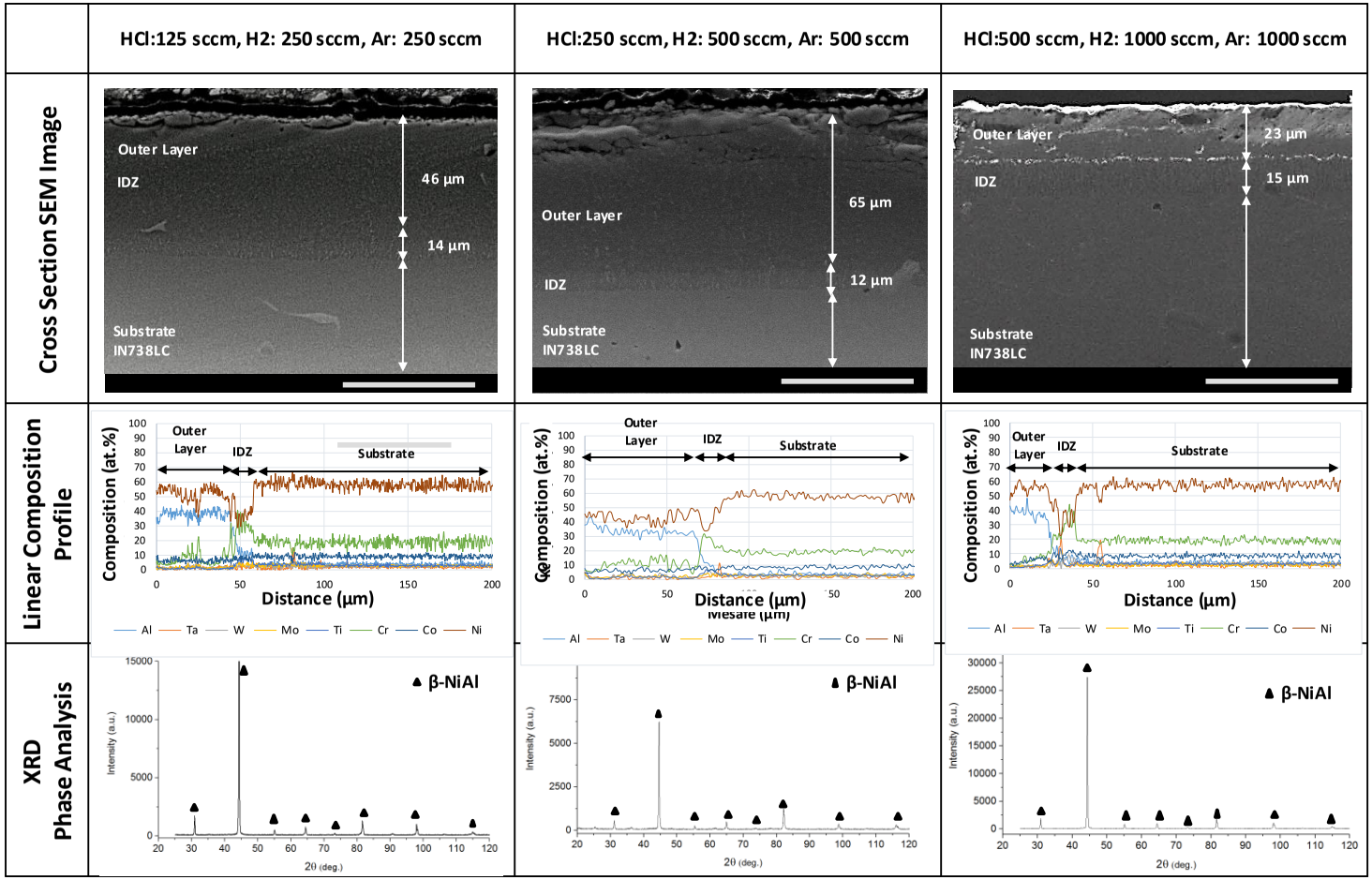

Figure 2.33 Cross section SEM images (The scale bar = 50 µm), linear composition profile and XRD pattern of aluminide coatings applied by using 125, 250 and 500 sccm HCl flow with 70/30 wt. % Al-Cr alloy at internal trays; for constant HCl:H_2 = 1:2 and HCl:Ar = 1:2 ratio.

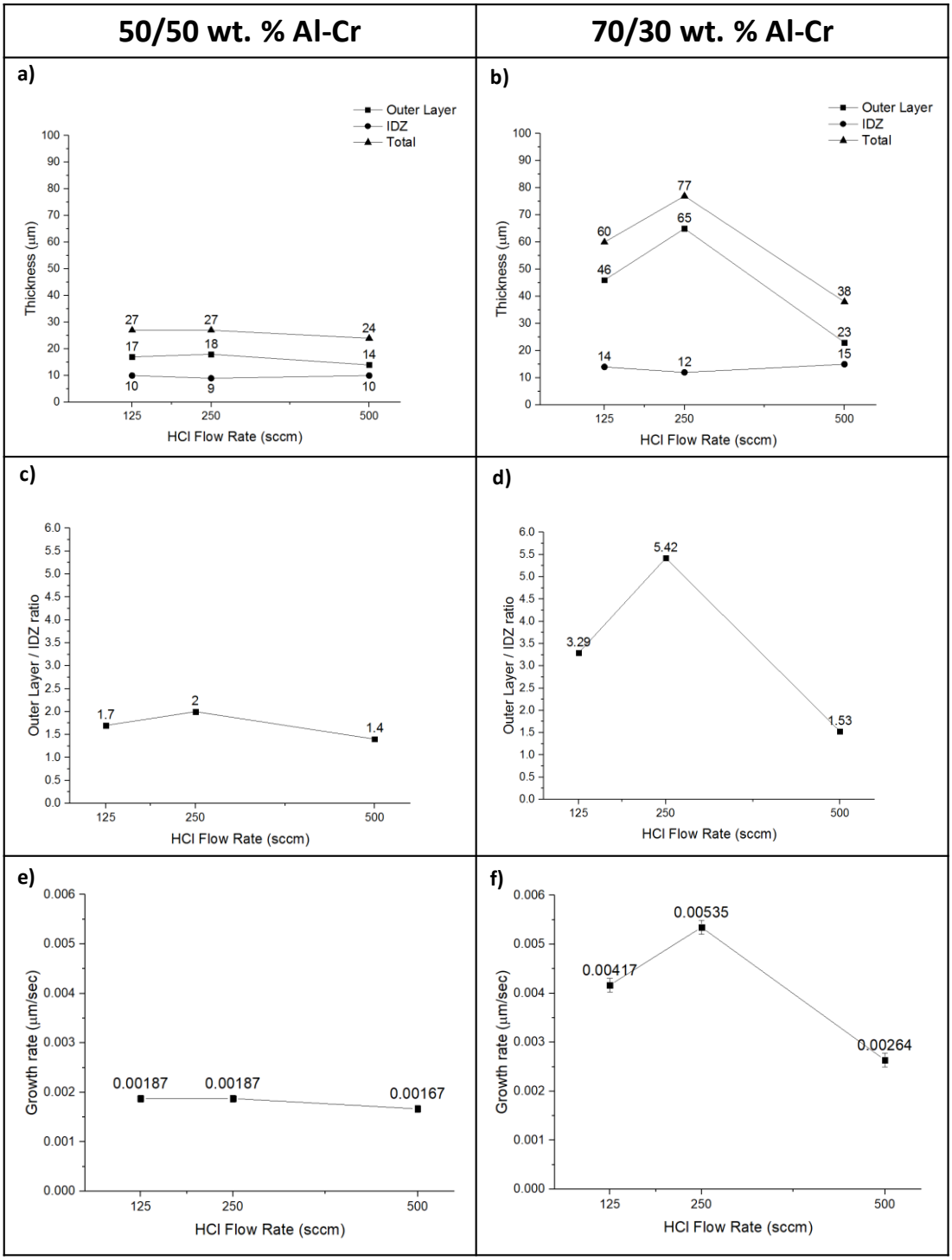

Figure 2.34 Outer layer, IDZ and total aluminide coating thickness change (a), outer layer/ IDZ ratio change (b) depending on gas flows, (e) growth rate change by 50/50 wt. %, (f) 70/30 wt. % Al-Cr alloy; for constant $HCl:H_2$ = 1:2 and HCl:Ar = 1:2 ratio.

Deposition rate has been increased by increasing the gas flows to two times at constant temperature and pressure. However, such effect of higher HCl flow has not been observed when 50/50 wt.% Al-Cr used at internal trays. It is assumed that higher HCl flow rates need more than 50 wt.% Al at internal trays to react and form aluminum chloride and sub-chloride gases. Therefore, the positive effect of higher HCl on growth rate have been observed when 70 wt.% Al containing alloy used at internal trays. On the other hand, when HCl flow increased from 250 sccm to 500 sccm, a significant decrease in growth rate and outer layer/IDZ ratio was observed (Fig. 2.34). A possible reason of such a massive decrease is the presence of unreacted HCl at coating chamber. While formation rate of aluminum chlorides at chlorinator is limited by the surface area of Al source (pellets), the amount of unreacted HCl transferred from the chlorinator to chamber increased by increasing HCl flow. Etching effect of HCl decreased the growth rate of the coating. Hence 23 μm outer layer and 15 μm IDZ thickness were obtained. Therefore, it is obvious that optimum HCl flow is around 250 sccm.

The amount of aluminum chloride gases was considerably increased by replacing 50/50 Al-Cr alloy with 70/30 Al-Cr alloy and optimizing the CVD process variables. As a result of increased partial pressures of aluminum sub-chloride gasses, the effect of system pressure on partial pressures of process gases could be more apparent. Therefore, the effect of lower and higher system pressure on aluminide coating formation was investigated by performing aluminizing experiments at 50 and 200 mbar system pressures.

2.3.1.6.3 Effect of System Pressure

The effects of the system pressure on the aluminide coating formation were examined by performing aluminizing experiments with 70/30 Al-Cr alloy. Two more aluminizing experiments were conducted at 50 and 200 mbar by using CVD parameters given in Table 2.16. Results were compared with the previously obtained coating at 100 mbar.

Table 2.16 CVD Process parameters for experiments conducted with 70/30 wt. % Al-Cr alloy at 50, 100 and 200 mbar system pressure.

Temperature	Pressure	HCl Flow	H_2 Flow	HCl : H_2	Ar Flow	HCl:Ar	Internal Trays	Time
1050 °C	50 mbar	250 sccm	500 sccm	1:2	500 sccm	1:2	**Al-Cr (70/30)**	4 h
1050 °C	100 mbar*	250 sccm	500 sccm	1:2	500 sccm	1:2	**Al-Cr (70/30)**	4 h
1050 °C	200 mbar	250 sccm	500 sccm	1:2	500 sccm	1:2	**Al-Cr (70/30)**	4 h

* Previous experiment

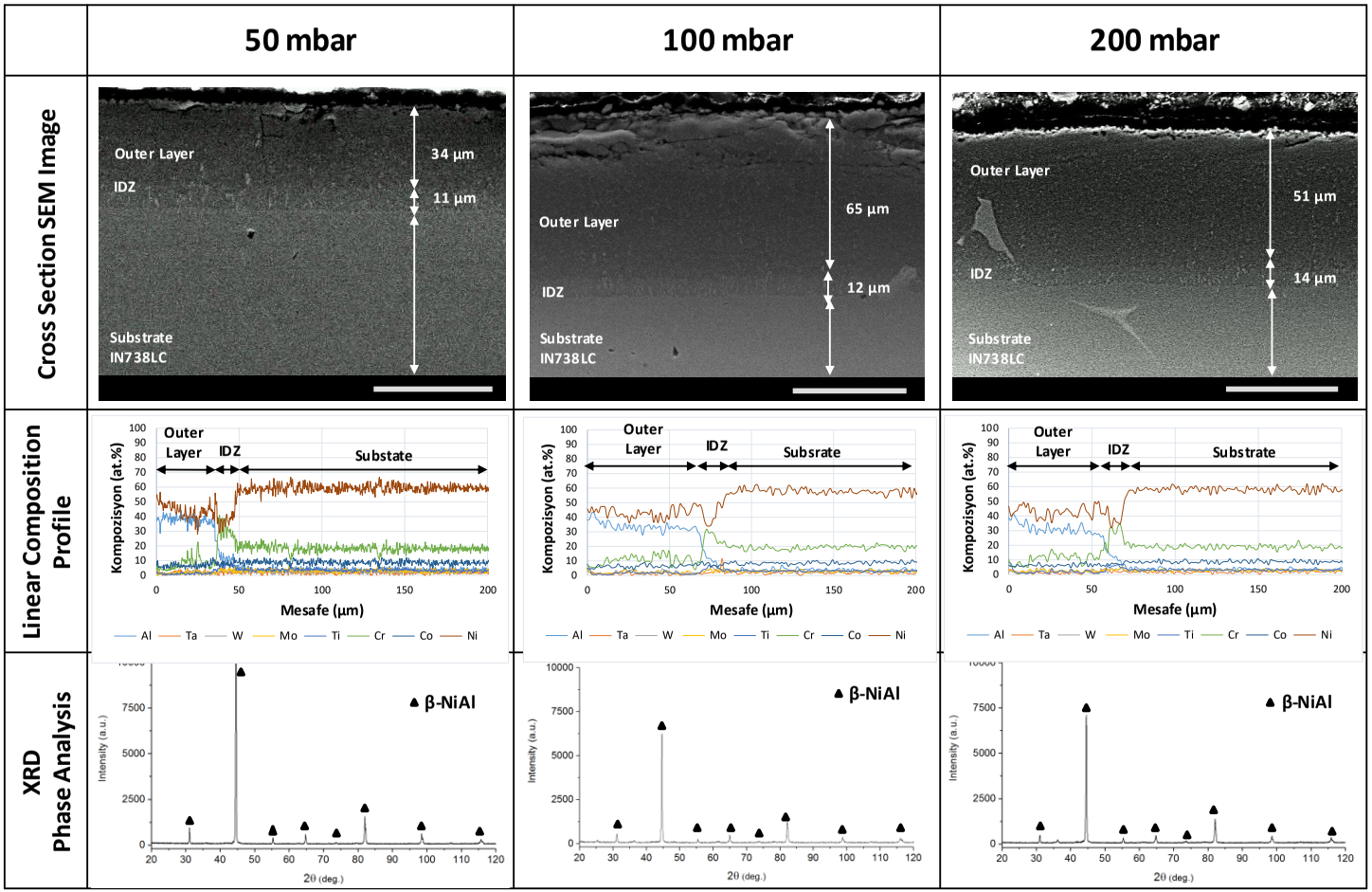

Figure 2.35 Cross section SEM images (The scale bar = 50 µm), linear composition profile and XRD pattern of aluminide coatings applied by using 70/30 wt. % Al-Cr alloy at 50, 100 and 200 mbar system pressure.

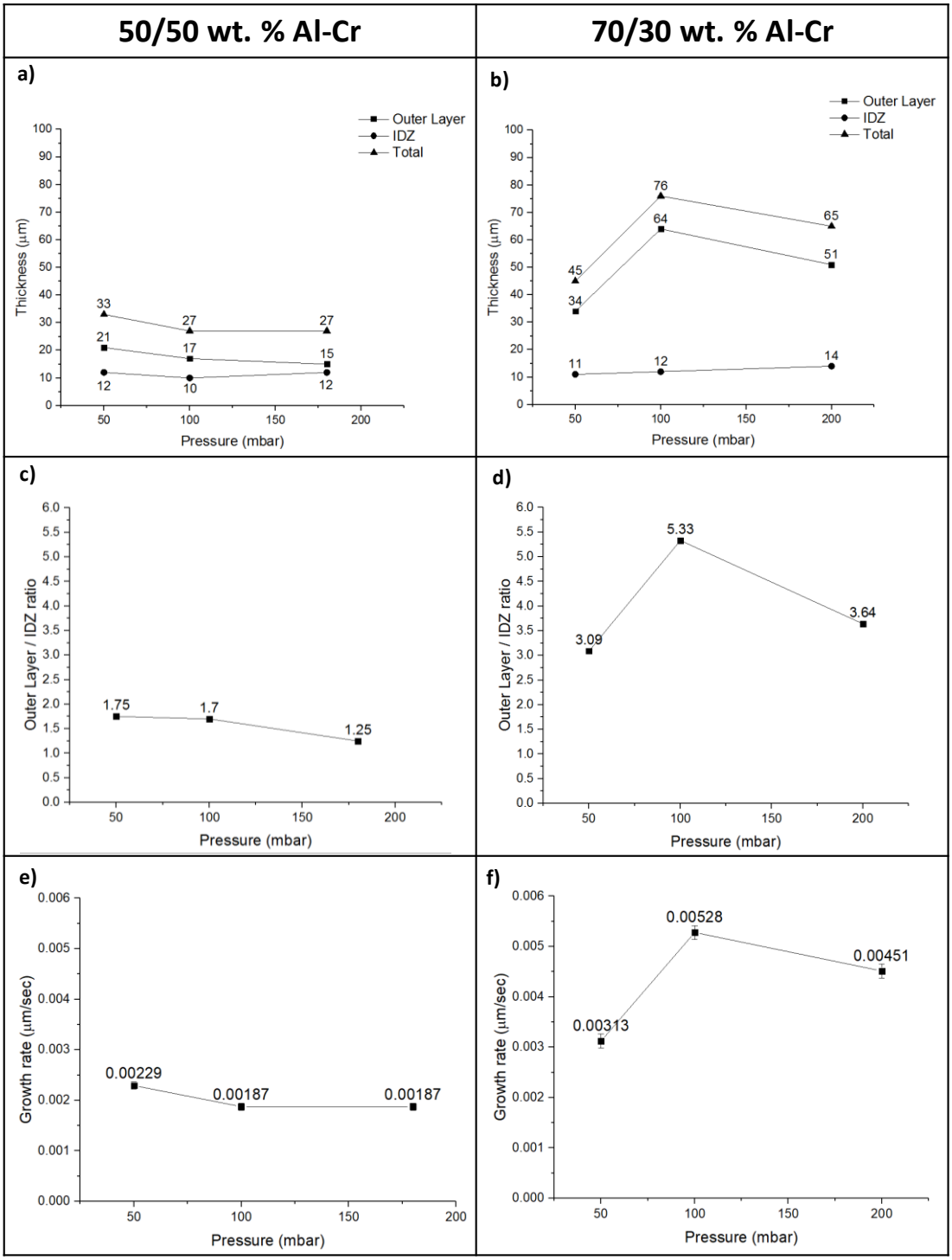

Figure 2.36 Outer layer, IDZ and total aluminide coating thickness change by 50/50 wt. % (a), 70/30 wt. % (b) Al-Cr alloy, outer layer/IDZ ratio change by 50/50 wt. % (c), 70/30 wt. % (d) Al-Cr alloy, (e) growth rate change by 50/50 wt. %, (f) 70/30 wt. % Al-Cr alloy; depending on system pressure.

When system pressure was reduced from 100 mbar to 50 mbar, a significant reduction in coating thickness was observed by 34 µm outer coating and 11 µm IDZ thickness as shown in Figure 2.35 and 2.36. Similarly, when the pressure was increased from 100 mbar to 200 mbar, the outer coating thickness decreased from 65 µm to 51 µm and the IDZ thickness increased from 12 µm to 14 µm. The pressure experiments show that the highest aluminide coating growth rate was obtained at 100 mbar pressure (Fig. 2.36 (f)). It is believed that the partial pressure of aluminum chloride gases decreased when system pressure decreased to 50 mbar. Therefore, the optimum growth rate was obtained at 100 mbar.

2.3.1.7 Process Time

Aluminizing is a solid state diffusion controlled process and follows parabolic rate law [77]. That means with increasing the process time, growth rate decreases by following the parabolic law. Therefore, to observe the effect of time on aluminide coating formation, three aluminizing experiments were performed for 4, 8, 12 hours by using identical process parameters as given in Table 2.17.

Table 2.17 CVD parameters of process time experiments conducted for 4, 8 and 12 hours.

Temperature	Pressure	HCl Flow	H_2 Flow	HCl : H_2	Ar Flow	HCl:Ar	Internal Trays	Time
1100 °C	100 mbar	125 sccm	1000 sccm	1:8	250 sccm	1:2	Al-Cr (50/50)	4 h
1100 °C	100 mbar	125 sccm	1000 sccm	1:8	250 sccm	1:2	Al-Cr (50/50)	8 h
1110 °C	100 mbar	125 sccm	1000 sccm	1:8	250 sccm	1:2	Al-Cr (50/50)	12 h

Figure 2.37 shows cross section SEM analysis of aluminide coatings. By 4 hours aluminizing process, 25 µm outer layer and 20 µm IDZ thickness (45 µm total) were obtained. When aluminizing time increased two times to 8 hours, outer layer thickness increased to 38 µm and IDZ thickness to 24 µm (62 µm total). While process time increased twice, total coating thickness increased only 37%. Similarly, 45 µm outer and 28 µm IDZ thickness (73 µm total) were obtained after 12 hours aluminizing. Even process time increased three times, the coating thickness only increased less than twice.

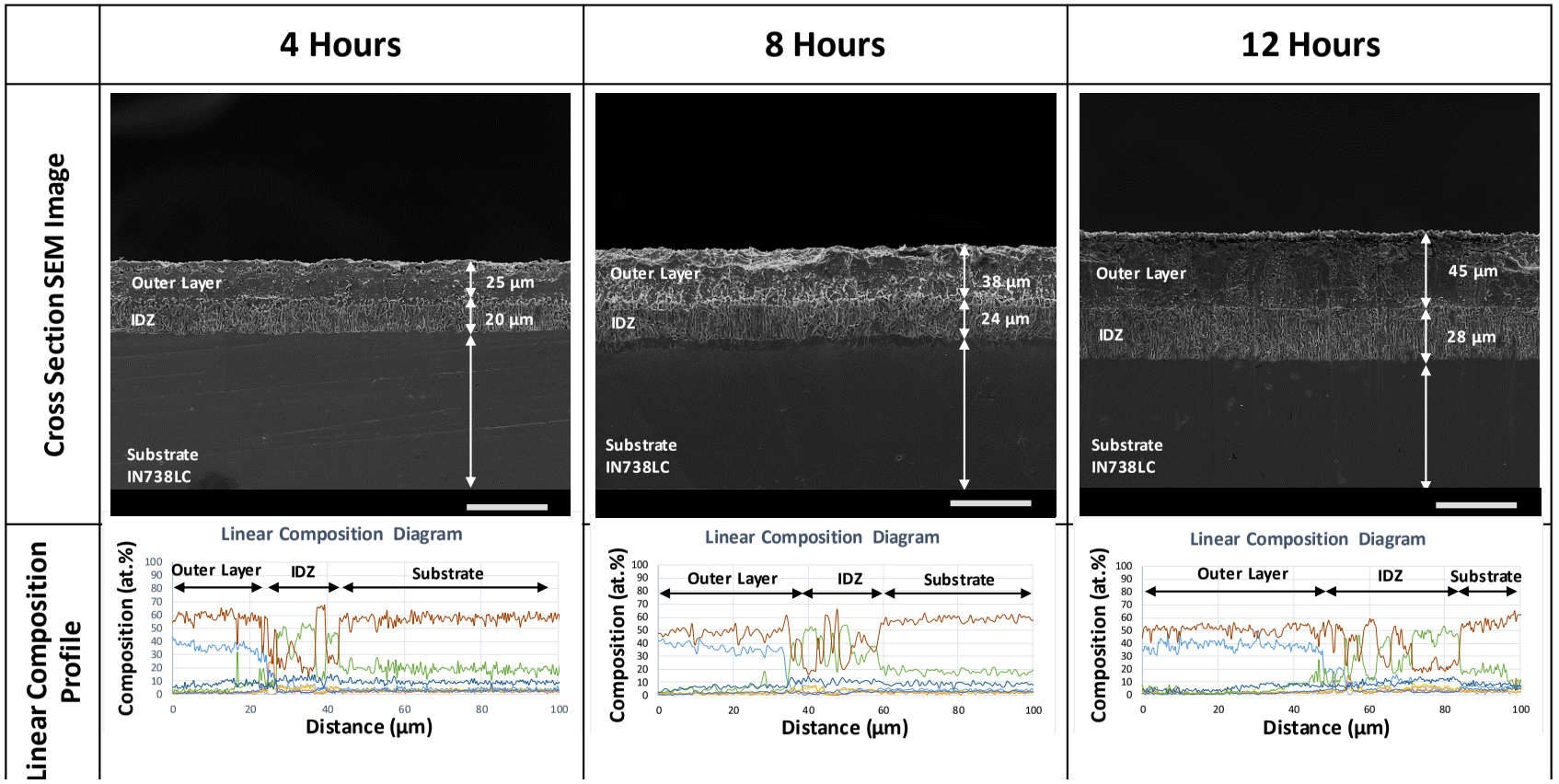

Figure 2.37 Cross section SEM images (The scale bar = 50 µm) and linear composition profile of aluminide coatings applied for 4, 8 and 12 hours.

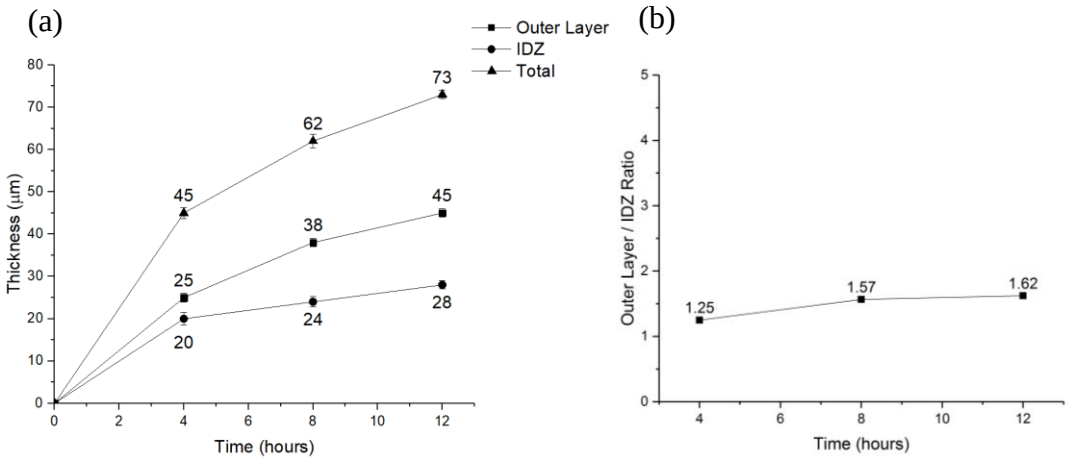

Figure 2.38 (a) Outer layer, IDZ and total aluminide coating thickness change, (b) outer layer/ IDZ ratio change depending on aluminizing process time.

Coating thicknesses were plotted against time as shown in Figure 2.38 (a) and graph extrapolated to zero value. It is obvious that maximum growth rate was obtained at the beginning of the process and then the growth rate decreased by following the parabolic rate law. Hickl and Heckel (1975) stated that aluminizing process obeys parabolic rate law after initial transient period [61]. Results showed that to increase process time does not mean a linear increase in coating thickness. Therefore, optimizing the CVD parameters is important production criteria for the feasibility of aluminizing process.

2.3.2 Effect of Surface Roughness on Aluminide Coating

Aluminide coating thickness and its homogeneity are directly affected by the surface roughness of substrate prior to aluminizing. Also, adhesion of thermally grown oxide that is α-Al_2O_3 for aluminide coatings could be influenced by the surface roughness of aluminide coating. Figure 2.39 shows that separation of TGO layer from the aluminide coating. Separation continues with cracking of oxide layer; hence the degradation of the coating system.

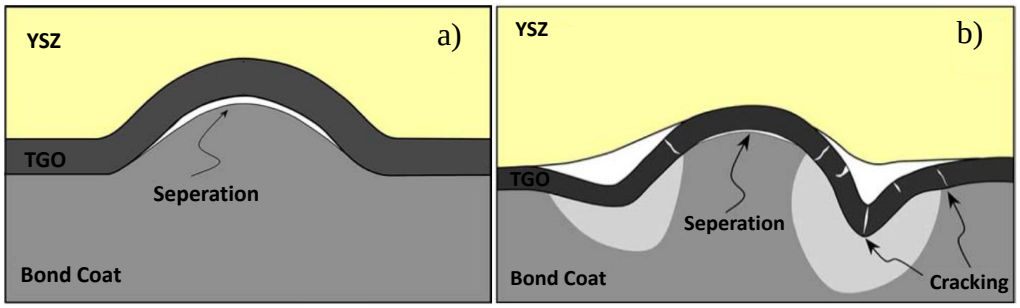

Figure 2.39 Illustration of TGO and thermal barrier coating failure due to bond coat surface geometry [84].

Surface roughness could be controlled and minimized easily for the substrates used in aluminizing experiments because of sample sizes. However, the surface roughness of turbine blades has importance due to difficulty in surface treatment processes such as grinding or blasting. Therefore, optimization of turbine blade surfaces by proper surface treatment methods is important production criteria. To reveal the importance of surface roughness, the effect of surface roughness prior to aluminizing on the physical and chemical properties of the aluminide coating was investigated. For this aim, surfaces of four specimens were ground by SiC paper have different grid size. Surfaces of the fifth sample were left as received (sandblasted casting surface) as shown in Figure 2.40.

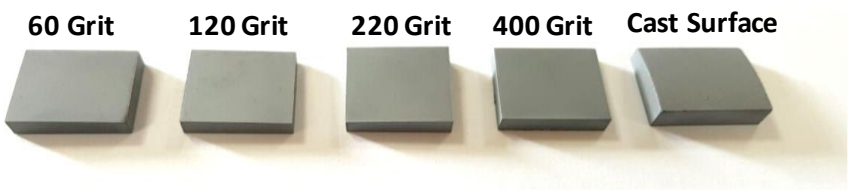

Figure 2.40 Images of test samples ground by 60, 120, 220, 400 grit SiC emery paper and test sample having cast surface.

After surface preparation, all samples were subjected to surface roughness measurement and were coated simultaneously by CVD aluminizing. After aluminizing surface roughness of samples were measured again to see any change. The results of the roughness measurements are shown in Table 2.18.

Table 2.18 Surface roughness measurements of specimens having varying surface roughness before and after CVD aluminizing.

Surface Roughness Measurements										
	60 Grid SiC		**120 Grid SiC**		**220 Grid SiC**		**400 Grid SiC**		**Cast Surface**	
	Before	After	Before	After	Before	After	Before	After	Before	After
Ra(µm)	0.287	0.946	0.190	0.887	0.097	0.864	0.067	0.773	2.947	2.726
Rz(µm)	2.428	6.840	1.608	6.828	0.995	6.361	0.773	5.821	18.358	16.440

It has been observed that the Ra and Rz values of all samples have ground surfaces were increased after the aluminide coating process. The highest increment in Ra and Rz values after aluminizing was observed on the sample ground by 400 grid SiC (Ra = 1150% increase, Rz = 750% increase). Moreover, the lowest increment was observed on sample ground by 60 grit SiC (Ra = 330% increase, Rz = 280% increase). On the contrary to the ground surfaces, the sample having cast surface showed 8% decrease in Ra and 11% in Rz after aluminizing.

In addition to surface roughness measurements, cross-sectional SEM examinations of all samples are shown in Figure 2.41.

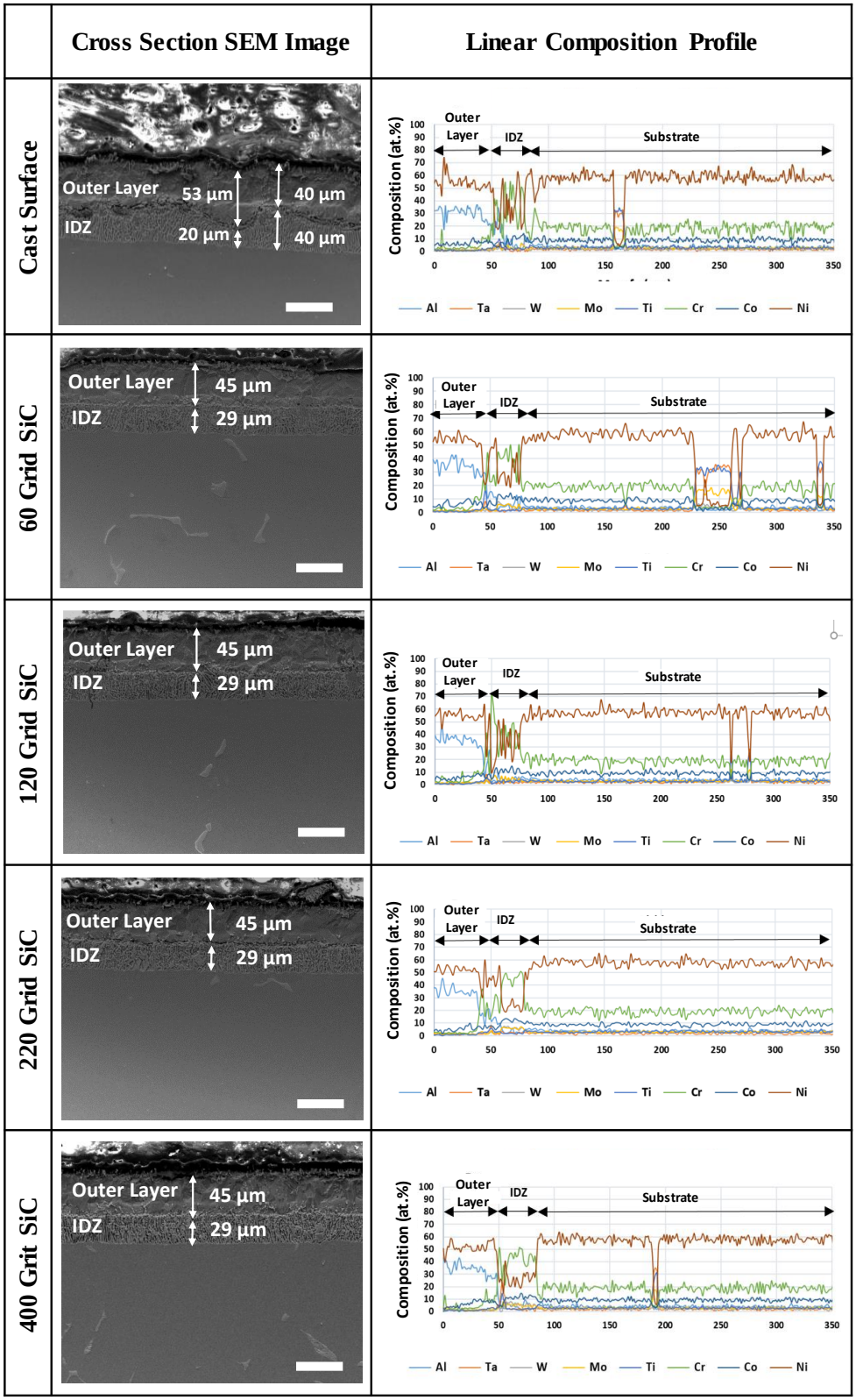

Figure 2.41 Cross section SEM images and EDS linear composition profile of aluminide coatings deposited on samples having altering surface roughness (The scale bar = 50 µm).

By cross-sectional SEM analysis, it was observed that the thickness of the outer coating zone of the sample have casting surface had changed between 40 - 53 μm and the IDZ thickness had changed in the range of 20 - 40 μm. Consequently, the total coating thickness was changing between 70 - 80 μm. In the samples having ground surfaces by 60, 120, 220 and 400 grit SiC, the coating thickness was measured as 45 μm outer layer and 29 μm IDZ (total 74 μm). It was determined that the average coating thicknesses were identical for ground samples regardless of SiC grit size and were altering within +/- 3 μm across the coating surface. On the other hand, the coating thickness of cast surface sample was heterogeneous with respect to the ground samples. Besides heterogeneous aluminide coating, surface cracks were found in the sample having cast surface. However, no surface cracks were observed in ground samples.

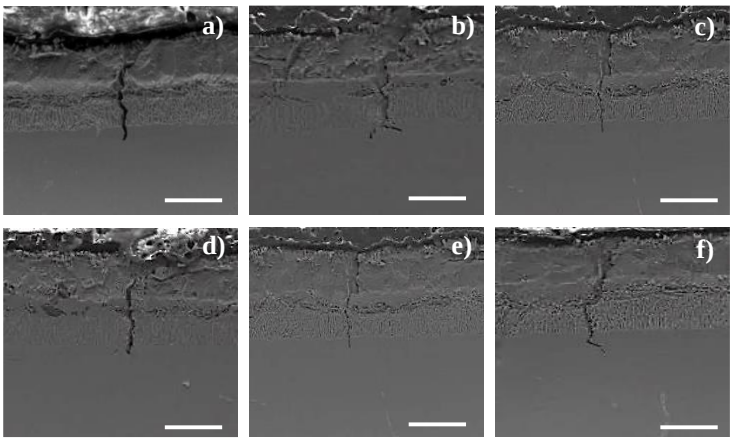

Figure 2.42 Surface crack analysis by cross section SEM images (The scale bar = 50 μm) of aluminide coating deposited on IN738LC specimen having cast surface.

Several surface cracks were observed along the aluminide coating cross-sectional region which is 20 mm in length (Fig. 2.42). The surface cracks in the coating layer could promote oxide layer (TGO) spallation in service condition; consequently, result in the consumption of substrate material due to internal oxidation and corrosion. To find the origin of surface cracks, an uncoated IN738 LC sample having cast surface were analyzed by SEM in cross-section (Fig. 2.43). Along the cast surface, there were many surface defects, voids, and cracks present. All surface imperfections prior to

aluminizing caused heterogeneous aluminide distribution and local coating cracks. Eventually, surface cracks and defects exist on aluminide coating would negatively affect the service life of the aluminide coating.

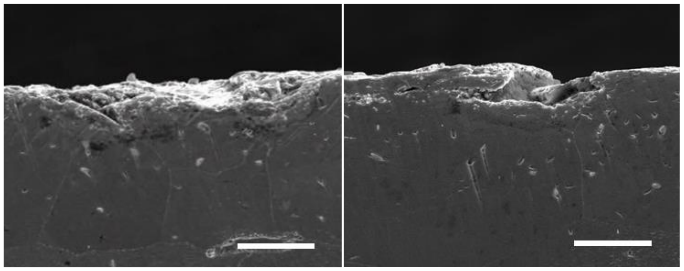

Figure 2.43 Surface morphology analysis by cross section SEM images (The scale bar = 50 µm) of uncoated IN738 LC specimen having cast surface.

2.3.3 Effect of Sample Thickness on Aluminide Coating

Turbine blades have a complex geometry including thin edges and thick body. Since aluminizing is a diffusion controlled process, the influence of sample thickness on growth kinetics was studied by using two different IN 738 LC samples having different thickness. The thin sample was sectioned from the edge of the turbine blade, while the thick sample was sectioned from the body of the turbine blade (Fig. 2.44).

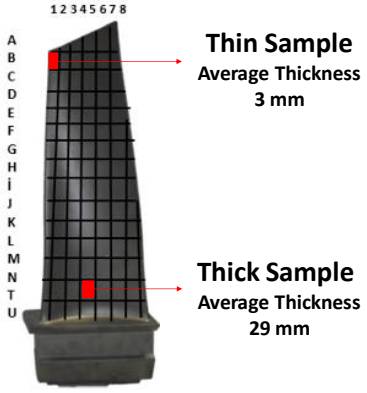

Figure 2.44 Original sample location of thin and thick samples sectioned on the turbine blade.

Thin and thick samples were coated simultaneously by using CVD process parameters given in Table 2.19.

Table 2.19 CVD process parameters used for the influence of sample thickness experiments.

Temperature	Pressure	HCl Flow	H_2 Flow	HCl : H_2	Ar Flow	HCl:Ar	Internal Trays	Time
1100 °C	100 mbar	125 sccm	250 sccm	1:2	250 sccm	1:2	Al-Cr (50/50)	12 h

Cross section SEM analysis given in Figure 2.45 showed that identical coating thickness and coating microstructures were obtained for both thick and thin samples. In addition to coating thickness, compositional distribution of both samples shows similar behavior. Microstructure and chemical analysis proved that thickness of samples greater than 3 mm does not affect growth kinetics. Due to the thinnest section of the turbine blade is 3 mm in thickness, aluminide coating along the turbine blade surface could be applied homogeneously without any additional treatment.

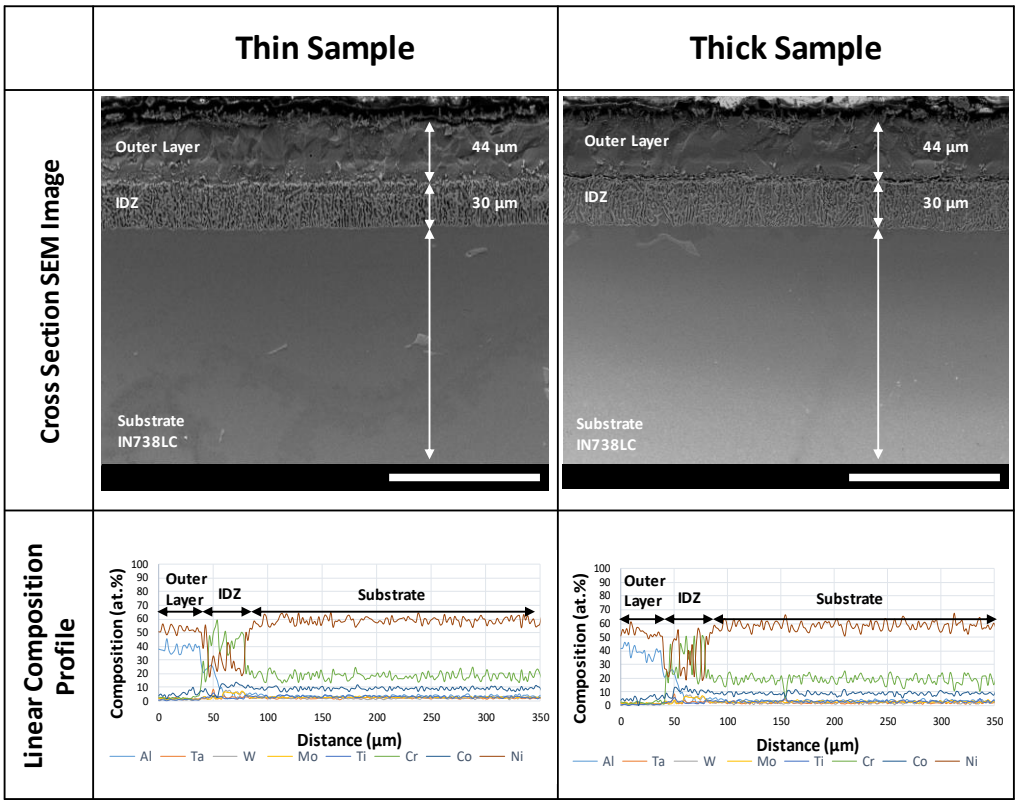

Figure 2.45 Cross section SEM images (The scale bar = 100 µm) and linear composition profile of aluminide coatings applied to thin and thick IN738 LC specimens.

2.3.4 Effect of Substrate Material on Aluminide Coating

Along with IN 738 LC, there are many other nickel based superalloys used in turbine applications. For instance, IN 939 is widely preferred for stationary turbine blades due to its better oxidation and corrosion behavior compared to IN 738 LC. While higher chromium content of IN 939 provides better corrosion resistance than IN 738 LC, it deteriorates mechanical strength and creep resistance. Therefore, each material used for different applications according to required mechanical and chemical properties. In this study, the effect of initial substrate composition on aluminide coating formation was studied by simultaneous aluminizing of IN 738 LC and IN 939 substrates. CVD process parameters used in substrate effect experiment is given in Table 2.20.

Table 2.20 CVD process parameters used for influence of substrate composition experiment.

Temperature	Pressure	HCl Flow	H_2 Flow	HCl : H_2	Ar Flow	HCl:Ar	Trays	Time
1100 °C	100 mbar	125 sccm	250 sccm	1:2	250 sccm	1:2	Al-Cr (50/50)	12 h

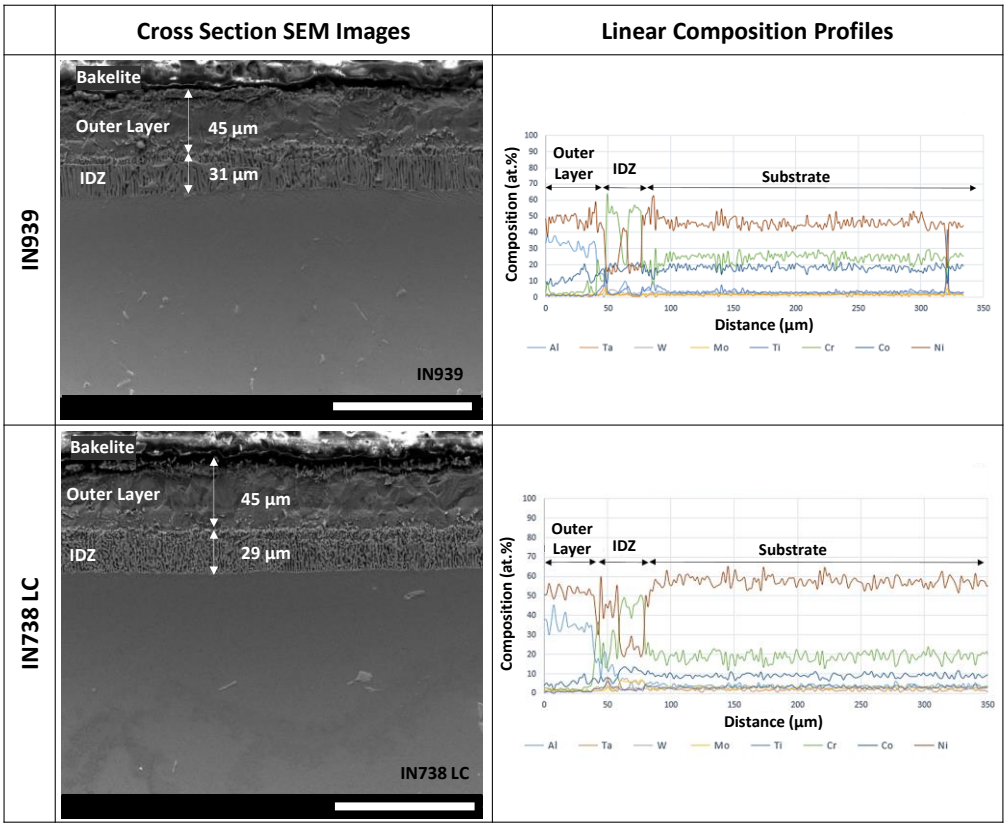

Figure 2.46 Cross section SEM images (The scale bar = 100 µm) and linear composition profile of aluminide coatings applied on IN939 and IN738 LC substrates.

Aluminizing is a diffusion controlled process which means initial substrate composition may affect growth kinetics. The composition of IN738 LC and IN939 are given in Table 1.2 and Table 1.3 in Chapter 1. SEM cross-section analysis showed that outer coating layer thickness of both IN939 and IN738 LC substrate was 45 μm (Fig. 2.46). There was only 2 μm difference in IDZ thickness, and 31 μm for IN939 and 29 μm for IN738 LC was obtained. The linear composition analyses performed by EDS exhibits that aluminum composition at outer coating layer is between 30 – 40 at. % for both substrate materials. Although Al contents were similar at the outer layer, more chromium build-up exists in IN939 at IDZ region. Since IN939 material has higher chromium content than IN738LC, it is considered that chromium accumulation is more at IDZ for IN939. In addition to chromium, cobalt composition was reached up to 20 at. % at outer coating layer of IN939. However, in IN738 LC, only 10 at. % cobalt present at outer layer due to its lower concentration in IN738 LC. Although effects of varying chromium and cobalt composition along aluminide coating on different substrate materials had not well-known during high temperature oxidation and corrosion, almost identical aluminide coatings were obtained for both substrate materials in terms of thickness and microstructure.

2.4 Conclusion

In this chapter, the influence of CVD process parameters on coating growth rate, outer layer/ IDZ ratio, and coating microstructure were studied by univariate experimental analysis.

- Aluminizing temperature is one of the most significant CVD process parameters which affect growth kinetics and final microstructure. Aluminide coating growth rate increases significantly with increasing furnace temperature for both 50/50 and 70/30 wt. % Al-Cr alloy. It is assumed that higher temperature promotes reduction reactions of aluminum sub-chloride gases, thereby increasing coating growth rate. The diffusibility of species also increases with temperature, lower outer layer/IDZ ratio was obtained for low aluminum activity (50/50 wt. %) aluminizing at 1100 °C. On the other hand, high Al deposition rate in high activity aluminizing suppresses IDZ thickness; therefore, outer layer/IDZ ratio increases with increasing temperature.

- Pressure has a minor effect on coating growth rate for low aluminum activity (50/50 wt. %) aluminizing. On the other hand, the influence of pressure on growth rate increases with increasing aluminum activity (70/30 wt. %). It is observed that there is a critical point which the surface boundary layer thickness and the partial pressure of aluminum sub-chlorides are in equilibrium for higher Al deposition rate.

- HCl flow rate in the range of 125-250 sccm was optimum level in low activity (50/50 wt. %) aluminizing, and higher growth rate was obtained. Above 250 sccm growth rate and outer layer/IDZ ratio decreased due to etching effect of excess HCl. On the other hand, the influence of HCl flow on coating growth rate increases in high activity (70/30 wt. %) aluminizing. Optimum HCl flow rate was obtained at 250 sccm rather than 125 or 500 sccm in high activity process. For both low and high aluminum activity, coating growth rate decreased considerably above 250 sccm HCl flow rate.

- Higher HCl to H_2 ratio favored the coating growth rate for low activity (50/50 wt. %) aluminizing. Maximum rate was obtained at 1:2 HCl to H_2 ratio rather than 1:4 or 1:8 ratios, but the outer layer/IDZ ratio decreased slightly.

- With increasing chlorinator temperature, aluminide coating growth rate slightly decreased, while outer layer/IDZ ratio increased. It is assumed that the partial pressures of aluminum sub-chloride gases increase with increasing chlorinator temperature. 400 °C was decided as maximum temperature limit of chlorinator to prevent unexpected melting of aluminum pellets at chlorinator.

- Aluminum activity has a major effect on growth rate and outer layer/IDZ ratio. When Al content of Al-Cr alloy increased from 50 wt. % to 70 wt. %, growth rate, and outer layer/IDZ ratio incredibly raised. It is assumed that aluminum activity significantly increases the partial pressures of aluminum sub-chloride gases; thereby, increasing aluminum deposition rate.

- Aluminide coating growth rate obeys parabolic rate law which means growth rate decreases with increasing process time. Therefore, optimizing the CVD parameters is important production criteria for the feasibility of aluminizing process.

Also, the effect of surface roughness on aluminide coating was investigated and optimum surface roughness range was specified to obtain homogeneously distributed coating along the surface.

- Proper surface pre-treatments are crucial to prevent surface defects after aluminizing. Surface cracks and varying coating thickness were observed on aluminide coating applied to cast surface (Ra = 0.287, Rz = 2.428) while no cracks were observed on surface ground samples before aluminizing.

- Grinding the substrate surfaces prior to aluminizing provides homogenous aluminide coating in terms of composition and thickness independent from SiC emery paper grit size.

Moreover, the effect of substrate material in terms of thickness and composition were studied by independent experiments.

- Substrate thickness does not affect aluminide coating formation if the substrate thickness is greater than 3 mm.
- No significant thickness difference was observed between aluminide coatings applied on IN 738 LC and IN 939 substrates. Due to higher chromium and cobalt content of IN 939, the composition of Cr and Co along the aluminide coating were greater than IN 738 LC.

Additionally, optimum CVD system parameters range in terms of growth rate, outer layer/IDZ ratio and safety limits were decided. The range of CVD growth parameters defined by the manufacturer and optimum ranges obtained by experiments is given in Table 2.21.

Table 2.21 Range of CVD system parameters defined by the manufacturer and optimum ranges obtained by experiments.

CVD System Parameters		
Variable	Limits defined by manufacturer	Optimum ranges for aluminizing process
Temperature	Up to 1200 ˚C	1000 – 1100 °C
Pressure	20 - 300 mbar	50 – 200 mbar
Al Chlorinator Temperature	Up to 800 ˚C	400 ˚C
Hf/Zr Chlorinator Temperature	Up to 800 ˚C	800 ˚C
Argon Flow Rate (MFC1)	5000 sccm	Up to user
Argon Flow Rate (MFC2)	5000 sccm	Up to user
Argon Flow Rate (MFC3)	5000 sccm	Up to user
Argon Flow Rate (MFC4)	5000 sccm	Up to user
H2 Flow Rate (MFC5)	5000 sccm	250 – 500 sccm
HCl Flow Rate (MFC6)	1000 sccm	125 - 250 sccm
HCl Flow Rate (MFC7)	1000 sccm	50 - 100 sccm

CHAPTER 3

REACTIVE ELEMENT AND ALLOYING ELEMENT ADDITION TO ALUMINIDE COATING BY CVD

3.1 Introduction

Reactive (Hf, Zr, Y, etc.) and alloying (Cr, Co, Pt, Si, etc.) elements can significantly improve oxidation and hot corrosion resistance of aluminide coatings as explained in Chapter 1. Figure 3.1 summarizes possible advantages and disadvantages of these ternary elements on aluminide coating. However, if their composition and distribution are not controlled precisely in aluminide coating, these elements may adversely affect the lifetime. In this thesis, co-deposition of Cr, Co, Hf, Zr and Y with Al were studied. As a future work, Pt and Si addition and their effect on aluminide coating lifetime will be studied.

Reactive elements have beneficial effects only if their compositions are in the limit of their solubility level in β-NiAl phase. Although actual solubility level of REs is changing depending on coating/substrate composition, excess REs precipitate along coating region and reduces scale adherence. Solubility level of Hf in β-NiAl phase was proposed by Kim et al. (2004) as around 0.005 at. % for CVD aluminide coating on pure nickel [85]. Pint et al. (1998) mentioned that Hf solubility is around 0.05 at. % for cast β-NiAl alloy [63]. In another study, Pint et al. (2003) also defined that cast β-NiAl with 0.05 at. % Hf is an ideal alumina former [86]. In addition, Y and Zr have similar solubility to Hf in β-NiAl phase. The maximum solubility of Y in β-NiAl is defined as 0.05 at. % [7]. Also, it was proposed that Zr in the level of 0.04 – 0.08 at. % improves oxidation resistance of aluminide coatings [63,87].

Elements	Advantages	Disadvantages
Cr	• Facilitates the formation of the slower growing, more protective α- Al_2O_3 scale than metastable Al_2O_3 scales. • Formation of Cr_2O_3 increases hot corrosion resistance of aluminide coatings.	• Formation of α-Cr and $AlCr_{(x)}$ phases degrades oxidation and hot corrosion resistance of aluminide coatings. • Cr_2O_3 scale is volatile especially in presence of water vapor and reduces the maximum operating temperature of aluminide coatings.
Co	• Promotes the formation of Al_2O_3 scale at a much lower Al concentration. • Co in β-NiAl could effectively reduce the internal diffusion of sulfur during hot corrosion, therefore improves oxidation and corrosion resistance.	• Excess level of Co promotes the formation of less protective oxides such as NiO.
Pt	• Improves the scale adherence. • Prevents the detrimental effect of sulfur. • Retards the formation of voids • Promotes the stable α- Al_2O_3	• Far more expensive. • Causes surface rumpling and degrade adherence of thermal barrier coating to aluminide coating surface. However, ternary elements (Si, Hf, Y, etc.) addition to Pt modified aluminide coatings can minimize the rumpling effect.
Y	• Improves the scale adherence. • Prevents the detrimental effect of sulfur.	• Degrades scale adherence, if composition of Y exceeds its solubility level in β-NiAl.
Hf	• Improves the scale adherence. • Prevents the detrimental effect of sulfur. • Retards the formation of voids.	• Degrades scale adherence, if composition of Hf exceeds its solubility level in β-NiAl.
Zr	• Improves the scale adherence. • Prevents the detrimental effect of sulfur.	• Degrades scale adherence, if composition of Zr exceeds its solubility level in β-NiAl.
Si	• Promotes the formation of Al_2O_3 scale.	• Volatile SiO_2 oxide significantly reduces the maximum operating temperature of aluminide coatings.

Figure 3.1 Advantages and disadvantages of ternary elements on aluminide coating lifetime.

Similar to the reactive elements, if the amount of Cr exceeds solubility level in β-NiAl (~10 at. % depending on phase composition), it precipitates as α-Cr which decreases beneficial effect of Cr on hot corrosion behavior [66]. Although there is a lack of information about Co, it is reported that presence of 14 wt. % Co in aluminide coating improves its hot corrosion behavior by restraining the internal diffusion of sulfur in the coating [67]. During this study, it was observed that Cr and Co are present in layer due to their diffusion from the IN 738 LC substrate to coating. However, their compositions are low (Cr ~1-4 at. % and Co ~2-5 at. %) in the coating layer. By co-deposition of these elements, their compositions were increased to 10 -15 at. % level.

In this chapter, co-deposition of reactive and alloying elements by CVD were studied to obtain aluminide coating having homogeneous ternary element distribution along coating layer. Y and Zr were added as reactive elements, Cr and Co were added as alloying elements to aluminide coating, separately. Also, CVD process parameters were optimized for Y addition to control its composition and distribution in β-NiAl phase. For this purpose, the effect of process temperature and pressure on co-deposition of Y was studied.

3.2 Experimental Details

3.2.1 Substrate and Sample Preparation

Inconel 738LC substrate material was used for reactive and alloying element addition to aluminide coating experiments. Samples were prepared by following the similar procedure mentioned in Chapter 2 in Section 2.2.1.

3.2.2 Reactive or Alloying Element Co-Deposition Process

The addition of ternary elements to aluminide coating can be achieved by different methods depending on aluminizing process. As mentioned in Chapter 1, one of the main advantages of CVD process is its ability to simultaneously deposit the additional elements together with aluminum, while pre- or post- treatments are usually necessary for pack aluminizing methods. The main challenge of ternary elements is to control

their composition in aluminide coating but it can be controlled by CVD process parameters.

The idea of ternary element deposition process is similar with aluminizing. Ternary elements can be in the form of halides like YCl_3, $CoCl_2$ and $CrCl_3$ or can be in the form of pure elements like Hf and Zr metal pellets. In our CVD system both forms of elements can be used for co-deposition process. For the deposition of Hf and Zr metal pellets, an external chlorinator (K2) is used to generate chlorides of Hf or Zr, while internal chamber trays are used for the YCl_3, $CoCl_2$ and $CrCl_3$ powder as shown in Figure 3.2. Y, Cr and Co cannot be used in the pure element form because their chlorination reactions occur at elevated temperature; however, halides of Zr and Hf can be formed at 800 °C chlorinator temperature. The main advantage of using external generator is the amount and distribution of RE elements in aluminide coating can be controlled more precisely rather than using their chlorides at the internal trays. The formation rate of chlorides and their deposition rate can be controlled by controlling the temperature of the generator (K2), gas flows and rates. However, controlling evaporation and deposition rate of chloride powders at internal trays are limited.

The addition of Y, Cr, and Co was achieved by using chlorides of those elements in powder form at top internal tray. Red colored internal tray in Figure 3.2 shows where the chloride powders placed. For each ternary element addition experiment, 50 gr of YCl_3 (99.99 %), $CoCl_2$ (99.7 %) or $CrCl_3$ (99.9 %) powders were loaded to coating chamber.

For co-deposition of Hf or Zr, 1 kg of high purity Zr (Grade 702, > 95 %) or Hf (99.9 %) metal pellets were filled to chlorinator unit (K2). High purity HCl gas (99.999 %) was used to form $HfCl_4$ or $ZrCl_4$ gasses at chlorinator unit. Argon (99.999 %) was used to dilute HCl gas and to transfer chlorides of Hf or Zr to coating chamber as a carrier gas.

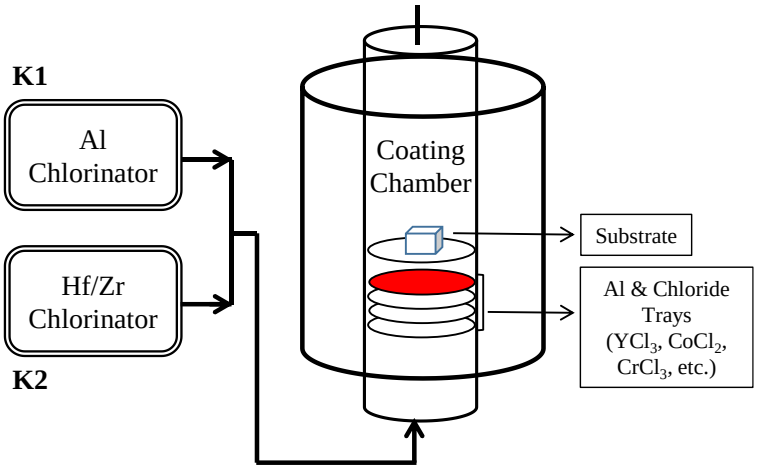

Figure 3.2 Diagram of external chlorinators and coating chamber belong to CVD system. Red colored tray represents where the chloride powders placed.

3.2.3 Coating Characterization

3.2.3.1 Metallographic Sample Preparation

Before EPMA – WDS analysis, all coated samples were sectioned by Buehler IsoMet 5000 Precision Saw. After that, samples were molded by Metkon EcoPress 100 into Bakelite. Each sample was ground by 220, 400, 800, 1200 grit SiC emery paper, respectively. 6 µm and 1 µm diamond was applied to polish cross section surfaces.

3.2.3.2 Wavelength Dispersive Spectroscopy (WDS)

The composition of reactive and alloying elements from the aluminide coating surface through the substrate was analyzed by wavelength dispersive spectroscopy detector belongs to Electron Probe Micro-Analysis (EPMA) equipment. Jeol JXA 8230 equipment was operated at 20 kV accelerating voltage. To increase the accuracy of measurement, three composition data was taken from each point, and the average values were calculated (Fig. 3.3).

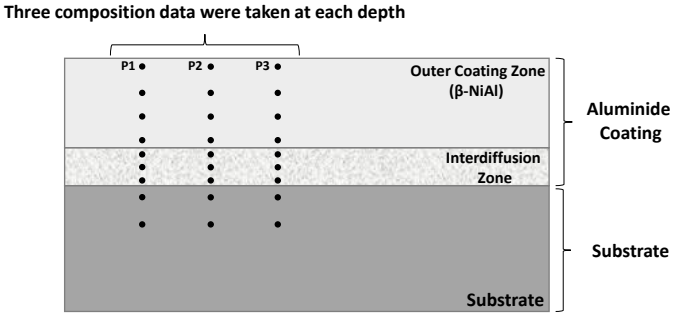

Figure 3.3 WDS composition analysis at three different points in each depth to calculate the average composition.

3.3 Results and Discussions

3.3.1 Chromium Addition

The chromium addition to the aluminide coating by CVD was carried out using the following CVD parameters.

Table 3.1 CVD process parameters used for Cr addition to aluminide coating.

Temperature	Pressure	HCl Flow	H_2 Flow	HCl : H_2	Ar Flow	HCl:Ar	Internal Trays	Time
1100 °C	100 mbar	125 sccm	250 sccm	1:2	250 sccm	1:2	Al-Cr* $CrCl_3$	4 h

* 50/50 wt. % Al-Cr

Co-deposition of chromium with the aluminum was achieved by placing chromium chloride ($CrCl_3$) powder to the internal tray in the coating chamber.

Although the amount of chromium element in the coating could be determined by EDS, WDS has been used for the accuracy of the composition analysis. Composition of only four major coating elements which are Al, Ni, Co, and Cr were measured by WDS. In simple aluminide coating, Cr composition was changing between 1 – 4 at. % along the coating, due to chromium diffused from IN 738 LC substrate as shown in Figure 3.4 (a). By the co-deposition of Cr, WDS analysis showed that Cr composition increased to 10-15 at. % along outer coating layer (Fig. 3.4 (b)). The maximum chromium level increased from 30 at. % to 50 at. % in the IDZ region. Chromium composition smoothly decreases from the peak point to substrate/IDZ interface. When

reached to the substrate, Cr level drops to 15 – 18 at. % level which indicates chromium composition of the substrate. Also, XRD analysis showed that there was no undesirable Cr containing phases formed at coating surface and the outer layer was composed of β-NiAl phase.

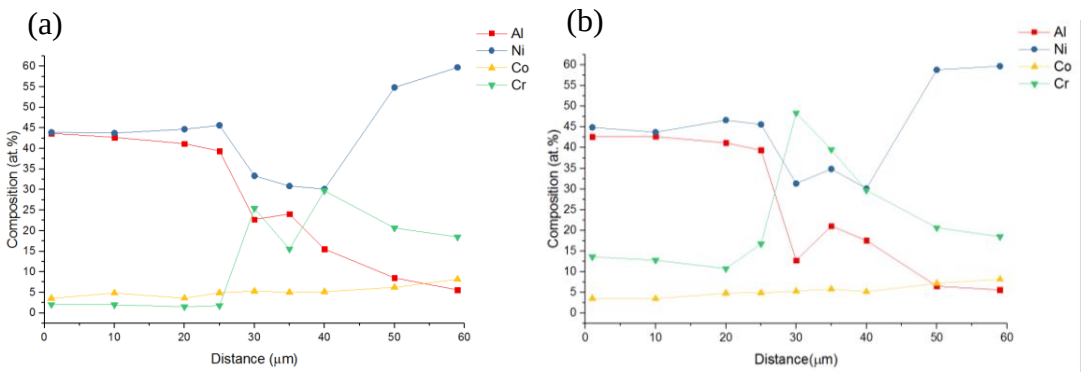

Figure 3.4 WDS linear composition profile of simple (a), Cr modified (b) aluminide coatings.

3.3.2 Cobalt Addition

The cobalt addition to the aluminide coating by CVD was carried out using the following CVD parameters.

Table 3.2 CVD process parameters used for Co addition to aluminide coating.

Temperature	Pressure	HCl Flow	H_2 Flow	HCl : H_2	Ar Flow	HCl:Ar	Internal Trays	Time
1100 °C	100 mbar	125 sccm	250 sccm	1:2	250 sccm	1:2	Al-Cr* $CoCl_2$	4 h

* 50/50 wt. % Al-Cr

Similar with chromium addition, co-deposition of cobalt with the aluminum deposition was achieved by placing cobalt chloride ($CoCl_2$) powder to the internal tray in the coating chamber.

Composition of only four major elements which are Al, Ni, Co, and Cr were measured by WDS. In simple aluminide coatings, Co composition was changing between 2 – 5 at. % along the coating, due to cobalt diffused from IN 738 LC substrate as shown in Figure 3.5 (a). By the co-deposition of Co, WDS analysis showed that Co composition

increased to 10-14 at. % along outer coating layer (Fig. 3.5 (b)). In the IDZ region, there was no significant change in the amount of Co, and it was present at 10-12 at. % levels. Cobalt composition smoothly reaches 8 at. % at substrate/IDZ interface. Also, XRD analysis showed that there was not undesirable Co containing phases formed at coating surface and the outer layer was composed of β-NiAl phase.

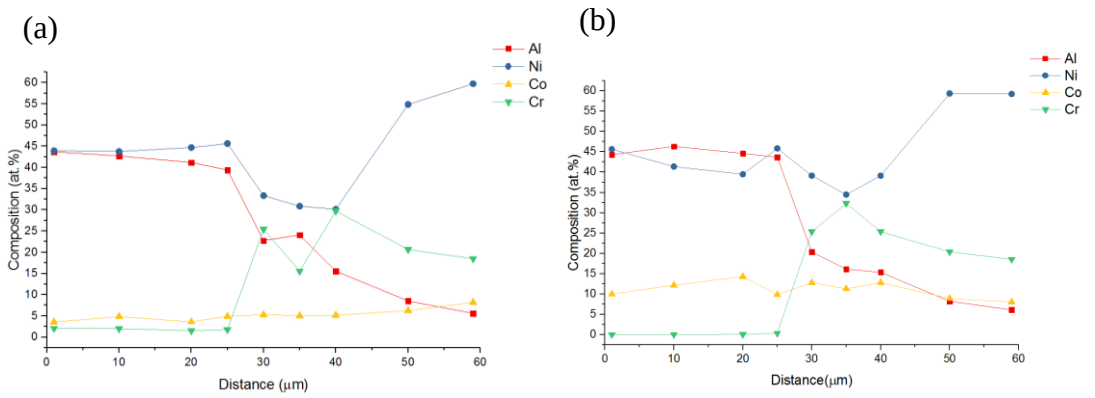

Figure 3.5 WDS linear composition profile of simple (a), Co modified (b) aluminide coatings.

3.3.3 Yttrium Addition

The yttrium addition to the aluminide coating by CVD was carried out using the following CVD parameters.

Table 3.3 CVD process parameters used for Y addition to aluminide coating.

Temperature	Pressure	HCl Flow	H_2 Flow	HCl : H_2	Ar Flow	HCl:Ar	Internal Trays	Time
1100 °C	100 mbar	125 sccm	250 sccm	1:2	250 sccm	1:2	Al-Cr* YCl_3	4 h
1050 °C	100 mbar	125 sccm	250 sccm	1:2	250 sccm	1:2	Al-Cr* YCl_3	4 h
1000 °C	100 mbar	125 sccm	250 sccm	1:2	250 sccm	1:2	Al-Cr* YCl_3	4 h
1050 °C	150 mbar	125 sccm	250 sccm	1:2	250 sccm	1:2	Al-Cr* YCl_3	4 h
1050 °C	200 mbar	125 sccm	250 sccm	1:2	250 sccm	1:2	Al-Cr* YCl_3	4 h

* 50/50 wt. % Al-Cr

Since yttrium was added to aluminide coating in a ppm level, composition analyses were carried out by WDS detector of the EPMA instrument.

In Y-modified aluminide coating which was applied at 1100 ˚C aluminizing temperature, no yttrium (below the detection limit, 80 ppm) element was detected at the coating surface (Fig. 3.6). It has been found that the amount of yttrium increases to 90 ppm at a depth of 10 µm, increased to 1280 ppm at 20 µm depth and raised to 7000 ppm level at the outer layer/IDZ interface. In the IDZ region, it was observed that the yttrium amount decreased at 100 ppm level and did not diffuse to the substrate material. Since the yttrium was not uniformly distributed in the aluminide coating, additional aluminizing experiments with different CVD parameters have been carried out.

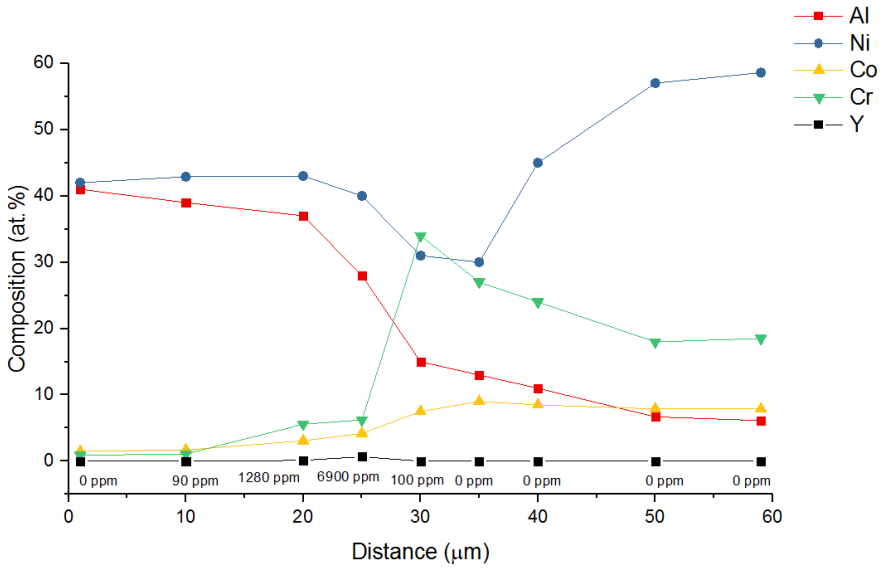

Figure 3.6 WDS linear composition profile of Y modified aluminide coating applied at 1100 °C chamber temperature.

Y addition to aluminide coating was achieved by YCl_3 powder which was placed on internal tray at coating chamber. It is believed that the YCl_3 powder evaporates rapidly due to the high process temperatures. During the first stages of the aluminide coating process, YCl_3 was completely consumed and aluminizing continued with the absence

of YCl_3. Consequently, the yttrium concentrated at inner coating region near to IDZ. For this reason, the coating chamber temperature has been gradually decreased to slow down evaporation rate of YCl_3 at coating chamber. Also, it is assumed that deposition rate of Y decreased with decreasing process temperature. In the Y-modified aluminide coating applied at 1050 ˚C, the thickness of the outer layer decreased to 20 µm and the IDZ thickness decreased to 17 µm due to lower aluminizing temperature.

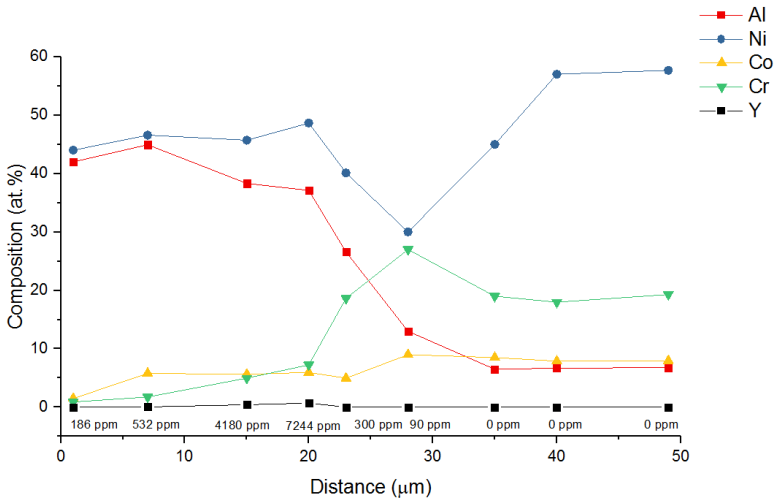

Figure 3.7 WDS linear composition profile of Y modified aluminide coating applied at 1050 °C chamber temperature.

The yttrium distribution in the aluminide coating applied at 1050 ˚C shows similarity with the coating applied at 1100 ˚C. Although yttrium composition at outer coating region increased by decreasing process temperature, Y distribution is still heterogeneous in aluminide coating (Fig. 3.7). 200 ppm Y presents at the coating surface, and it rises to 7200 ppm near the outer layer/IDZ interface. It is believed that reducing the process temperature by 50 °C did not reduce the evaporation rate of yttrium chloride powder as expected. For this reason, the chamber temperature has been reduced by 50 ˚C and another coating operation at 1000 ˚C has been carried out.

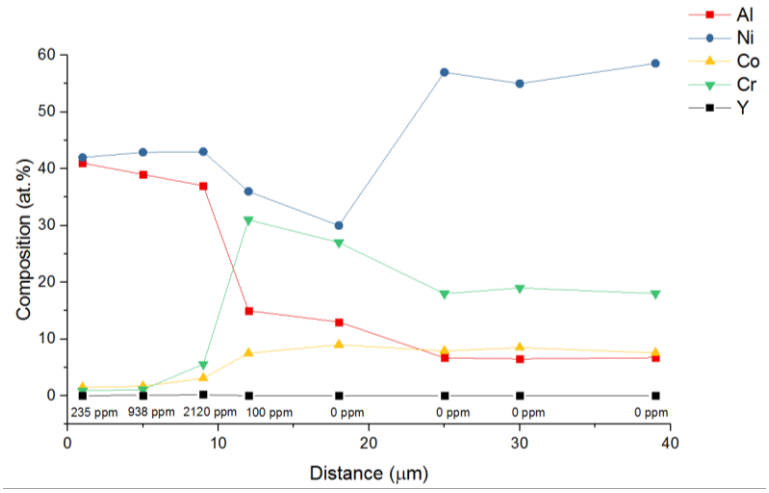

Figure 3.8 WDS linear composition profile of Y modified aluminide coating applied at 1000 °C chamber temperature.

At 1000 ˚C, 10 μm outer layer and 7 μm IDZ thickness were obtained. Along with the decreasing coating thickness, the composition of yttrium in coating noticeably reduced as shown in Figure 3.8. Y level at coating surface is 235 ppm and rises to 2120 ppm levels towards the IDZ region, and more homogenous Y distribution was obtained at 1000 ˚C chamber temperature. Results indicate that evaporation rate of YCl_3 and deposition rate of yttrium decreases with decreasing the temperature. However, the aluminide coating growth rate is greatly reduced at 1000 ˚C aluminizing temperature. Therefore, to obtain thicker coatings, aluminizing is needed to be performed over 20 hours which is impractical. As a result, YCl_3 evaporation rate must be decreased at higher coating temperatures to keep aluminide growth rate relatively high.

The evaporation rate of YCl_3 depends on the system pressure as well as the chamber temperature. Increasing the system pressure could reduce the YCl_3 evaporation rate without affecting the aluminide coating growth rate. Therefore, the effect of system pressure on Y addition to aluminide coating was investigated by two more aluminizing experiment which were performed at 150 and 200 mbar system pressure. The aim is to distribute the yttrium in the coating homogeneously without reducing the aluminide coating growth rate.

When the system pressure is increased, the distribution of yttrium in aluminide coating is greatly affected. Figure 3.9 shows Y distribution along the coating surface at 100, 150 and 200 mbar system pressure. When the system pressure is increased from 100 mbar to 150 mbar, the yttrium content at outer layer / IDZ boundary is reduced from 7000 ppm levels to 4500 ppm levels. Also, the amount of yttrium at outer coating region has increased from 0-200 ppm levels to 200-400 ppm levels. When the system pressure was increased to 200 mbar, the yttrium amount in the outer coating area increased to 500-1000 ppm range, and it decreased to 1300 ppm levels near the outer coating / IDZ interface. Results indicate that the evaporation rate of YCl_3 significantly decreased by increasing the system pressure and the yttrium element was more homogeneously distributed along the coating. Through the experiments carried out step by step, CVD process parameters of Y-modified aluminide coating was enhanced to obtain more homogeneously dispersed Y along alumina coating.

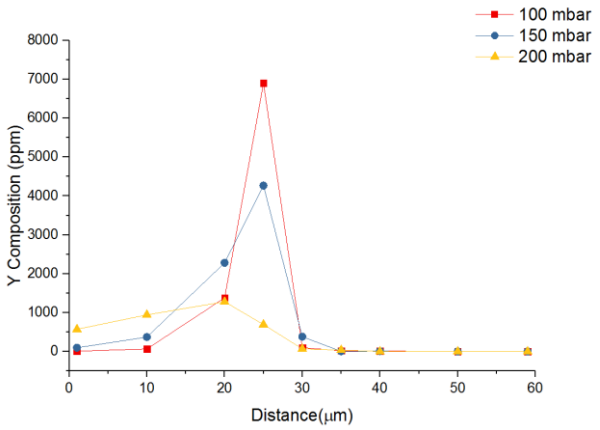

Figure 3.9 WDS linear Y profile of Y modified aluminide coating applied at 100, 150 and 200 mbar system pressures.

3.3.4 Zirconium Addition

The zirconium addition to the aluminide coating by CVD was carried out using the following CVD parameters.

Table 3.4 CVD process parameters used for Zr addition to aluminide coating.

Temperature	Pressure	HCl Flow	H_2 Flow	HCl : H_2	Ar Flow	HCl:Ar	Internal Trays	Time
1100 °C	100 mbar	125 sccm	250 sccm	1:2	250 sccm	1:2	Al-Cr*	4 h

* 50/50 wt. % Al-Cr

Co-deposition of zirconium with the aluminum was achieved by using external Hf/Zr chloride generator which is filled with high purity Zr pellets. $ZrCl_4$ gas was formed by reaction between HCl gas and Zr metal at generator rather than using $ZrCl_4$ powder at internal trays. $ZrCl_4$ gas is transferred to coating chamber by using Argon as a carrier gas. Advantages of using the external generator for the co-deposition process is high ability to control process variables; hence, the composition of doping element in aluminide coating.

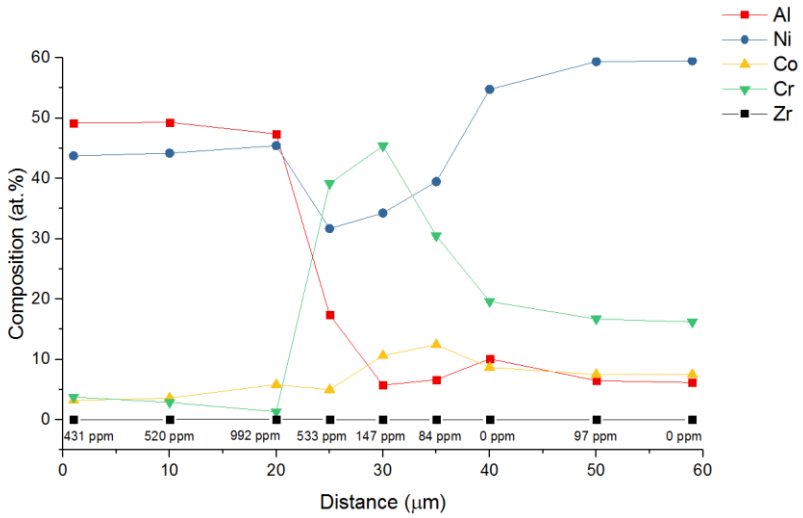

Figure 3.10 WDS linear composition profile of Zr modified aluminide coating.

The amount of zirconium in the aluminide coating was determined by EPMA - WDS. To increase the accuracy of measurement in ppm level, three composition data was

taken from each point, and the average values were calculated. The sensitivity of WDS detector is 80 ppm for zirconium.

Compositional analysis indicates that Zr composition is changing between 400 – 900 ppm range at outer coating layer as shown in Figure 3.10. Near the outer layer/IDZ interface, Zr amount slightly raised to 1000 ppm level. Zirconium composition smoothly decreases from outer coating/IDZ to substrate/IDZ interfaces. When reached to the substrate, Zr level drops to 97 ppm, and it changes between 0 – 200 ppm level. It is believed that the zirconium detected at substrate comes from the alloy itself and it is not affected by zirconium addition to the coating. Results demonstrate that amount and distribution of RE elements in aluminide coating could be controlled more precisely by using external generator rather than using their chlorides at the internal generator. Because formation rate of chlorides, its partial pressure and deposition rate could be controlled by controlling the temperature of the generator, gas flows and rates. However, to control evaporation rate for chloride powder at internal trays are limited. However, in both ways, the addition of RE and alloying elements to aluminide coating is feasible to improve its oxidation and corrosion resistance at high temperatures.

3.4 Conclusion

In this chapter, co-deposition of ternary elements with Al, Cr and Co as alloying elements, Zr and Y as reactive elements were studied by CVD method.

- Chromium was added to aluminide coating in the level of 10 – 15 at. % by using $CrCl_3$ powder at the internal tray, while simple aluminide coating contains 1 – 4 at. % chromium at outer coating region.
- Cobalt was incorporated to aluminide coating in the level of 10 – 14 at. % by using $CoCl_2$ powder at internal tray, while cobalt content of simple aluminide coating is between 2 – 5 at. % at outer coating region.
- The decrease in aluminizing temperature from 1100 ˚C to 1000 ˚C was not sufficient to decelerate evaporation rate of YCl_3. On the other hand, the evaporation rate of YCl_3 was greatly decreased by increasing the pressure from

100 mbar to 200 mbar. Thus, homogeneous distribution of Y along the outer coating layer was obtained.

- By the optimization of CVD process parameters, yttrium was added to aluminide coating in the range of 500 – 1000 ppm by using YCl_3 powder at 200 mbar, 1050 °C.
- Zirconium was added to aluminide coating in the level of 400 – 900 ppm range by using pure Zr pellets at external chlorinator.

CHAPTER 4

COMPARATIVE ANALYSIS OF ALUMINIDE COATINGS CORROSION BEHAVIOR WITH THE ADDITION OF TERNARY ELEMENTS

4.1 Introduction

Simple aluminide coatings are extensively used to protect turbine blades from oxidation and hot corrosion. However, further improvements can be achieved by the addition of ternary elements to aluminide coating, as explained in Chapter 1, to prolong coating/substrate lifetime and decrease maintenance costs.

Chromium, yttrium, zirconium, and hafnium are most prevalent elements which have a beneficial effect on oxidation and corrosion resistance of the coating. However, if the composition of ternary elements exceeds a critical point, they may have an adverse effect which deteriorates coating lifetime. Table 4.1 shows possible advantages and disadvantages of Cr, Y, Zr and Hf on aluminide coating lifetime. Although the addition of cobalt to aluminide coating promotes the formation of continuous and dense Al_2O_3 scale on the coating surface [67], chromium as an alloying element promotes not only Al_2O_3 formation but also increase hot corrosion resistance by the formation of Cr_2O_3 [88].

Also, main improvement mechanism of Cr as an alloying element is different from the mechanism of reactive elements (Zr, Y, and Hf). While Cr promotes the formation of more stable, slower growing α-Al_2O_3 scale [64], reactive elements improve scale adherence by preventing detrimental effect of sulfur [63]. Sulfur segregation to coating/scale interface weaken the chemical bonding and degrade the scale adhesion. For that reason, simultaneous addition of Cr and Y on aluminide coating was included to comparative corrosion test analysis.

Table 4.1 Advantages and Disadvantages of Ternary Elements on Aluminide Coating Lifetime.

Advantages	**Cr**	**Y**	**Zr**	**Hf**
Facilitates the formation of more protective α- Al_2O_3	+			
Improves the resistance to hot corrosion attack	+			
Decreases surface rumpling		+	+	+
Prevents sulfur segregation to grain boundaries and interfaces		+	+	+
Improves adherence of alumina scale		+	+	+
Retards the formation of internal voids				+
Disadvantages	**Cr**	**Y**	**Zr**	**Hf**
Decreases ductility of substrate/coating system	−			
Undesirable phase formations	−	−	−	−
Grain boundary segregation if added more than solubility level		−	−	−
Forms volatile oxides	−			

In this chapter, the effect of Cr, Y, Cr/Y, Hf, and Zr addition to aluminide coating were comparatively examined by hot corrosion test.

4.2 Experimental Procedure

4.2.1 Sample Preparation For Coating

IN 738 LC samples were prepared by following sample preparation procedure which is given in Chapter 2, Section 2.2.1. Table 4.2 summarizes the history of corrosion test samples before aluminizing.

Table 4.2 Specifications of the test samples to be aluminized for corrosion test.

Material	**Casting Method**	**Heat Treatments Prior to Coating**	**Sample Sizes**	**Surface Roughness**
IN738 LC	Vacuum Casting	HIP and Solutionizing	10 x 10 x 5 mm	Ra<0.14 µm Rz<1.2 µm

4.2.2 Aluminide Coating Process

For comparative analysis of hot corrosion, six sample set (10 sample in each set) were aluminized by using identical CVD process parameters which is given in Table 4.3.

Table 4.3 CVD process parameters of corrosion test samples.

Temperature	Pressure	HCl Flow	H_2 Flow	HCl : H_2	Ar Flow	HCl:Ar	Internal Trays	Time
1100 °C	200 mbar	125 sccm	250 sccm	1:2	250 sccm	1:2	Al-Cr (50/50)	12 h

Cr and Y elements were co-deposited with aluminum by using $CrCl_3$ and YCl_3 powder at internal trays. For Cr, Y and Cr/Y addition, 80 gr of YCl_3 (99.99 %) and/or $CrCl_3$ (99.9 %) powders were loaded into internal chamber trays. On the other hand, Hf and Zr were co-deposited by using pure Zr and Hf pellets at external chlorinator. For co-deposition of Hf or Zr, 1 kg of high purity Zr (Grade 702, > 95 %) or Hf (99.9 %) metal pellets were filled to chlorinator unit (K2). A mixture of HCl gas (50 sccm) and argon (150 sccm) was used to form $HfCl_4$ or $ZrCl_4$ gasses at chlorinator unit. Details of co-deposition process are explained in Chapter 3 in Section 3.2.2.

4.2.3 Corrosion Test Procedure

4.2.3.1 Optimization of Corrosion Test Procedure

Prior to hot corrosion test of reactive and alloying element modified aluminide coatings, test condition and parameters were optimized by performing a pilot hot corrosion test. Ten pieces of aluminide coated and five pieces of uncoated IN 738 LC test samples were used for the hot corrosion test optimization study. Testing method and conditions were decided by our project partners and hot corrosion tests were performed in SDM R&D facility. Hot corrosion test conditions are as follows:

1- Hot Corrosion Test Method and Test Equipment
2- Surface Preparation
3- Hot Corrosion Test Condition
4- Sampling Frequency

All these conditions were optimized according to results of the pilot hot corrosion test and technical equipment limitations.

Corrosion Test Procedure and Condition to Be Optimized:

1- Hot Corrosion Test Method and Equipment

Numerous hot corrosion test methodologies have been proposed in the literature to evaluate hot corrosion behavior of materials and coatings. These test methodologies involve furnace test, crucible test, thermo-gravimetric test, electrochemical methods, and burner rig test [89]. Among all testing methods, burner rig test is the most proper method which simulates the operating conditions of gas turbine engines. In this test, gas velocity and pressure, temperature, fuel to air ratio, and corrosive salt concentrations can be controlled depending on test condition. Although burner rig is more appropriate testing method, it requires expensive and complex test equipment. In contrast with burner rig, crucible test is easier and cheaper method to assess hot corrosion behavior. It involves direct immersion of the samples to molten salt but does not reflect the operating conditions of gas turbines. Another test method is electrochemical test which involves continuous electrochemical reactions and provides rapid corrosion rates. However, it is difficult to correlate the test results with the hot corrosion behavior of materials in a real gas turbine.

Furnace test and thermos-gravimetric test are other methods which are used to evaluate hot corrosion behavior of materials. Furnace test consists of two independently controlled furnaces, one of them is used for sample placement and the other is used to vaporize corrosive salts. By using a carrier gas like argon, salt vapors are transferred to test furnace where it deposits on the sample surface. In this method, salt deposition rate and test temperature can be controlled precisely. In thermos-gravimetric test, on the other hand, salt is applied to sample surfaces externally. After that, the salt coated sample is placed to test furnace. Both methods are widely used to evaluate hot corrosion behavior of materials. Table 4.4 summarizes the advantages and disadvantages of testing methods.

Table 4.4 Advantages and disadvantages of hot corrosion testing methods.

Technique	Advantages	Disadvantages
Burner Rig Test	Simulates gas pressure and velocity, temperature, corrosive environments, mechanic stress and loads of gas turbine	Requires expensive equipment and involves complex process.
Furnace Test	Hot corrosion test conditions can be controlled precisely (salt deposition rate, temperature, etc.)	Difficult to maintain salt deposition rate for longer times.
Crucible Test	The simplest and cheapest method.	Corrosion rate is high and difficult to control.
Thermo-gravimetric Test	Precise weight measurements. Test conditions can be controlled (test temperature, salt composition, gas composition).	Not useful for predicting the life of materials and coatings.
Electrochemical Test	Fast and easy technique to assess hot corrosion.	Difficult to correlate with gas turbine conditions.

In this study, cruciable test method was chosen by our project partners for the pilot hot corrosion test and performed in a custom design test equipment belong to SDM company. Technical drawing of test equipment is shown in Figure 4.1 (a). Protherm Chamber Furnaces were modified to perform hot corrosion tests under air or burned natural gas atmosphere. Test system includes five separate test furnaces and two pieces of sealed sample holder to use burned natural gas in test furnaces (Fig. 4.1 (b)). Although equipment is capable to conduct hot corrosion test under burned natural gas atmosphere, corrosion tests were conducted under hot air due to technical limitations of corrosion test equipment. First limitation is the sealed sample holder are designed for continuous test and difficult to unload the samples for short sampling intervals. Second limitation of equipment is stainless steel pipes are used to transfer burned natural gas to sample holders. It was realized that stainless steel pipes are rapidly oxidized at elevated test temperatures. Changing the design and materials of equipment was not possible due to limited time of this study. Therefore, hot corrosion tests were

performed without using natural gas. Corrosive environment of turbine engine was simulated by applying Na_2SO_4 and V_2O_5 salts to sample surfaces.

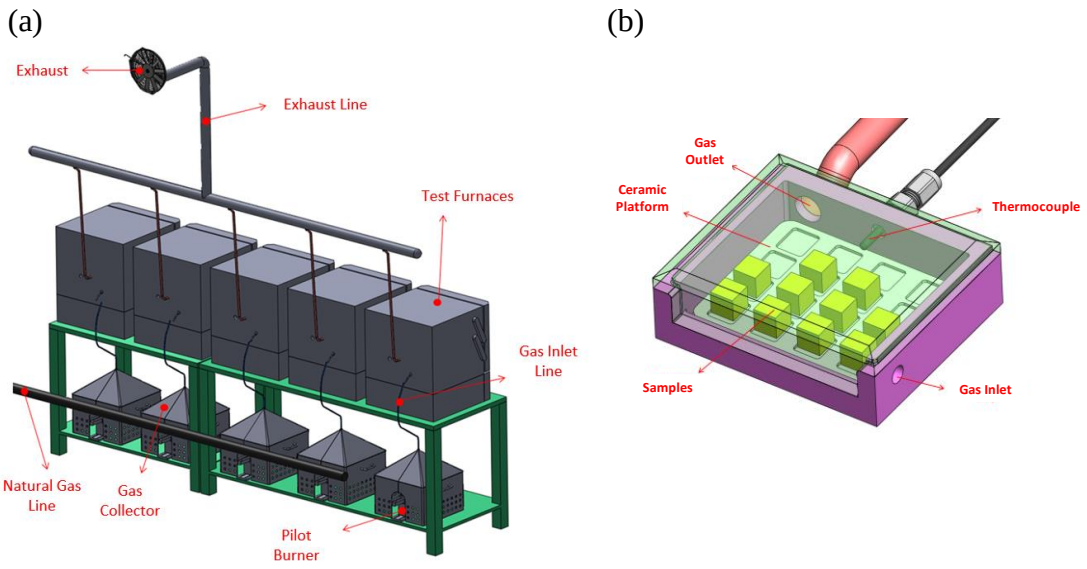

Figure 4.1 Custom design (a) oxidation and corrosion test equipment, (b) sealed sample holder for burned natural gas, belong to SDM Company.

2- Surface Preparation:

Crucible method was used in the pilot hot corrosion test. Na_2SO_4 and V_2O_5 compounds were used to simulate corroding environment of the gas turbine. A mixture of Na_2SO_4 (50 wt.%) and V_2O_5 (50 wt.%) was prepared. Then the salt mixture was put in ceramic crucibles, and test samples were placed on the top of salt mixture. After that, the test samples in the ceramic crucibles were loaded to test furnace at 800 °C. Since the corrosive salt mixture completely dissolved at the test temperature, the samples were exposed to hot corrosion in the molten salt mixture. Hot corrosion test was performed for 120 hours and one sample from each sample set was removed for characterizations in every 24 hours. When the samples were cooled down to room temperature, the corroding salt mixture completely solidified and covered the test specimen surfaces. Also, it was visually observed that all samples were completely destroyed regardless of exposure time to hot corrosion as shown in Figure 4.2.

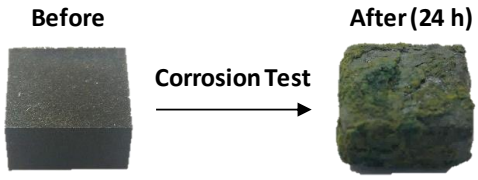

Figure 4.2 Image of aluminide coated IN738 LC test sample before and after (24 h) hot corrosion test.

To clean the residual salt deposits on the sample surfaces, samples were washed with water, but the salts were not dissolved and the samples still were completely covered by solidified salts. Since the weight change and weight gain of samples should be measured during the hot corrosion test for the comparative analysis, huge amount of solidified salts on the surface of samples have to be removed. Therefore, surface cleaning study was performed on four different corrosion test sample by following surface cleaning procedure which is given below:

Surface Cleaning Procedure:

1- Corrosion test sample 1 was cleaned in a beaker filled with 1000 ml DI water at 100 °C. Cleaning was applied for 30 min and stirred by using 100 rpm agitation speed.

2- Corrosion test sample 2 was cleaned in a beaker filled with 500 ml DI water at 70 °C. Cleaning was applied for 30 min in an Ultrasonic Cleaner.

3- Corrosion test sample 3 was cleaned in a pressurized vessel filled with 1000 ml DI water at 2.5 bar (~128 °C). Cleaning was applied for 30 min.

4- Corrosion test sample 4 was cleaned by flowing DI water at RT. Cleaning was applied for 30 min.

By using cleaning methods mentioned above, only 20% wt. of the salt mixture was solved from the sample surfaces. To completely solve salt mixture, a chemical solution was prepared. The composition of the solution is given in Table 4.5. To compare the

effect of the chemical solution with water, one sample was cleaned with DI water, and another sample was cleaned by solution in same conditions.

Table 4.5 Composition of cleaning solution used for surface cleaning of corrosion test sample.

Chemical Composition of Cleaning Solution	18g NaOH + 5g $KMnO_4$ + 77ml H_2O

Surface Cleaning Procedure by Chemical Solution:

1- First test sample was cleaned in a beaker filled with 500 ml of cleaning solution at boiling point. Cleaning was applied for 30 min and stirred by using 100 rpm agitation speed.

2- Second test sample was cleaned in a beaker filled with 500 ml DI water at boiling point. Cleaning was applied for 30 min and stirred by using 100 rpm agitation speed.

Before and after cleaning, the weight of test samples was measured to observe the effect of the chemical solution compared to DI water. It was obvious that chemical solution is more effective than DI water to clean salt mixture from sample surfaces. Table 4.6 shows weight measurements of both sample before and after cleaning.

Table 4.6 Weight measurements of corrosion test samples before and after the surface cleaning process.

Cleaning Solution	Before	After	Weight of Solved Salt
500 ml H_2O	3.391 g	3.377 g	0.014 g
90g NaOH + 25g KMnO4 + 385ml H2O	3.270 g	3.236 g	0.034 g

Although test sample surfaces partially cleaned by the chemical solution (Table 4.5), surfaces were not sufficiently salt-free for weight change measurements.

Also, microstructures of coated (aluminized) and un-coated IN738 LC test samples were analyzed after exposure to hot corrosion (Fig. 4.3). Following the first 24 hours of hot corrosion exposure, all coated and un-coated sample surfaces were corroded at a depth of 100 - 200 μm from the surface. No aluminide coating layer was observed at

coated sample surfaces which show complete depletion of Al. Corrosion progressed to the depth of 300 – 400 μm after 48 hours exposure. On the surface of the samples, oxide layers were observed in the thickness of 50 - 100 μm which mainly consist oxides of Cr, Ni, Al, Co and Ti elements. When reached to 120 hours, samples were completely corroded. Results prove that aluminide coating was completely dissipated after first 24 hours exposure to hot corrosion by the crucible (salt immersion) method. No effect of aluminide coating on hot corrosion behavior of IN 738 LC was observed. It is seen that immersion to Na_2SO_4 and V_2O_5 mixture aggressively dissolved protective alumina scale from the coating surface and cause depletion of aluminum in less than 24 hours.

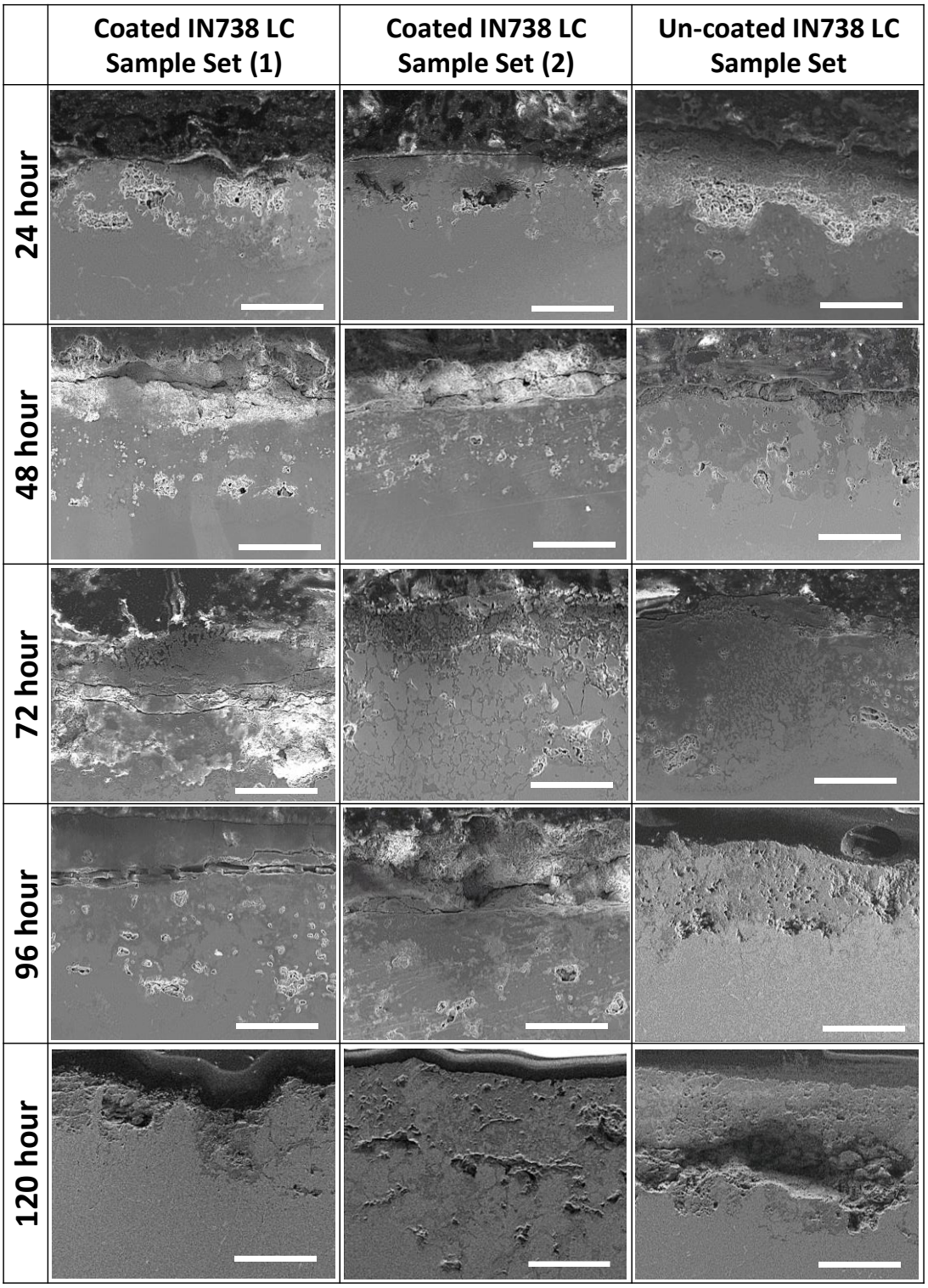

Figure 4.3 Cross-section SEM analysis of coated (aluminized) and un-coated IN 738 LC test samples after exposure to hot corrosion in increasing exposure time.

Results of pilot hot corrosion test showed that crucible (salt immersion) method causes not only the surface cleaning problem, but also it is so aggressive for comparative hot corrosion analysis of different coatings. Crucible method does not reflect real operating conditions of the turbine engine. In a turbine engine, corrosive salt vapors are transferred by hot exhaust gas to turbine blade surfaces and cover the surfaces like a thin film. Therefore, corrosion test procedure was changed from the crucible (immersion) method to thermos-gravimetric (salt spray) method to eliminate not only surface cleaning problem but also perform hot corrosion test under more accurate conditions with the real turbine. Also, composition of salt mixture was changed because V_2O_5 compound is present in turbine engine only if fuel oil is used rather than natural gas. That means turbine blades are exposed to V rarely because natural gas is the main fuel of the turbine engines. For that reason, the ratio of V_2O_5 in salt mixture was decreased from 50 wt. % to 10 wt. %. Consequently, following procedure were developed to apply corrosive salts to sample surfaces (thermo-gravimetric method).

1- Na_2SO_4 (90 wt. %) and V_2O_5 (10 wt. %) were solved in a 500 ml DI water at 100 °C on a hot plate & stirrer.
2- Test samples were heated up to 200 ˚C on a hot plate.
3- Salt mixture solved in hot water was sprayed to test samples for 15 min. Samples were left to dry before each spray.

Corrosive salt mixture was applied on samples surfaces once at the beginning of the hot corrosion test. Table 4.7 summarizes surface preparation for hot corrosion test before and after optimization studies.

Table 4.7 Surface preparation for hot corrosion test before and after optimization.

	Corrosive Salts	**Test Method**
Before Optimization	Na_2SO_4 (50 wt. %) and V_2O_5 (50 wt. %)	Crucible Method (Salt Immersion)
After Optimization	Na_2SO_4 (90 wt. %) and V_2O_5 (10 wt. %)	Thermo-gravimetric Method (Salt Spray)

3- Hot Corrosion Test Condition

Hot corrosion is mostly divided into two as Type I (high temperature hot corrosion) and Type II (low temperature hot corrosion), mostly depending on exposing temperature. While, Type I hot corrosion, also called as HTHC, is mainly observed at the temperature range of 850 – 950 °C [70], Type II hot corrosion (LTHC) is mainly observed at the temperature range of 650 – 800 °C which is below the melting point of Na_2SO_4 [73].

The pilot hot corrosion test for optimization study was conducted at 800 °C furnace temperature which is at the maximum limit of Type II corrosion. However, SO_3 is required in the gas phase with high partial pressure to LTHC reactions occur, while HTHC is observed in air or pure oxygen atmosphere [70]. As mentioned before, hot corrosion tests could not be performed under natural gas atmosphere due to limitation of test equipment. Therefore, 800 °C test temperature could not be suitable to observe LTHC under hot air atmosphere. Also, the melting point of Na_2SO_4 which is used in hot corrosion test is above 800 °C. At higher test temperatures, corrosive effect of Na_2SO_4 will be more apparent. For that reason, test temperature was increased from 800 °C to 900 °C which is in the range of HTHC.

Table 4.8 Hot corrosion test temperature before and after optimization.

	Test Temperature	**Hot Corrosion Type**
Before Optimization	800 °C	In between Type I (HTHC) & Type II (LTHC)
After Optimization	900 °C	Type I (HTHC)

4- Sampling Frequency

Sampling frequency for weight measurements and characterization is an important test condition to observe the effect of hot corrosion on aluminide coated test samples. In this study, discontinuous (interrupted) measurement of hot corrosion method was used which involves the interruption of the test process, by cooling the samples to room

temperature. Following the sample removal for corrosion assessment, rest of the samples were reloaded to test furnace for further exposure.

Total hot corrosion exposure time was 120 hours for pilot hot corrosion test. One piece of sample in each sample set was removed from test furnace in 24 hour intervals for detailed investigations. However, characterizations of test samples showed that all samples were totally corroded after first 24 hours and hot corrosion aggressively continued to the end of the test as mentioned latter topic. Results demonstrate that incubation period of oxidation and hot corrosion is short; therefore, in a form of logarithmic scale was adopted for sampling frequency rather than equal sample removal intervals. By this way, the effect of hot corrosion at the beginning of the exposure would be investigated in more details.

In addition, total exposure time was prolonged from 120 hours to 400 hours. The main reason of such a destructive corrosion was the crucible test method. However, the effect of hot corrosion would be less aggressive by using thermos-gravimetric (salt spray) method. Therefore, test duration was extended to 400 hours to compare the effect of ternary elements on aluminide coating for a longer period.

Table 4.9 Hot corrosion test conditions as test temperature, total test time, weight measurements and sample take out intervals.

	Total Test Time	**Weight Measurement Intervals (h)**	**Sample Removal Intervals (h)**
Before Optimization	120 hours	-	24, 48, 72, 96, 120
After Optimization	400 hours	1, 2, 5, 10, 20, 50, 100, 150, 200, 250, 400	1, 2, 5, 10, 20, 50, 100, 150, 200, 400

4.2.3.2 Optimized Hot Corrosion Test Procedure:

After hot corrosion test optimization study, surface preparation, test conditions, test duration, and sampling frequency were decided. Consequently, following procedure was used in hot corrosion test of simple, Cr, Cr/Y, Zr, and Hf modified aluminide coatings.

1- All test samples were weighted by KERN & Sohn ABJ 220-4M precision scales with 0.1 mg readability.
2- 10g Na_2SO_4 (Carlo Erba, 99%) ve 1g V_2O_5 (ACROS Organics, 99+%) were solved in a 500 ml DI water at 100 °C by using 100 rpm agitation speed on a Mtops MS300HS Hot Plate&Stirrer.
3- Test samples were heated up to 200 ˚C on a hot plate set to 350 °C.
4- Salt mixture solved in hot water was sprayed to test samples for 15 min. Samples were left to dry before each spray. Images of test samples before and after the salt spray is shown in Figure 4.4. Corrosive salt mixture was applied on samples surfaces once at the beginning of the hot corrosion test.

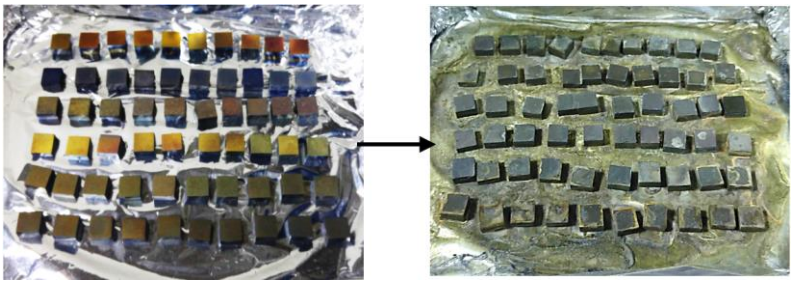

Figure 4.4 Corrosion test samples on a hot plate before salt spray (a) after salt spray (b).

5- Samples were weighed again to measure accumulated salt amount on sample surfaces.

6- Test samples were divided into two group as characterization and weighing samples. One test sample from each coating sets was selected and placed in a separate test furnace by placing in the alumina crucible for weight measurements. Characterization samples, on the other hand, were placed into

two separate furnaces as 27 samples for each furnace. Figure 4.5 sample placement on test furnaces.

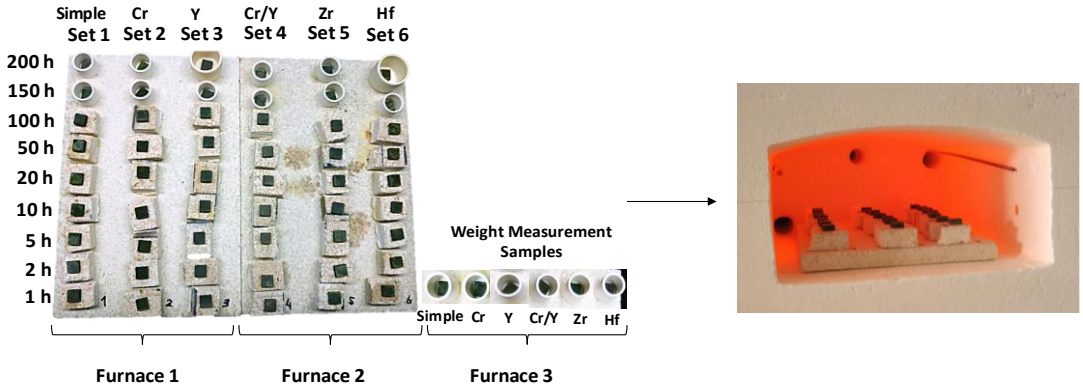

Figure 4.5 Corrosion test sample arrangements for six coating sets.

7- Hot corrosion tests were carried out at 900 °C and samples were loaded to pre-heated furnaces.

8- The total exposure time of the corrosion test was 400 hours. Since meta-stable oxide formations on the coating surface are observed at the beginning of the corrosion test, the sample take-out intervals for characterizations, and weight measurements were determined as more frequent at the beginning (Table 4.9).

9- In given time intervals, characterization and weight measurements samples were removed from hot furnaces and cooled in air.

10- Weight gain and change of weight measurement samples were taken by KERN & Sohn ABJ 220-4M precision scales with 0.1 mg readability. The corrosion test was continued by loading them back into the furnace after weight measurements. The weight of the samples (with spalled oxides) and net weights (without spalled oxides) were measured separately.

4.3 Results and Discussion

4.3.1 Characterizations of Coatings Before Corrosion Test

Before the hot corrosion test, one sample from each coating set was characterized to observe the beginning coating thickness, microstructure, and composition.

Simple Aluminide Coating

Simple aluminide coating test samples were coated by using CVD process parameters given in Table 4.3.

For simple aluminide coated samples, an average 45 µm outer coating layer and 27 µm IDZ thickness (total 72 µm) were obtained. The composition analysis by WDS shows that in 43-47 at. % aluminum is present in the outer coating layer, and it demonstrates the presence of β-NiAl phase at outer layer (Fig. 4.6). Also, chemical mapping by WDS represents that Al homogeneously distributed and no unexpected phases present at outer coating layer (Fig. 4.7).

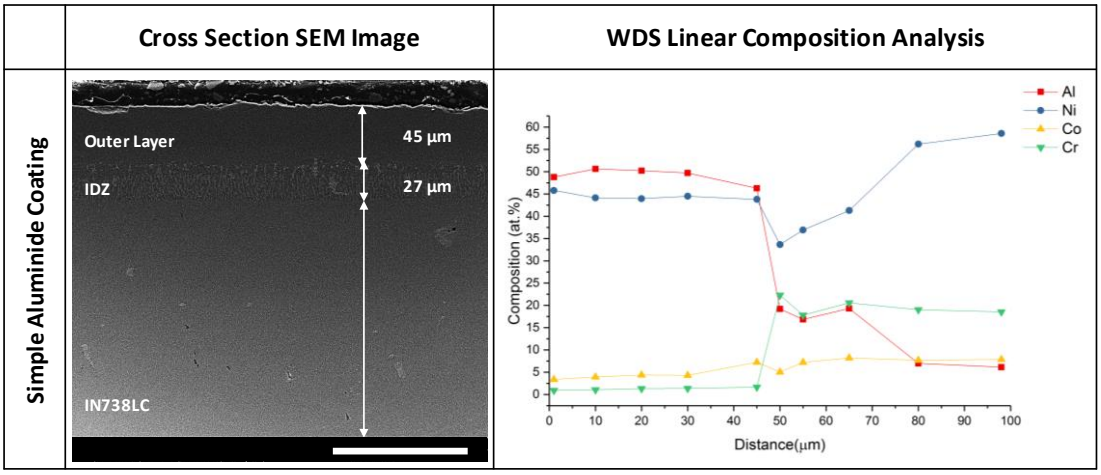

Figure 4.6 Cross section SEM image and WDS linear composition analysis of the simple aluminide coating prepared for corrosion tests. (The scale bar = 100 µm)

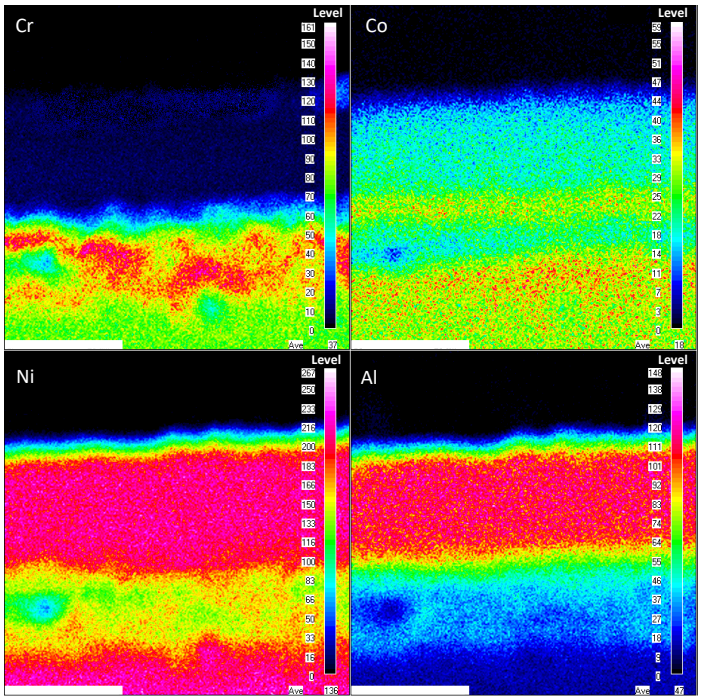

Figure 4.7 WDS Cross-sectional chemical mapping of the simple aluminide sample coated sample for corrosion tests. (The scale bar = 50 μm)

Chromium Addition

Cr modified aluminide coating test samples were coated by using CVD process parameters given in Table 4.3.

For Cr modified aluminide coated samples, an average 43 μm outer coating layer and 30 μm IDZ thickness (total 73 μm) were obtained. The chemical analysis shows that 43-47 at. % aluminum is present in the outer coating layer and it demonstrates the presence of β-NiAl phase at outer layer (Fig. 4.8). Cr composition is changing between 8-13 at. % along outer coating layer which is around the expected Cr composition (10 at.%). Cr content increases to 50 at. % at IDZ. When reached to the substrate, Cr level drops to 15 – 18 at. % level. Also, chemical mapping by WDS demonstrates that Al and Cr homogeneously distributed at outer coating layer and there are no undesired precipitates of Cr as α-Cr (Fig. 4.9).

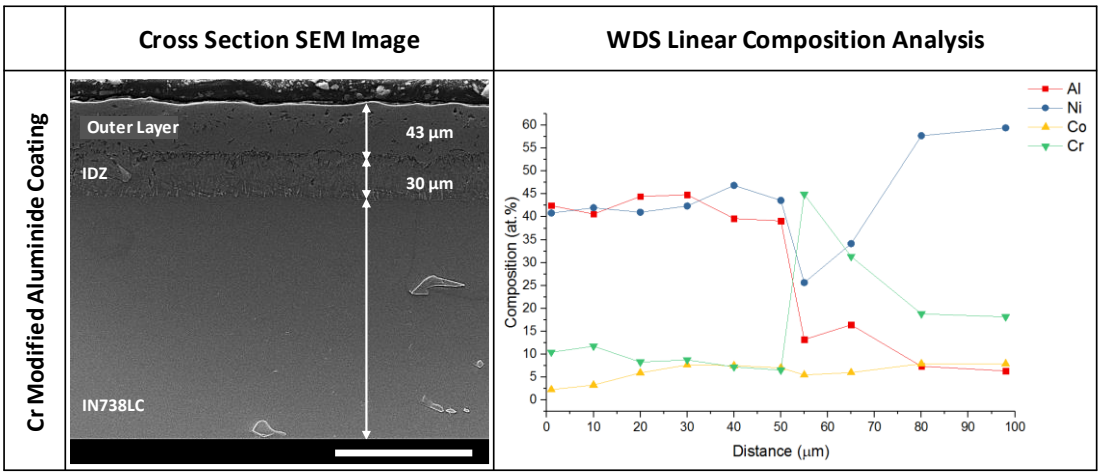

Figure 4.8 Cross Section SEM Image and WDS linear composition analysis of the Cr modified aluminide coating prepared for corrosion test. (The scale bar = 100 µm)

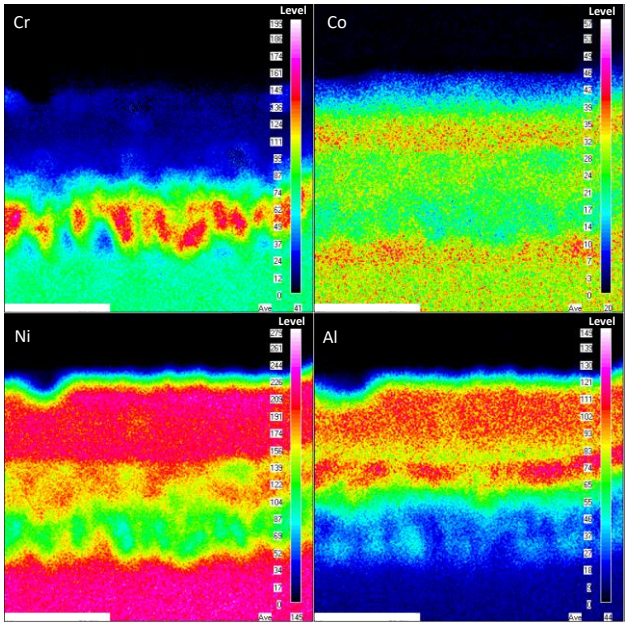

Figure 4.9 WDS Cross-sectional chemical mapping of the Cr modified aluminide coated sample for corrosion tests. (The scale bar = 50 µm)

Hafnium Addition

Hf modified aluminide coating test samples were coated by using CVD process parameters given in Table 4.3.

For Hf modified aluminide coated samples, an average 48 µm outer coating layer and 30 µm IDZ thickness (total 78 µm) were obtained. The chemical analysis shows that 43-46 at. % aluminum is present in the outer coating layer, and it demonstrates the presence of β-NiAl phase at outer layer (Fig. 4.10). Hf composition is fluctuating between 430-730 ppm along outer coating layer which is around the expected Hf content (500 ppm). Also, chemical mapping by WDS represents that Al and Hf homogeneously distributed at outer coating layer as shown in Figure 4.11.

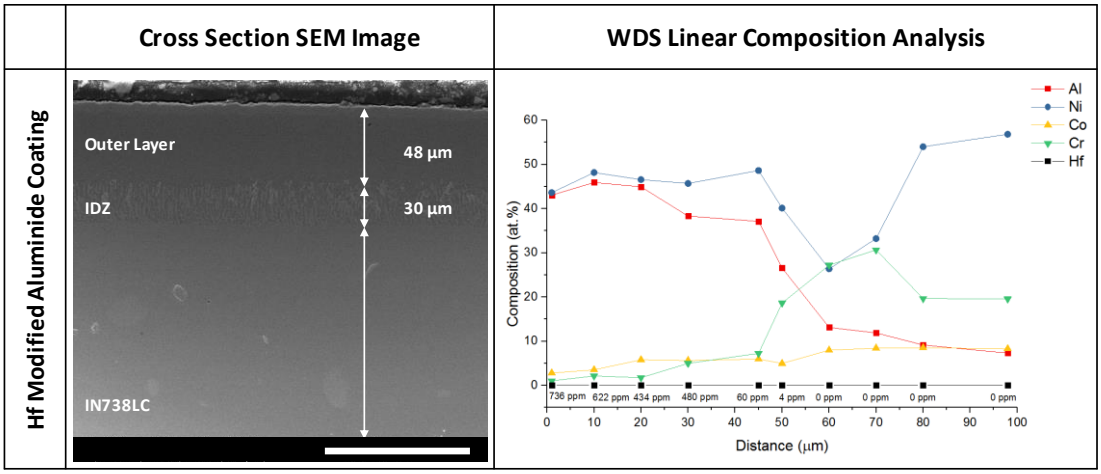

Figure 4.10 Cross Section SEM Image and WDS linear composition analysis of the Hf modified aluminide coating prepared for corrosion test. (The scale bar =100 µm)

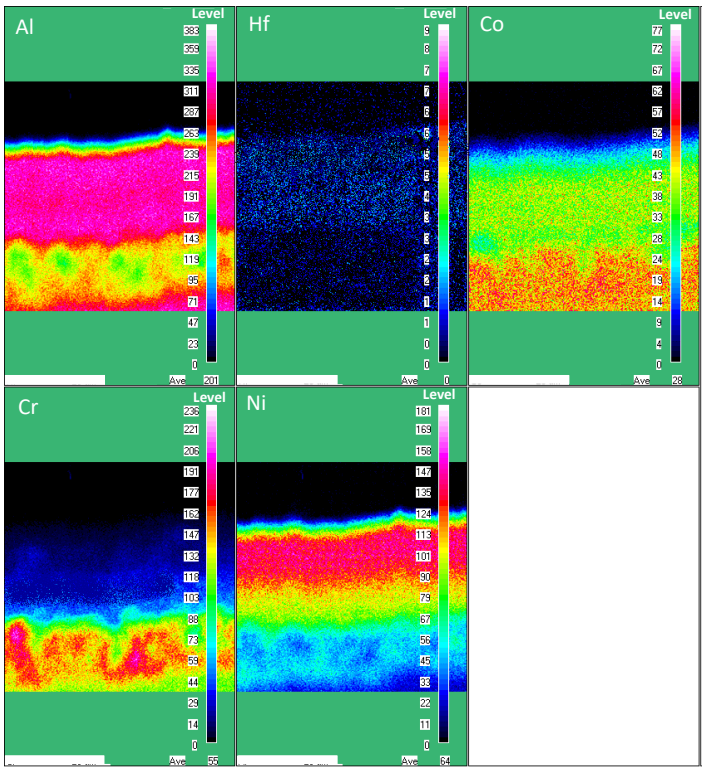

Figure 4.11 WDS Cross-sectional chemical mapping of the Hf modified aluminide coated sample for corrosion tests. (The scale bar = 50 μm)

Yttrium Addition

Y modified aluminide coating test samples were coated by using CVD process parameters given in Table 4.3.

Average 46 μm outer coating layer and 27 μm IDZ thickness (total 73 μm) were obtained in Y modified aluminide coated samples. The chemical analysis shows that 45-51 at. % aluminum is present in the outer coating layer, and it demonstrates the presence of β-NiAl phase (Fig 4.12). Y composition is altering between 320-600 ppm along outer coating layer which is around the expected Y composition (500 ppm). However, Y level sharply increases to 4000 ppm at outer layer/IDZ interface. Still, chemical mapping by WDS represents that Y homogeneously distributed at outer coating layer (Fig. 4.13).

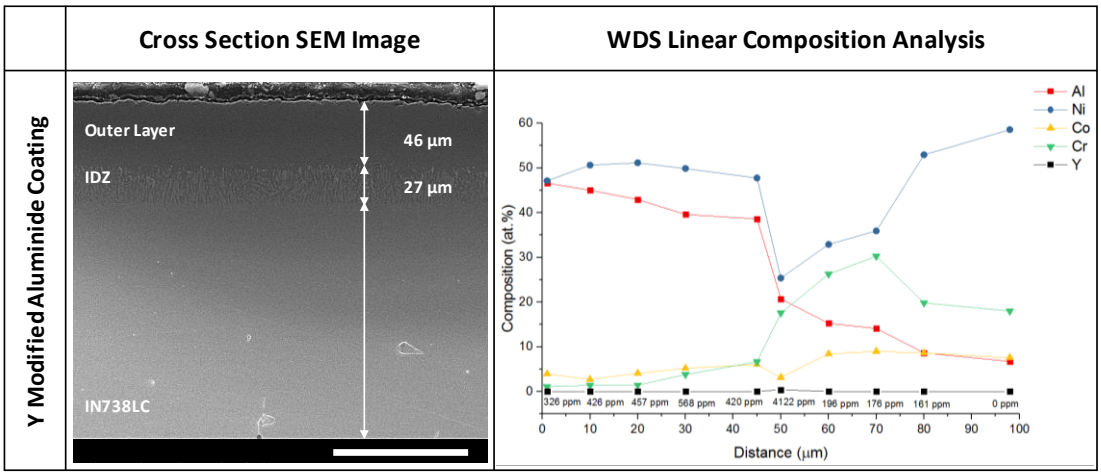

Figure 4.12 Cross Section SEM Image and WDS linear composition analysis of the Y modified aluminide coating prepared for corrosion test. (The scale bar = 100 µm)

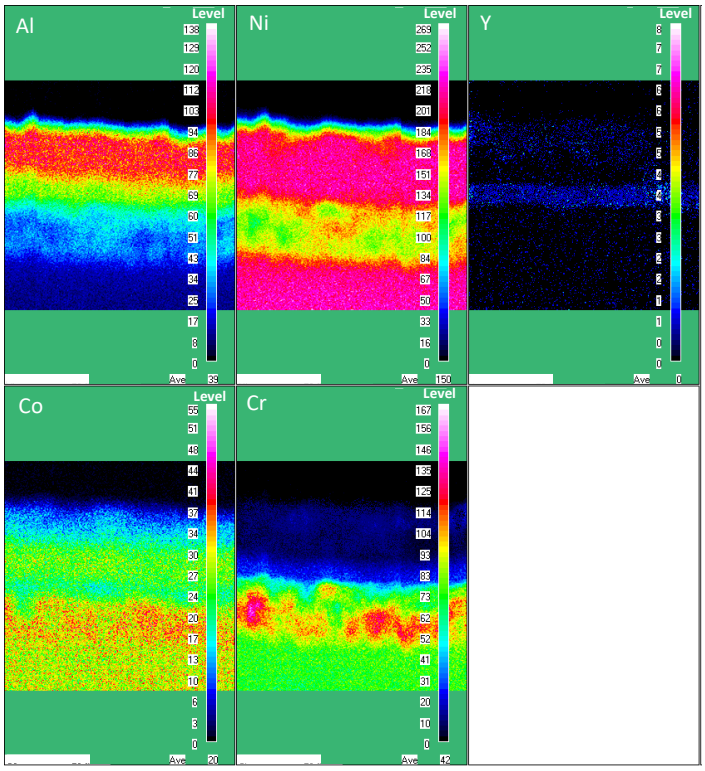

Figure 4.13 WDS Cross-sectional chemical mapping of the Y modified aluminide coated sample for corrosion tests. (The scale bar = 50 µm)

Zirconium Addition

Zr modified aluminide coating test samples were coated by using CVD process parameters given in Table 4.3.

For Zr modified aluminide coated samples, an average 47 µm outer coating layer and 29 µm IDZ thickness (total 76 µm) were obtained. The chemical analysis shows that 40-45 at. % aluminum is present in the outer coating layer, and it demonstrates the presence β-NiAl phase (Fig. 4.14). Zr composition is at the level of 500 ppm along outer coating layer which is close to expected Zr composition (500 ppm). Also, chemical mapping by WDS represents that Zr homogeneously distributed at outer coating layer (Fig. 4.15).

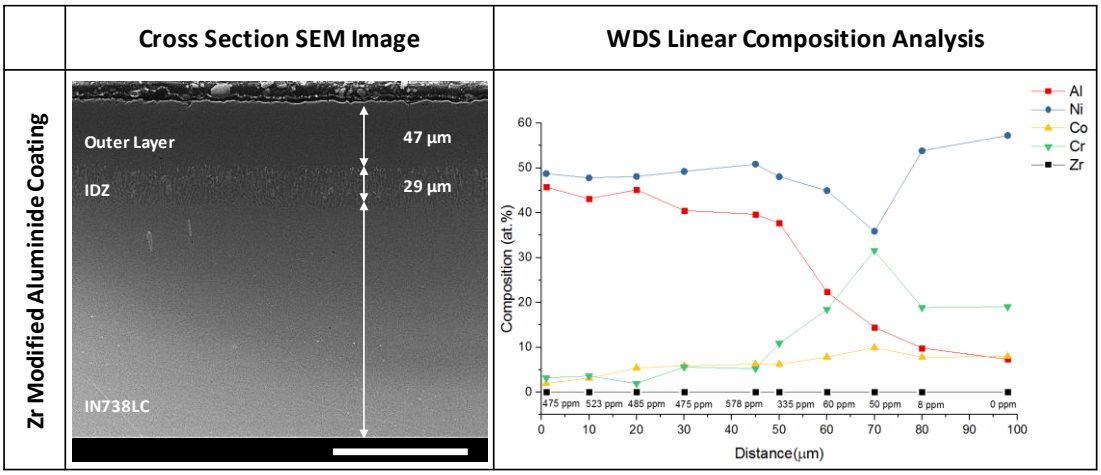

Figure 4.14 Cross Section SEM Image and WDS linear composition analysis of the Zr modified aluminide coating prepared for corrosion test. (The scale bar =100 µm)

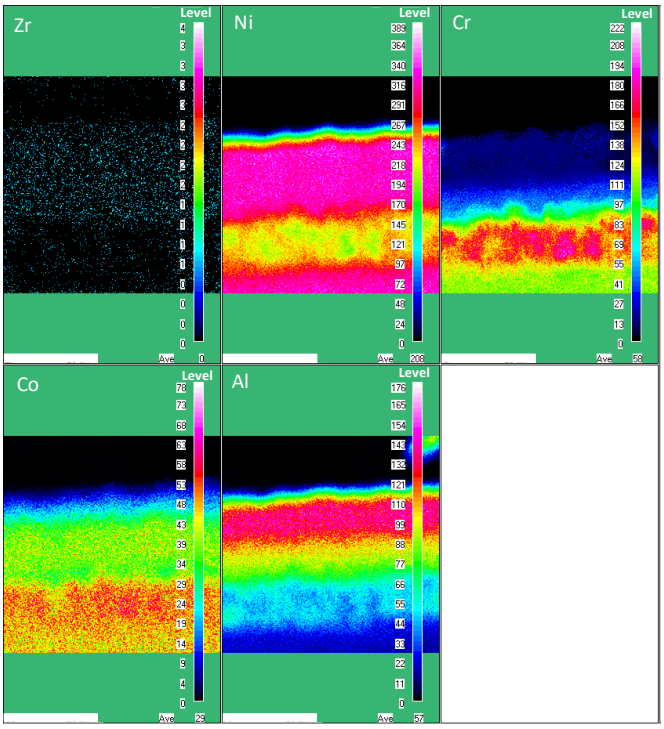

Figure 4.15 WDS Cross-sectional chemical mapping of the Zr modified aluminide coated sample for corrosion tests. (The scale bar = 50 μm)

Chromium/Yttrium Addition

Cr/Y modified aluminide coating test samples were coated by using CVD process parameters given in Table 4.3.

Similar with other coatings, an average 45 μm outer coating layer and 27 μm IDZ thickness (total 72μm) were obtained. The chemical analysis shows that 45-50 at. % aluminum is present in the outer coating layer, and it demonstrates the presence of β-NiAl phase (Fig. 4.16). Y composition is changing between 350-600 ppm along outer coating layer which is around the expected Y concentration (500 ppm). However, Y level increases to 2650 ppm at outer layer/IDZ interface. Besides Y, Cr composition is changing between 6-10 at. % at outer coating layer, while expected Cr content is around 10 at. %. Cr composition increases to 35 at. % at IDZ. When reached to the substrate, Cr level drops to 15 – 18 at. % level. Chemical mapping by WDS represents that Cr and Y homogeneously distributed at outer coating layer and their content increases near to outer layer/IDZ interface (Fig. 4.17).

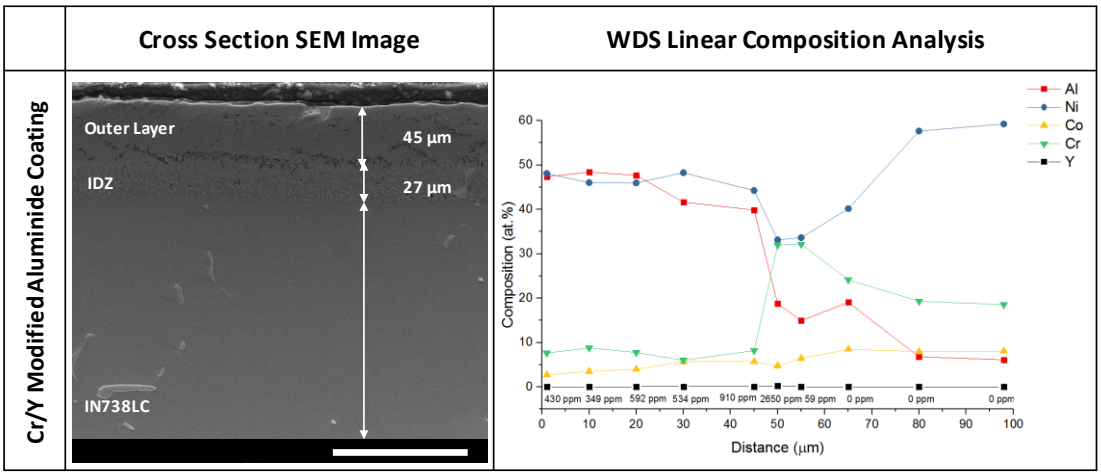

Figure 4.16 Cross Section SEM Image and WDS linear composition analysis of the Cr/Y modified aluminide coating prepared for corrosion test.
(The scale bar = 100 µm)

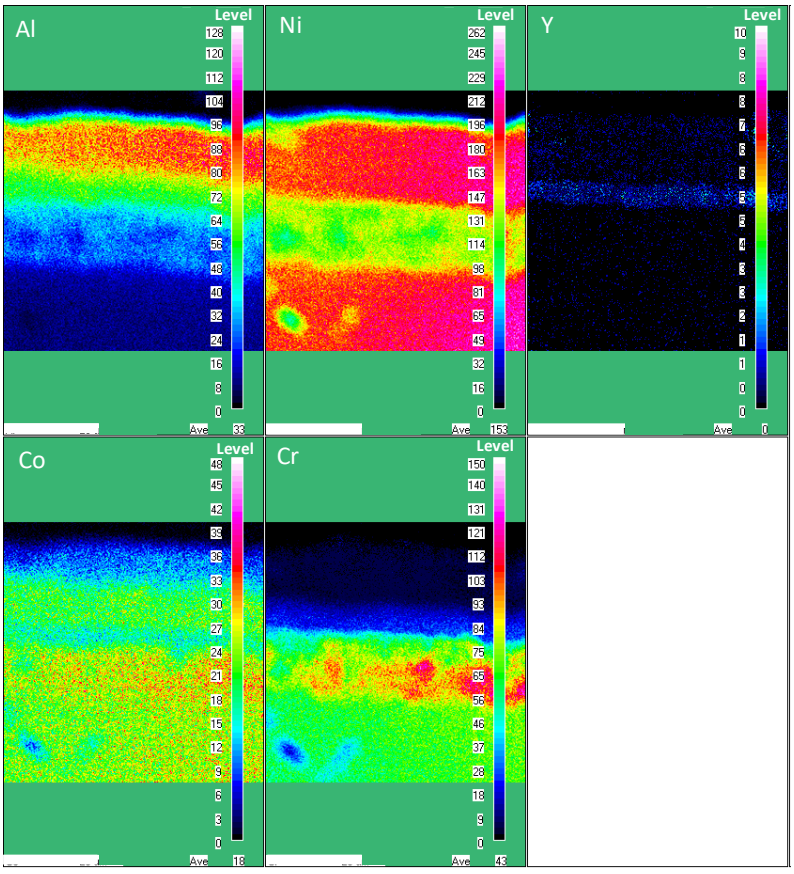

Figure 4.17 WDS Cross-sectional chemical mapping of the Cr/Y modified aluminide coated sample for corrosion tests. (The scale bar = 50 µm)

4.3.2 High Temperature Corrosion Test Results

Total mass gains (Fig. 4.18) and mass changes (Fig. 4.19) of hot corrosion test samples were plotted for comparative analysis. Also, XRD analysis was performed to identify the surface phases as shown in Figure 4.20.

As a side note, total weight gain graph shows the weight gain caused by oxidation of samples. If the weight gain rate of a sample is high, it means rapid oxide formation occurred at sample surfaces. On the other hand, weight change graph represents not only oxidation rate but also oxide spallation. If there is a weight loss, it means surface oxides spalled due to weak adherence. Therefore, if total weight gain and weight loss of a coating are less, it indicates the formation of slow growing and adherent oxides which are preferred for better hot corrosion resistance. Also, the presence of α-Al_2O_3 and Cr_2O_3 at the substrate surface is expected for better hot corrosion behavior, while Ni, Ti, Nb, W containing oxides indicates depletion of the coating due to hot corrosion. Hot corrosion behavior of aluminide coatings was compared accordingly.

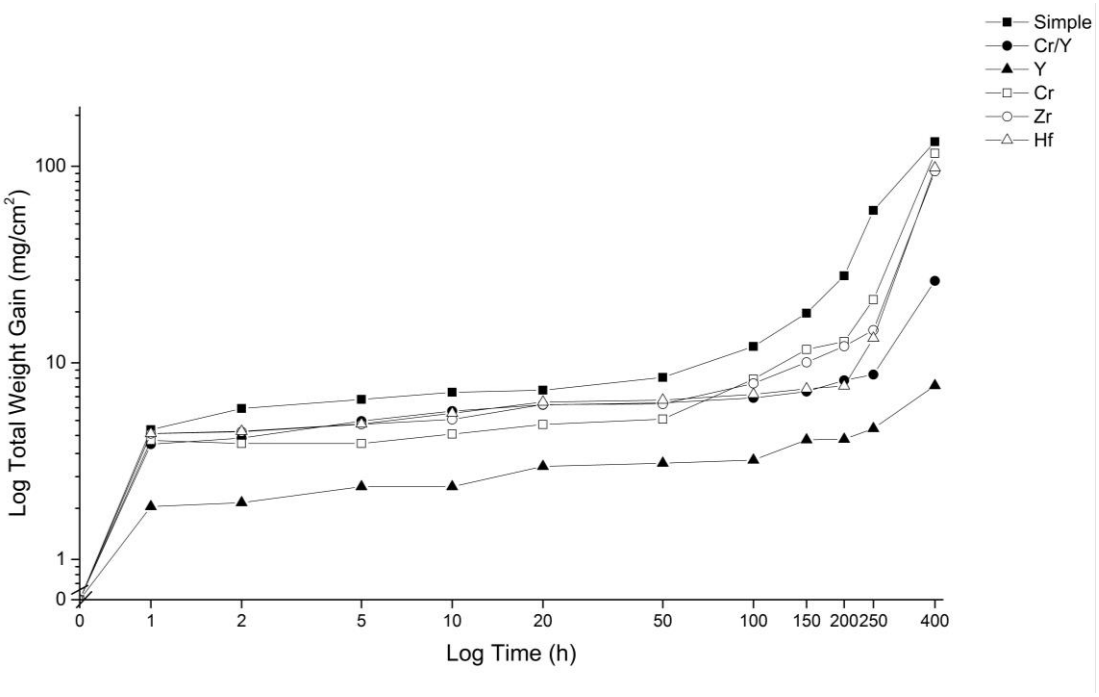

Figure 4.18 Specimen total mass gains during 400 hours isothermal hot corrosion test at 900°C.

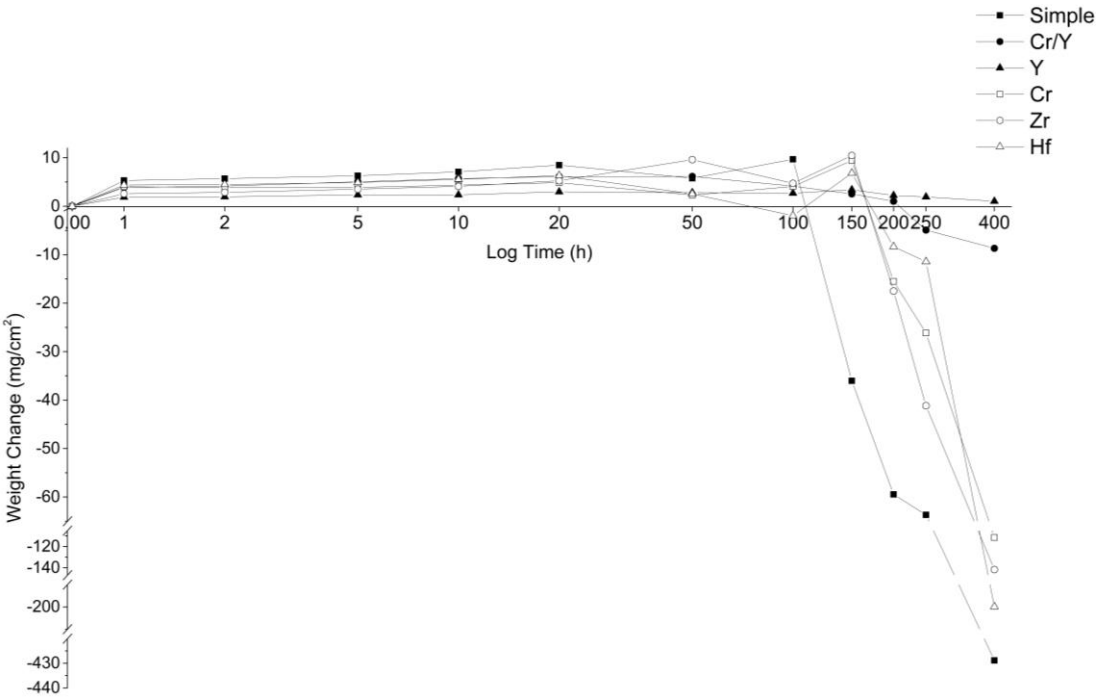

Figure 4.19 Specimen mass changes during 400 hours isothermal hot corrosion test at 900°C.

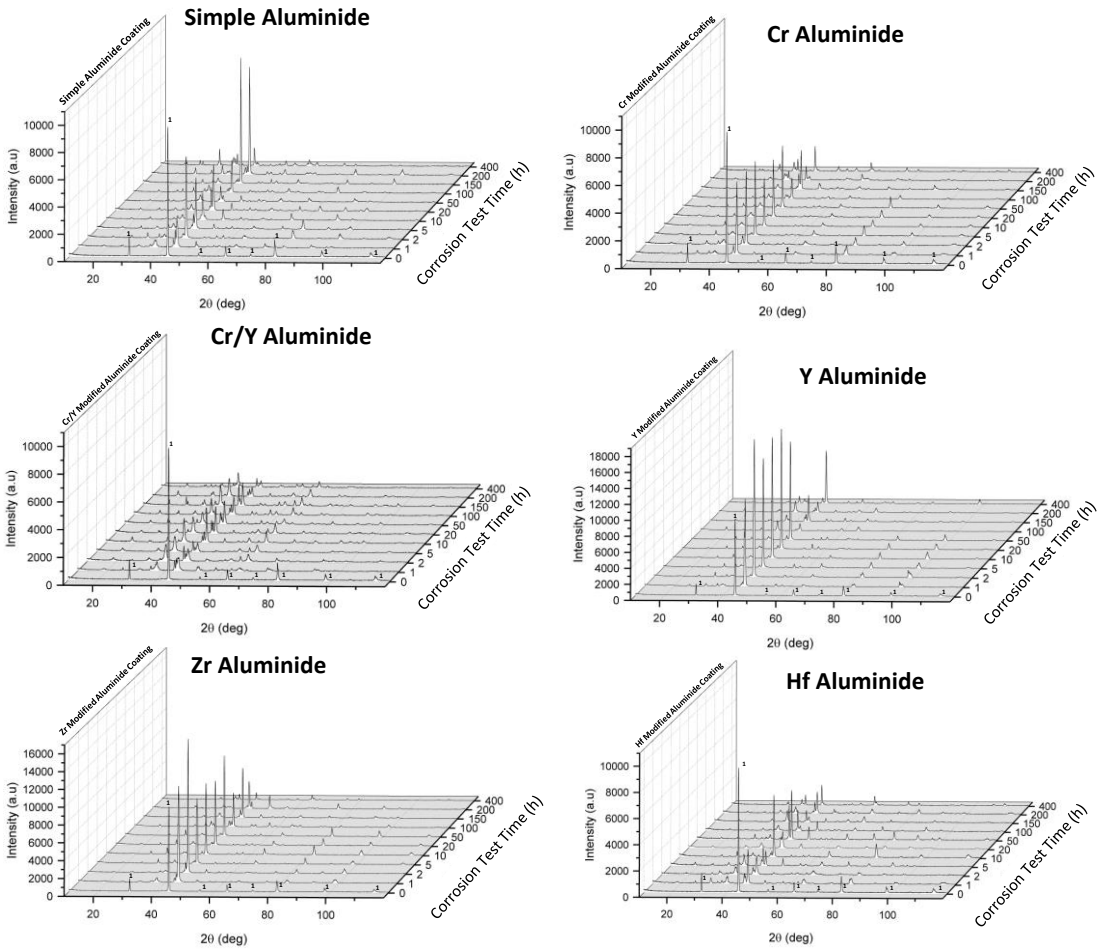

Figure 4.20 XRD patterns of corrosion test specimens after varying exposure periods to hot corrosion.

A similar weight gain profiles were observed for all coatings except the Y modified aluminide after the first hour of corrosion test. Rapid weight gains indicate the formation of the fast growing oxides at the beginning of hot corrosion. However, the total weight gain of Y-aluminide was less than the other coatings. Fewer mass gain signifies the formation of slow growing oxides which is preferred for better oxide adherence. Also, XRD phase analysis showed that α-Al_2O_3 and Cr_2O_3 formed on all coating surfaces with low levels of Co and Ni containing oxides. According to EDS analysis taken from surface oxides, the amount of Cr_2O_3 was higher at the surface of Cr and Cr/Y modified aluminide coatings.

Until 50th hour, weight increments showed a similar trend for all coatings. The most weight gained coating was simple aluminide while the least weight gained was Y modified aluminide coating. The most significant increase was seen in the simple aluminide coating, indicating rapid oxide growth on the surface. However, slow growing, dense and homogeneous oxide layer is preferred for better oxidation and corrosion resistance. After 20 hours exposure, some fluctuations in the mass change profiles of simple, Cr, Zr and Hf aluminides were observed that indicates oxide spallation and new oxide formation at the exposed surfaces. However, no spallation was observed in Y and Cr/Y aluminide coatings.

After 100 hours exposure, simple aluminide coating quickly began to gain weight, and a significant increase was observed. Such weight gain indicates continuous oxide spallation and reformation. Still, α-Al_2O_3 and Cr_2O_3 were present on coating surface with the small amount of Co, Ni, and Ti containing oxides. However, a steady weight increase was observed in Y, and Cr/Y modified coatings up to 250 h.

After 250 hours exposure, the Zr, Hf, and Cr modified coatings rapidly gained weight up to 100 mg/cm^2 at the end of corrosion test. Also, a large weight loss was seen after 100 hours in the simple coating, and after 150 hours in Zr, Hf and Cr modified aluminide coatings. Weight loss indicates the oxide spallation from coating surfaces which causes Al depletion in aluminide coating due to new oxide formation at the spalled areas.

At the end of hot corrosion test, NiO, NiO_2, TiO_2, $NiCr_2O_4$, and $Ni(WO_4)$ formed at the surface of simple and Zr, Hf, Cr aluminides. Figure 4.21 shows surface XRD analysis of simple aluminide coating at the end of hot corrosion test. Similar oxide formations were observed in Zr, Hf, and Cr aluminides at the end of hot corrosion test. Formation of such oxides at specimen surfaces indicates internal corrosion and oxidation due to depletion of aluminide coating. However, surface of Y and Cr/Y aluminide coatings consist of mainly Al_2O_3 which shows presence of protective oxides at substrate surfaces.

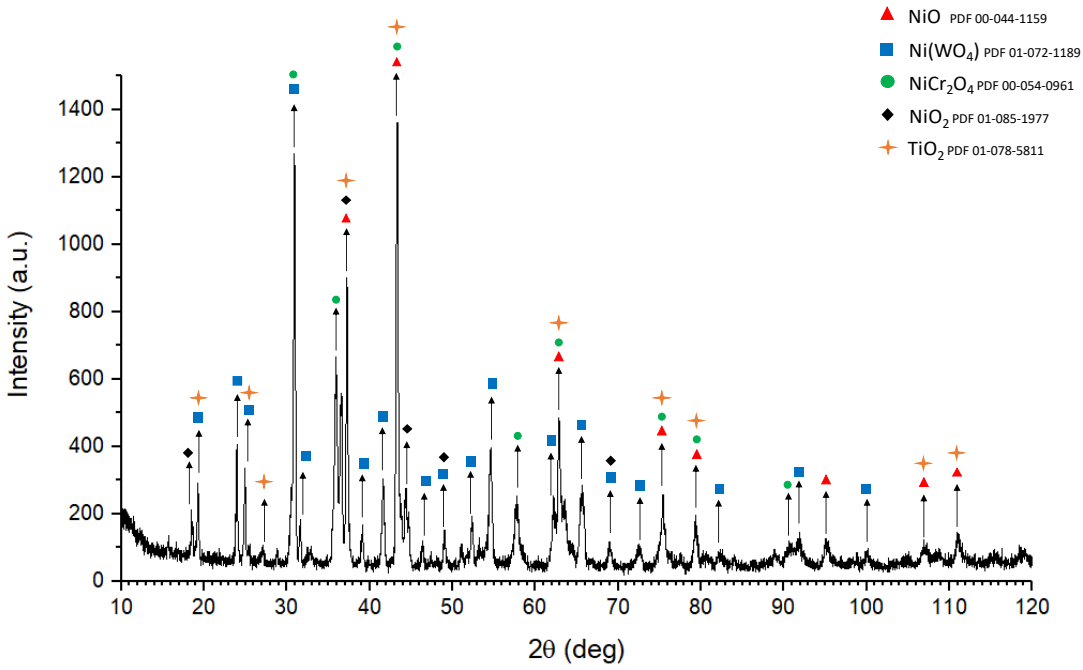

Figure 4.21 XRD pattern of corrosion test specimen (simple aluminide) at the end of corrosion test.

Cr/Y and Y modified coatings did not show a significant decrease in weight until 200 h. The weight loss of Cr/Y aluminide was only 9 mg/cm^2 after 400 hours. On the other hand, no weight loss was observed for Y aluminide coating. At the end of hot corrosion test, Y aluminide only gained 8 mg/cm^2 weight which indicates slow growing and adherent oxide formation on the substrate surface. Yttrium sulfide phase was also found at the surface of Y containing coatings. It is supposed that Y enhances the corrosion resistance by preventing sulfur segregation to boundaries and interfaces by forming stronger sulfides compared to other reactive and alloying elements (Fig. 4.22). Total mass gain and mass loss analysis show that the most excellent hot corrosion resistance is obtained by Y addition to aluminide coating. Similarly, Cr/Y modified aluminide showed better corrosion resistance compared to Cr, Hf, Zr, and simple aluminide coatings, in decreasing order.

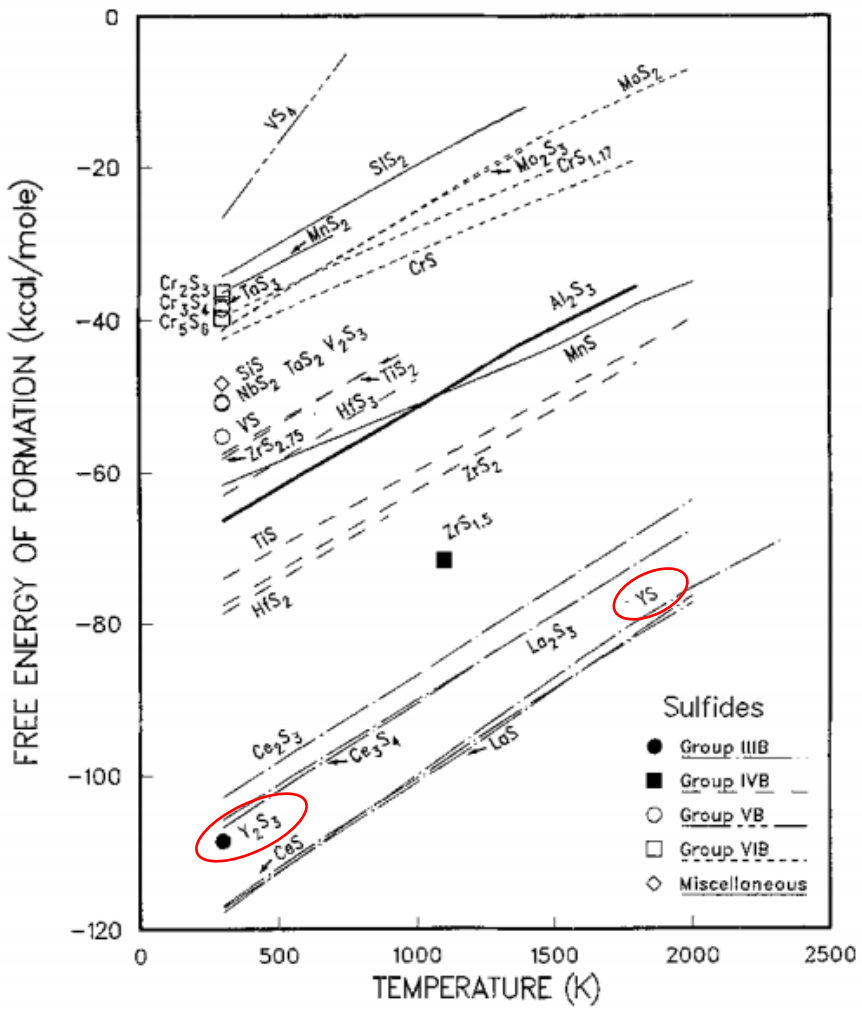

Figure 4.22 Standard free energy of formation (per mole of sulfur as S_2 gas) vs. temperature for various sulfides [90].

In addition to weight change and XRD analysis, cross-sectional SEM surface analysis was done to examine oxide formations, spallation, and microstructure in details. In the first 20 hours, it appears that a thin oxide layer on the coating surfaces was started to form as shown in Figure 4.23 and 4.24. The thickest oxide layer was observed in the simple aluminide coated specimen with an average 20 μm oxide layer. It is supposed that the reason for rapid oxide formation is meta-stable alumina formation in the first stage of oxidation. The addition of reactive and/or alloying elements promotes the formation of fine and dense α - alumina by suppressing formation of metastable phases. In modified aluminide coatings, the average oxide thickness is in between 5 - 10 μm.

After 100 hours exposure, it was observed that the thickness of the oxide layer together with outer coating layer began to decrease in the simple aluminide coating (Fig. 4.25). The reason of decreasing oxide layer and coating thickness is oxide spallation following with new oxide formation at poured regions. By continuous oxide formation, the thickness of β-NiAl layer decreases until Al in outer layer is totally consumed.

In modified aluminide coatings, no significant decrease in coating thickness was observed up to 150 hours (Fig. 4.26). The thickness of the oxide layer varies from 5 to 15 μm across the entire surfaces. Although local oxide spallation was observed, internal oxidation and corrosion were not observed on the sample surfaces. When reached 200 hours, Cr and Cr / Y modified coatings began to show gaps at the outer coating / IDZ interface. Due to high chromium content of Cr and Cr/Y modified coatings, chromium starts to precipitate along the β-NiAl/IDZ boundary. It causes void formation in this region by weakening the bonds as a result of high temperature exposure for a long time.

At the end of the 200th hour, precipitates up to 7-8 μm size and containing a high amount of sulfur were observed at the outer surface of simple aluminide coated specimen. Also, sulfur containing small precipitates were present in Cr aluminide which shows inner diffusion of sulfur. No sulfur-containing precipitates were found in the coatings containing reactive elements. It is supposed that reactive elements slow down the segregation and inner diffusion of sulfur.

At the end of corrosion test (400 h), the coating layer was completely consumed in the rest of the coatings with no Y. Also, high amount of nickel and chromium rich oxides were observed at the specimen surfaces with a thickness in the range of 50-100 μm. However, in Y and Cr/Y coatings, a dense and continuous α-Al_2O_3 layer was present in 15 - 25 μm thickness which prevents internal oxidation and corrosion. Also, the β-NiAl was still the dominant phase at the surface of Y containing coatings, while coatings with no Y were completely destroyed by hot corrosion after 400 hours.

The Y modified aluminide coating showed the best hot corrosion resistance and followed by the Cr/Y modified aluminide coating. The beneficial effect of Y was more significant compared to Hf, Zr, and Cr, due to Y forms stronger sulfides than other elements. The addition of Cr to aluminide coating improved the hot corrosion resistance of simple aluminide coating. The adverse effect of Cr on Cr/Y aluminide could be related to the formation α-Cr precipitates along the oxide/coating interface. A chain like Cr-rich precipices caused the formation of voids which decrease the adherence of oxide layer. The composition of Cr in Cr/Y modified aluminide coating was changing between 6 - 10 at. %. If it is decreased to a lower level like 5 at. %, the hot corrosion resistance could be improved by preventing the formation of α-Cr.

In short, the addition of ternary elements improved the hot corrosion resistance of aluminide coating, and the Y modified aluminide coating showed the best hot corrosion resistance.

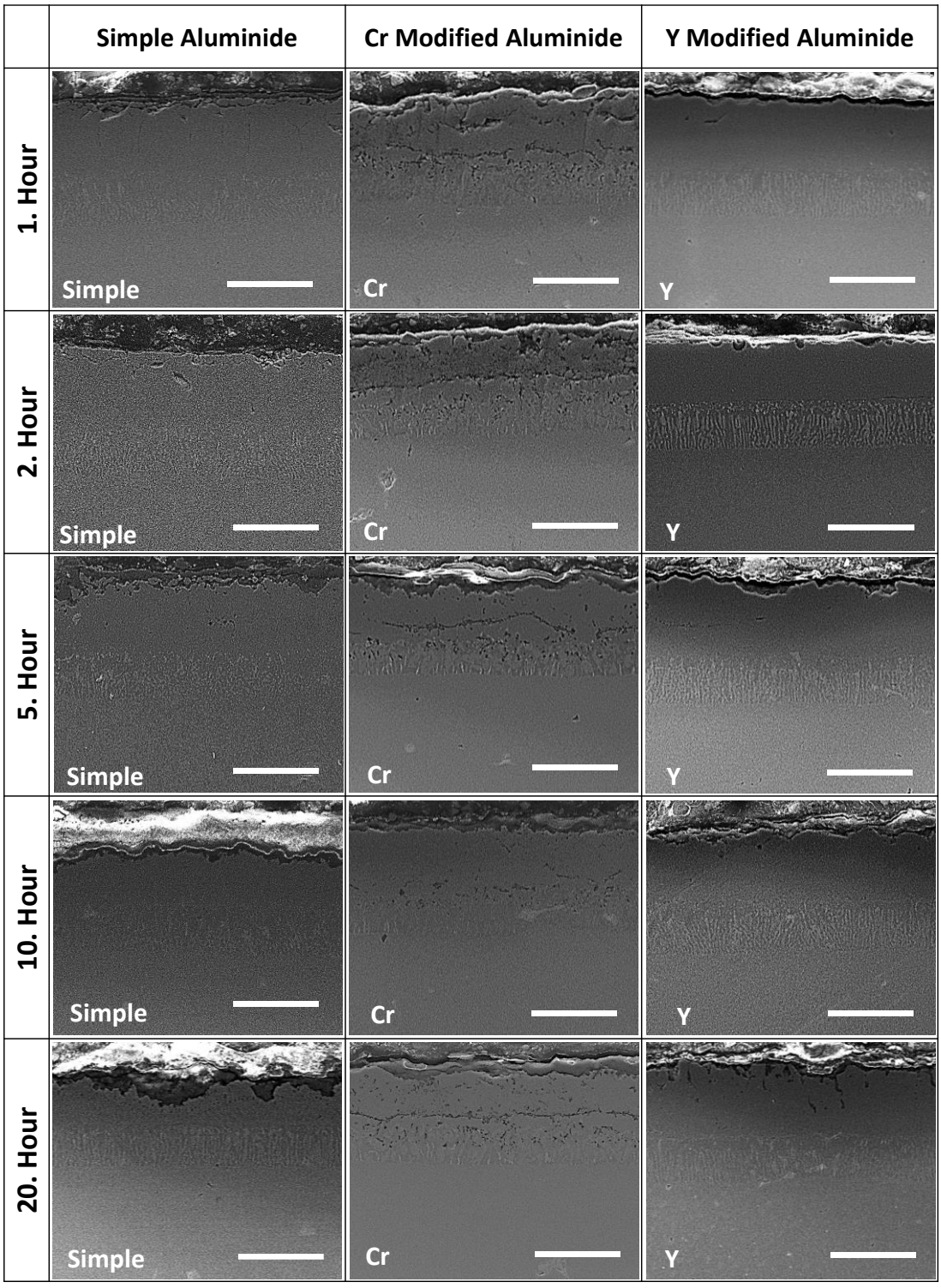

Figure 4.23 Cross section SEM images (The scale bar = 50 μm) of simple, Cr and Y aluminide coated samples after 1, 2, 5, 10 and 20 hours exposure to hot corrosion.

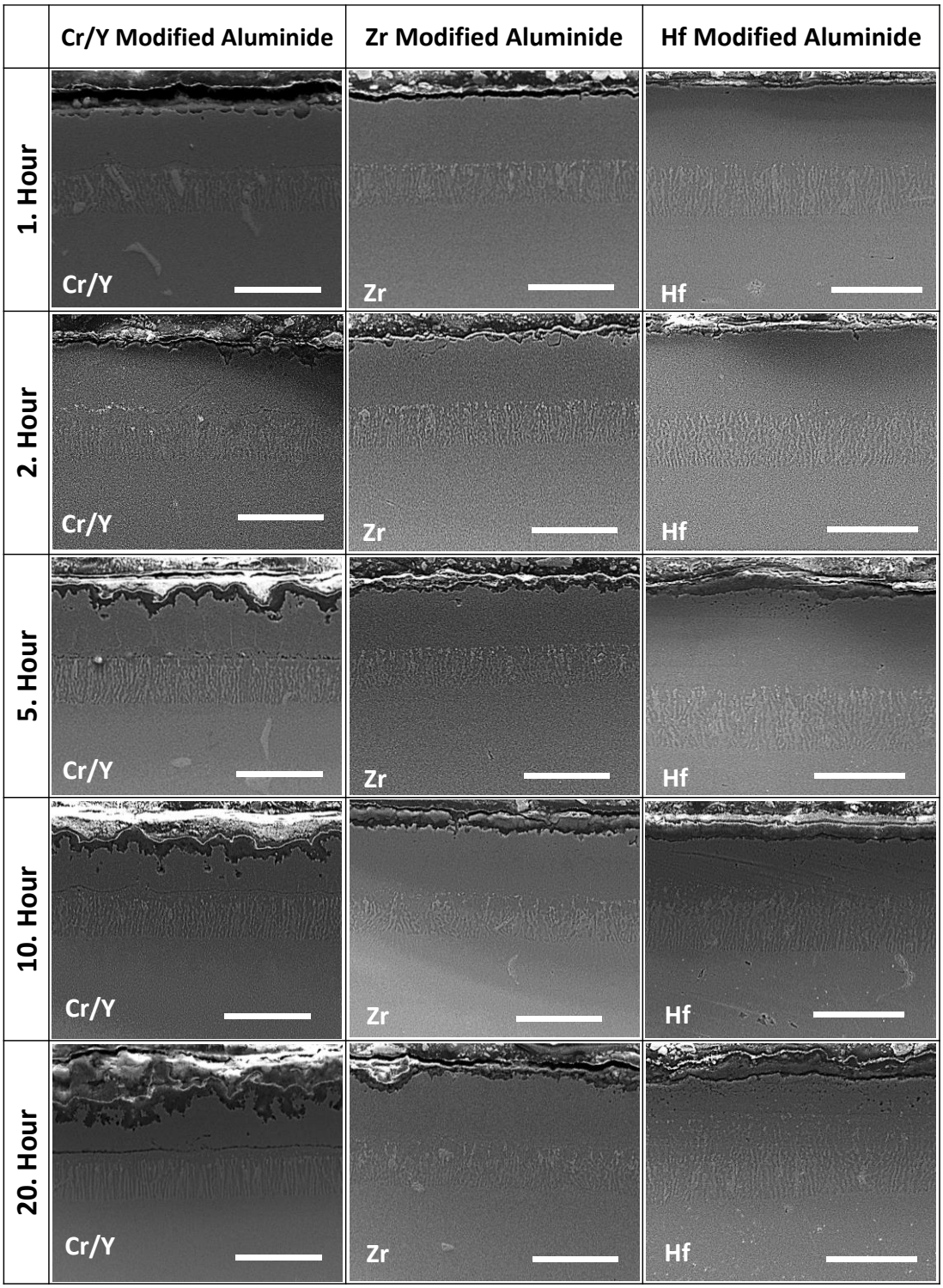

Figure 4.24 Cross section SEM images (The scale bar = 50 μm) Cr/Y, Zr and Hf aluminide coated samples after 1, 2, 5, 10 and 20 hours exposure to hot corrosion.

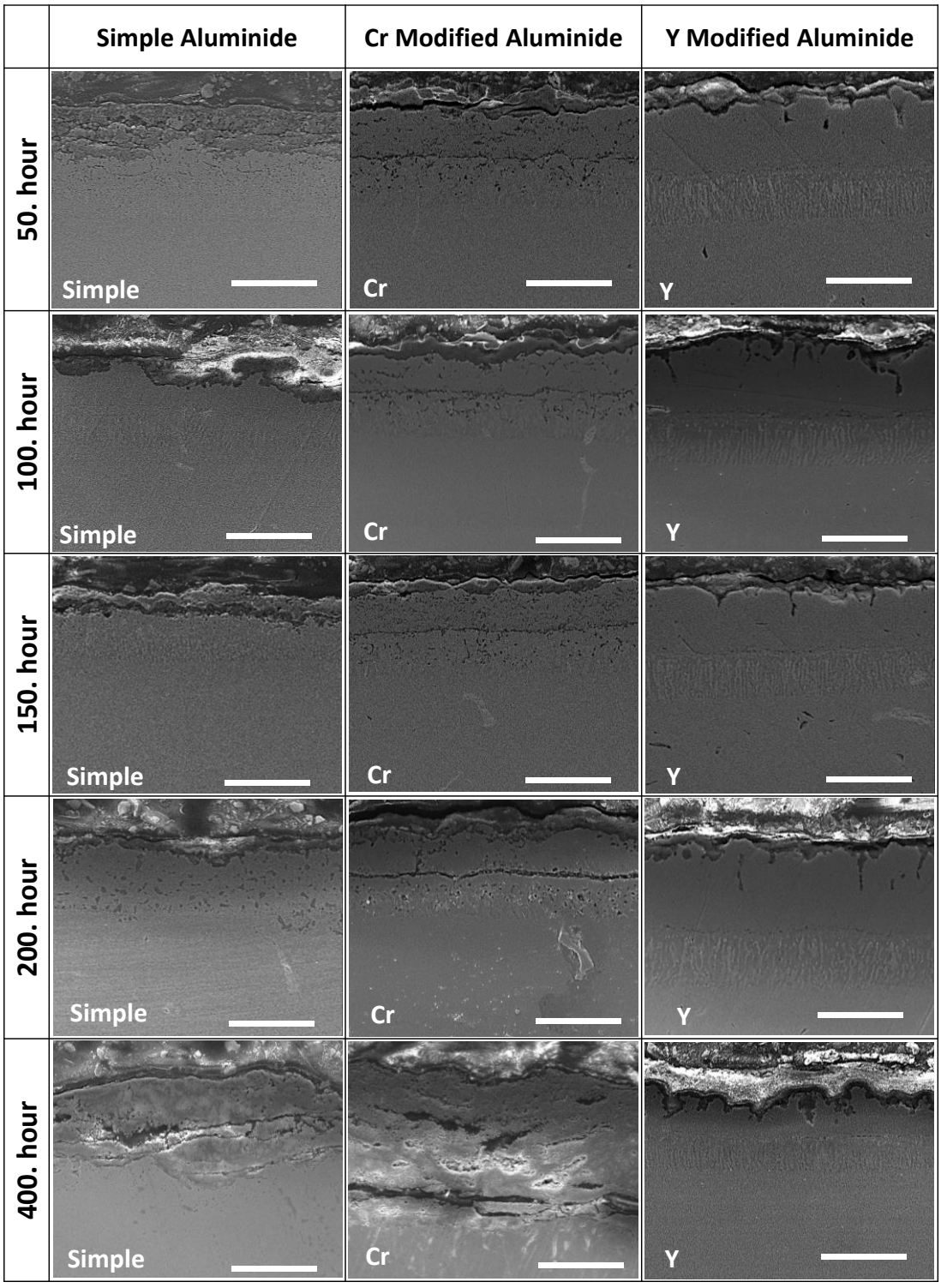

Figure 4.25 Cross section SEM images (The scale bar = 50 µm) of simple, Cr and Y aluminide coated samples after 50, 100, 150, 200 and 400 hours exposure to hot corrosion.

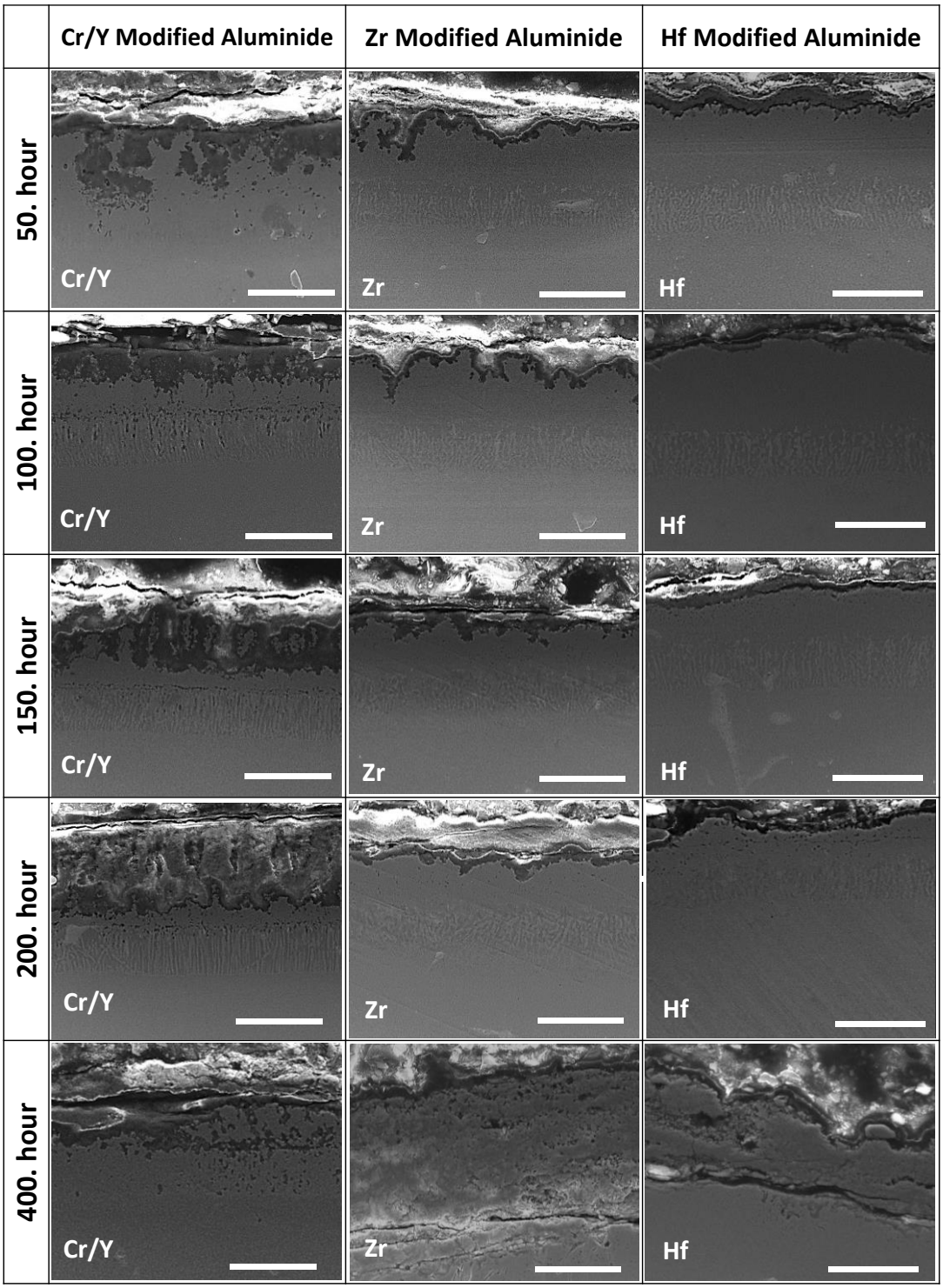

Figure 4.26 Cross section SEM images (The scale bar = 50 µm) Cr/Y, Zr and Hf aluminide coated samples after 50, 100, 150, 200 and 400 hours exposure to hot corrosion.

4.4 Conclusion

In this chapter, the influence of ternary element addition on the hot corrosion resistance of aluminide coating was studied by discontinuous measurement of hot corrosion method. Simple, Cr, Y, Cr/Y, Zr, and Hf modified aluminide coated samples were exposed to hot corrosion for 400 hours.

- Simple aluminide coating showed weakest hot corrosion resistance and lost 430 mg/cm^2 weight after 400 hours exposure.
- The beneficial effect of Cr on the hot corrosion resistance of aluminide coating was more significant than Zr and Hf.
- All coatings except Y containing aluminides were totally destroyed due to hot corrosion after 400 hours exposure.
- Cr/Y and Y modified aluminide coatings survived after hot corrosion test. Y aluminide coating showed better hot corrosion resistance compared to Cr/Y aluminide in terms of coating depletion and weight loss.
- The beneficial effect of Y on hot corrosion behavior of aluminide coating was more significant than other ternary elements, possibly due to Y is more effective to prevent detrimental effect of sulfur.

CHAPTER 5

FUTURE RECOMMENDATIONS

5.1 Future Recommendations

This research addressed the optimization of CVD aluminizing process to maximize growth rate and outer layer/IDZ ratio. Also, improvement of aluminide coating hot corrosion resistance and lifetime by the addition of reactive or alloying elements were studied. However, there is some important acquired information that needs further investigations to optimize aluminizing process and improve aluminide coating oxidation and hot corrosion resistance. The following list includes some research studies which are suggested for future works.

- The aluminum activity is a major CVD process parameter which significantly affects growth rate and outer layer/IDZ thickness ratio of the coating. In this study, only 50/50 and 70/30 wt. % Al-Cr alloy were used at internal trays to observe the influence of aluminum activity. Further studies by using alloys containing different Al and Cr compositions (such as 20/80, 30/70, 40/60, 50/50, 60/40, 70/30, 80/20 wt.%) should be performed to understand the aluminum activity effect better. However, there is a risk of exhaust graphite blockage caused by aluminum deposition when using 80/20 wt. % Al-Cr alloy. Therefore, experiments should be performed with caution.

- It was observed that the influence of pressure on growth rate increases with increasing aluminum activity (70/30 wt. %). There is a critical point which the surface boundary layer thickness and the partial pressure of aluminum sub-

chlorides are in equilibrium for higher Al deposition rate. Therefore, the influence of pressure on growth rate should be studied for various Al-Cr alloys having different composition.

- Coating formation mechanism and time dependency of process should be studied in more details by performing interrupted aluminide coating growth (e.g. 1 h, 2 h, 3 h, 4 h, 5 h, etc.).

- Experiments demonstrate that HCl gas is not consumed completely in the chlorinator. The presence of unreacted HCl at coating chamber etches the coating surface and decreases coating growth rate. One of the possible explanation for low reaction rates in the chlorinator is the temperature difference between actual value and thermocouple reading. Therefore, actual temperature of chlorinator can be measured by placing reference thermocouple near to reaction zone to ensure thermocouple readings are correct.

- Net reaction rate in chlorinator is limited by surface area of aluminum pellets. Therefore, the influence of aluminum surface area on coating growth rate can be studied by placing varying size aluminum pellets in the chlorinator.

- Several aluminizing experiments were performed to incorporate reactive and alloying elements to aluminide coating. However, process parameters were not optimized to control the content of REs or alloying elements along the coating. The effect of ternary elements on oxidation and corrosion resistance of aluminide coating is also depended on their composition in the coating. Therefore, CVD process parameters should be optimized for each ternary elements to precisely control their composition in aluminide coating.

- A comparative hot corrosion test was performed for simple, Cr, Cr/Y, Y, Zr, and Hf modified aluminide coatings. Although improvement in hot corrosion resistance of aluminide coating was obtained, further enhancement could be

achieved by optimizing their composition in coating and combinations of those elements.

- Platinum has beneficial effect on oxidation and hot corrosion behavior of aluminide coatings. Addition of platinum to aluminide coating can be studied by electrochemical process or gas phase deposition with CVD. Also, its beneficial effect can be compared with other reactive and alloying elements by performing oxidation and hot corrosion test.

- Only hot corrosion test was performed to compare the influence of ternary elements. However, to better understand their effect on the lifetime of aluminide coating, oxidation tests should be performed under hot air, hot air with corrosive salts mixture, burned natural gas, burned natural gas with corrosive salts mixture. Also, composition and content of corrosive salt mixture can be altered to observe the influence of corroding environment.

- In this study, discontinuous (interrupted) measurement of hot corrosion method was used for comparative analysis of aluminide coatings hot corrosion behavior with the addition of ternary elements. However, continuous measurement method provides more precise weight measurement data during the hot corrosion test. Therefore, hot corrosion tests can be performed by continuous measurement method using special equipment.

- Burner rig and furnace test methods are more proper methods to simulate the operating conditions of gas turbine engines. Therefore, oxidation and hot corrosion behavior of aluminide coatings can be studied by using these methods rather than thermos-gravimetric method.

REFERENCES

[1] S. Bose, High temperature coatings, Elsevier Butterworth-Heinemann, 2007.

[2] E.F. Bradley, Superalloys : A technical guide, ASM International, 1988.

[3] R.I. Jaffee, J. Stringer, High-Temperature Oxidation and Corrosion of Superalloys in the Gas Turbine (A Review), in: E.F. Bradley (Ed.), Source B. Mater. Elev. Appl., American Society for Metals, 1979: p. 19.

[4] Y. Tamarin, Protective Coatings for Turbine Blades, 2002.

[5] G.W. Goward, Progress in coatings for gas turbine airfoils, Surf. Coatings Technol. 108–109 (1998) 73–79.

[6] B. Pint, Progress in understanding the reactive element effect since the Whittle and Stringer literature review, in: P.F. Tortorelli, P.Y. Hou (Eds.), Proc. John Stringer Symp., ASM International, 2001.

[7] R. Bianco, Pack Cementation Aluminide Coatings on Superalloys: Codeposition of Cr and Reactive Elements, J. Electrochem. Soc. 140 (1993) 1181.

[8] J. Day, Engines: The Search for Power, St. Martin's Press, 1980.

[9] N. Davey, The Gas Turbine, D. Van Nostrand Company, 1914.

[10] T. Giampaolo, Gas turbine handbook : principles and practice, Third Edit, Fairmont Press, 2006.

[11] W.J. Watson, The "success" of the combined cycle gas turbine, in: Int. Conf. Oppor. Adv. Int. Power Gener., IEE, 1996: pp. 87–92.

[12] W.W. Bathie, Fundamentals of gas turbines, Wiley, 1996.

[13] A.J. Scalzo, R.L. Bannister, M. DeCorso, G.S. Howard, Evolution of Heavy-Duty Power Generation and Industrial Combustion Turbines in the United States, in: Vol. 4 Heat Transf. Electr. Power; Ind. Cogener., ASME, 1994.

[14] D. Eckardt, Gas Turbine Powerhouse: The Development of the Power Generation Gas Turbine, 2014.

[15] S. Isser, Electricity restructuring in the United States, Cambridge University Press, 2015.

[16] GE LM 6000 Gas Turbine, (n.d.). https://powergen.gepower.com (accessed April 1, 2017).

[17] F. Keskinel, Türkiye'de Elektrik Üretimi ve Doğalgaz Kombine Çevrim Santralleri, İstanbul Bülten (IMO). (2006) 19–26.

[18] Türkiye İstatistik Kurumu TUIK, (n.d.). http://www.tuik.gov.tr/UstMenu.do?metod=temelist (accessed July 24, 2017).

[19] R.J. Hunt, The History of the Industrial Gas Turbine (Part 1 The First Fifty Years 1940-1990), Inst. Diesel Gas Turbine Eng. 15 (2011) 50.

[20] J. Stringer, I.G. Wright, The Future for High Temperature Materials and Coatings in the New Millennium, Mater. Sci. Forum. 369–372 (2001) 1–22.

[21] M.F. Stroosnijder, R. Mévrel, M.J. Bennett, The interaction of surface engineering and high temperature corrosion protection, Mater. High Temp. 12 (1994) 53–66.

[22] E.F. Bradley, M.J. Donachie, Role of Materials In Flight Propulsion Systems, J. Met. 22 (1970) 25-.

[23] G.W. Meetham, Requirements for and factors affecting high temperature capability, Mater. Des. 9 (1988) 244–252.

[24] C.T. Sims, N.S. Stoloff, W.C. Hagel, Superalloys II: High-Temperature Materials for Aerospace and Industrial Power, John Wiley and Sons, New York, 1987.

[25] W.G. Meetham, The development of gas turbine, 1981.

[26] W. Betteridge, S.W.K. Shaw, Development of superalloys, Mater. Sci. Technol. 3 (1987) 682–694.

[27] K.A. Green, T.M. Pollock, H. Harada, eds., Superalloys 2004, Proceedings of the Tenth International Symposium on the Superalloys, Metals and Materials Society (TMS), 2004.

[28] R.C. Reed, The Superalloys: Fundamentals and Applications, Cambridge University Press, 2006.

[29] S.S. Handa, Precipitation of Carbides in a Ni-based Superalloy, (2014) 1–33.

[30] S. Kalpakjian, S.R. Schmid, Manufacturing processes for engineering materials,

Prentice Hall, 2003.

[31] B. George, J.J. Galka, Alloy IN-738 Technical Data, 1969.

[32] The International Nickel Company, Properties of Some Metals and Alloys, (1982) 1–4.

[33] S.R.J. Saunders, J.R. Nicholls, Oxidation, Hot Corrosion and Protection of Metallic Materials, in: R.W. Cahn, P. Hassen (Eds.), Phys. Metall. Fourth Ed., Elsevier Science, Netherlands, 1996.

[34] P. Hancock, J.R. Nicholls, Fundamental and Engineering Aspects of Coatings for Diesel and Gas Turbines, NATO Work. into Adv. Coatings Diesel Gas Turbines. (1994) 31–58.

[35] C. Coddet, Environmental Protection of Metal Structures at High Temperature: State of the Art and Future Trends, Mater. Sci. Forum. 461–464 (2004) 193–212.

[36] T.J. Rayner, Development and evaluation of yttrium-modified aluminide diffusion coatings, University of Toronto, 1998.

[37] D.D. Hass, Thermal Barrier Coatings via Directed Vapor Deposition, University of Virginia, 2001.

[38] D.R. Gaskell, Introduction to the thermodynamics of materials, Taylor & Francis, 1995.

[39] T. Van Aller, Treatment of Metals, 1,155,974, 1911.

[40] H.B.C. Allison, L.A. Hawkins, Calorizing: A Protective Treatment for Metals, in: Gen. Electr. Rev., Vol. 17, 1914: pp. 947–951.

[41] C.B. Meher-Homji, The Development of the Whittle Turbojet, J. Eng. Gas Turbines Power. 120 (1998) 249.

[42] G. Goward, L. Cannon, Pack Cementation Coatings for Superalloys. A Review of History, Theory, and Practice, J. Eng. Gas Turbines Power(Trans. ASME). (1988) 150–154.

[43] J.A. David, Applying protective coating from powdered material utilizing high temperature and low pressure, 1960.

[44] M.P. Brady, B.A. Pint, P.F. Tortorelli, I.G. Wright, R.J. Hanrahan, High-Temperature Oxidation and Corrosion of Intermetallics, in: Corros. Environ. Degrad., Wiley-VCH Verlag GmbH & Co. KGaA, Weinheim, Germany, 2000:

pp. 229–325.

[45] Z. El Majid, M. Lambertin, High temperature oxidation of aluminide coatings, Mater. Sci. Eng. 87 (1987) 205–210.

[46] P. Nash, P. Nash, A.S.M. International, Phase diagrams of binary nickel alloys, ASM International, 1991.

[47] M.J. Pomeroy, Coatings for gas turbine materials and long term stability issues, Mater. Des. 26 (2005) 223–231.

[48] R. Bianco, R.A. Rapp, N.S. Jacobson, Volatile species in halide-activated diffusion coating packs, Oxid. Met. 38 (1992) 33–43.

[49] A. Squillace, R. Bonetti, N.J. Archer, J.A. Yeatman, The control of the composition and structure of aluminide layers formed by vapour aluminising, Surf. Coatings Technol. 120 (1999) 118–123.

[50] B.M. Warnes, D.C. Punola, Clean diffusion coatings by chemical vapor deposition, Surf. Coatings Technol. 94–95 (1997) 1–6.

[51] R.S. Parzuchowski, Gas phase deposition of aluminum on nickel alloys, Thin Solid Films. 45 (1977) 349–355.

[52] Z. Yu, D.D. Hass, H.N.G. Wadley, NiAl bond coats made by a directed vapor deposition approach, Mater. Sci. Eng. A. 394 (2005) 43–52.

[53] B.M. Warnes, A.L. Purvis, D.L. Near, Chemical vapor deposition apparatus and method, US6793966, 2001.

[54] B. Nciri, L. Vandenbulcke, Theoretical and experimental study of the aluminization of iron and steel in the pack and in the gas phase, Thin Solid Films. 139 (1986) 311–324.

[55] B.K. Gupta, A.K. Sarkhel, L.L. Seigle, On the kinetics of pack aluminization, Thin Solid Films. 39 (1976) 313–320.

[56] L. Seigle, B.K. Gupta, A.R. Shankar, A.K. Sarkhel, Kinetics of pack aluminisation, NASA Contract. Rep. 2939. (1978).

[57] G.W. Goward, D.H. Boone, Mechanisms of formation of diffusion aluminide coatings on nickel-base superalloys, Oxid. Met. 3 (1971) 475–495.

[58] R. Pichoir, Aluminide coatings on nickel and cobalt-base superalloys: Principal parameters determinig their morphology and composition, in: D. Coutsoradis, P. Felix, H. Fischmeister, L. Habraken (Eds.), High Temp. Alloy. Gas Turbines,

Applied Science, London, 1978: pp. 191–208.

[59] G.W. Goward, Current Research on Surface Protection of Superalloys for Gas Turbine Engines, J. Met. 22 (1970) 31-.

[60] S. Shankar, L.L. Seigle, Interdiffusion and intrinsic diffusion in the NiAl phase of the Al-Ni system, Metall. Trans. A. 9 (1978) 1467–1476.

[61] A.J. Hickl, R.W. Heckel, Kinetics of phase layer growth during aluminide coating of nickel, Metall. Trans. A. 6 (1975) 431.

[62] M.P. Brady, I.G. Wright, B. Gleeson, Alloy design strategies for promoting protective oxide-scale formation, Jom. 52 (2000) 16–21.

[63] B.A. Pint, I.G. Wright, W.Y. Lee, Y. Zhang, K. Prüßner, K.B. Alexander, Substrate and bond coat compositions: factors affecting alumina scale adhesion, Mater. Sci. Eng. A. 245 (1998) 201–211.

[64] H.J. Grabke, M. Brumm, M. Steinhorst, Development of Oxidation-resistant High Temperature Intermetallics, 8 (1992) 339–344.

[65] G.H. Meier, Research on Oxidation and Embrittlement of Intermetallic Compounds in the U.S., Oxid. Intermet. 618 (2007) 15–58.

[66] C. Leyens, B.A. Pint, I.G. Wright, Effect of composition on the oxidation and hot corrosion resistance of NiAl doped with precious metals, Surf. Coatings Technol. 133–134 (2000) 15–22.

[67] M. Qiao, C. Zhou, Hot corrosion behavior of Co modified NiAl coating on nickel base superalloys, Corros. Sci. 63 (2012) 239–245.

[68] F. Pettit, Hot corrosion of metals and alloys, Oxid. Met. 76 (2011) 1–21.

[69] K.-H. Keienburg, B. Deblon, B. Deblon, Refurbishing procedures for blades of large stationary gas turbines, Mater. Sci. Technol. 1 (1985) 620–628.

[70] I.G. Wright, High-Temperature Corrosion, in: Met. Handb., 9th ed., Metals Park: ASM, 1987: pp. 97–103.

[71] P. Hancock, Vanadic and chloride attack of superalloys, Mater. Sci. Technol. 3 (1987) 536–544.

[72] R.A. Rapp, Y.-S. Zhang, Hot corrosion of materials: Fundamental studies, JOM. 46 (1994) 47–55.

[73] J. Stringer, High-temperature corrosion of superalloys, Mater. Sci. Technol. 3 (1987) 482–493.

[74] K.B. Small, D.A. Englehart, T.A. Christman, Guide to etching specialty alloys, Adv. Mater. Process. 166 (2008) 32–37.

[75] B. Wierzba, K. Tkacz-Śmiech, A. Nowotnik, K. Dychtoń, Aluminizing of nickel alloys by CVD. the effect of HCl flow, Chem. Vap. Depos. 20 (2014) 80–90.

[76] H. Rafiee, H. Arabi, S. Rastegari, Effects of temperature and Al-concentration on formation mechanism of an aluminide coating applied on superalloy IN738LC through a single step low activity gas diffusion process, J. Alloys Compd. 505 (2010) 206–212.

[77] P.J. Masset, A. Bogusz, J. Sieniawski, B. Wierzba, K. Tkacz-Śmiech, Optimisation of Nickel Aluminising by CVD, Defect Diffus. Forum. 323–325 (2012) 367–372.

[78] T. Kikuchi, T. Kurosawa, T. Yagihashi, Equilibrium of the 2Al(l)+AlCl3(g)=3AlCl(g) Reaction in the Subhalide Process of Aluminium, Trans. Japan Inst. Met. 5 (1964) 122–126.

[79] Z. Xu, Z. Wang, J. Niu, L. He, R. Mu, K. Wang, Effects of deposition temperature on the kinetics growth and protective properties of aluminide coatings, J. Alloys Compd. 632 (2015) 238–245.

[80] A. Nowotnik, J. Sieniawski, M. Góral, M. Pytel, K. Dychton, Microstructure and kinetic growth of aluminide coatings deposited by the CVD method on Re 80 superalloy, Arch. Mater. Sci. Eng. 55 (2012) 22–28.

[81] H.O. Pierson, W.A. Publishing, N. York, Handbook of chemical vapor deposition: principles, technology and applications, 1999.

[82] W.-P. Sun, H.J. Lin, M.-H. Hon, CVD aluminide nickel, Metall. Trans. A. 17 (1986) 215–220.

[83] J.E. Hatch, A. Association, A.S. Metals, Aluminum: Properties and Physical Metallurgy, American Society for Metals, 1984.

[84] K. Vaidyanathan, Surface geometry and strain energy effects in the failure of a (Ni,Pt)Al/EB-PVD thermal barrier coating, Acta Mater. 52 (2004) 1107–1115.

[85] G.Y. Kim, L.M. He, J.D. Meyer, W.Y. Lee, A. Quintero, J.A. Haynes, Mechanisms of Hf dopant incorporation during the early stage of chemical vapor deposition aluminide coating growth under continuous doping conditions,

Metall. Mater. Trans. A. 35 (2004) 3581–3593.

[86] B.A. Pint, K.L. More, I.G. Wright, Effect of quaternary additions on the oxidation behavior of Hf-doped NiAl, Oxid. Met. 59 (2003) 257–283.

[87] S. Naveos, G. Oberlaender, Y. Cadoret, P. Josso, M.P. Bacos, Zirconium Modified Aluminide by a Vapour Pack Cementation Process for Thermal Barrier Applications: Formation Mechanisms and Properties, Mater. Sci. Forum. 461–464 (2004) 375–382.

[88] R. Bianco, R.A. Rapp, J.L. Smialek, Chromium and Reactive Element Modified Aluminide Diffusion Coatings on Superalloys - Environmental Testing, J. Electrochem. Soc. 140 (1993) 1191–1203.

[89] I. Gurrappa, I.V.S. Yashwanth, I. Mounika, H. Murakami, S. Kuroda, The Importance of Hot Corrosion and Its Effective Prevention for Enhanced Efficiency of Gas Turbines, Gas Turbines - Mater. Model. Perform. (2015) 55–102.

[90] D.R. Sigler, Aluminum Oxide Adherence on Fe-Cr-A1 Alloys Modified with Group IIIB, IVB, VB, and VIB Elements, Oxid. Met. 326 (1989).